A STUDY ON PROCESSING OF CELLULOSE AND ITS INTERACTION WITH SUPERCRITICAL CARBON DIOXIDE AND CO-SOLVENT

By

ANIKET SELARKA

A DISSERTATION PRESENTED TO THE GRADUATE SCHOOL
OF THE UNIVERSITY OF FLORIDA IN PARTIAL FULFILLMENT
OF THE REQUIREMENTS FOR THE DEGREE OF
DOCTOR OF PHILOSOPHY

UNIVERSITY OF FLORIDA

2011

This dissertation is dedicated to the late Dr. Charles L. Beatty, Barbara Beatty, John Matthews, and Olive Matthews.

ACKNOWLEDGMENTS

At first, I would like to convey my gratitude to my former adviser, the late Dr. Charles L. Beatty for his endless support. I am very grateful to Dr. Ronald H. Baney and Dr. Siobhan Matthews for extending their support after demise of Dr. Beatty in the year of 2010. They always encouraged me to stay focused on my research and provided valuable feedback throughout my studies. I am very thankful to Dr. Siobhan Matthews for letting me use her facility in Ireland and her family for their kind love and support. Irrespective of the time difference between USA and Ireland, Dr. Siobhan Matthews was always available to discuss and provide inputs. I would like to extend my thanks to Dr. Kirk Ziegler for his generosity on use of equipment and valuable suggestions in progress of my research. I would also like to thank Dr. Joanna Long for her involvement and support.

My sincere acknowledgement also goes to Dr. Laurie Gower and Dr. Hassan El-Shall for serving on my committee and guiding me through the research work. I appreciate my colleagues and friends for helping me in several academic and personal ways. I would like to take this opportunity to extend my gratitude to the department of Materials Science and Engineering at University of Florida for providing me course work and research opportunities to develop the ability for advanced level research.

Finally, I am very thankful to my family for encouraging me to pursue higher studies and for their blessings.

TABLE OF CONTENTS

page

LIST OF TABLES

LIST OF FIGURES

LIST OF ABBREVIATIONS

AGU	Anhydroglucose Unit
ATR	Attenuated Total Reflection
CP	Cross Polarized
DMSO	Dimethyl Sulfoxide
DRIFT	Diffused Reflectance Infrared Fourier Transform Spectroscopy
EC	Ethyl Cellulose
FTIR	Fourier Transform Infrared Spectroscopy
LDPE	Low Density Polyethylene
L/D	Length/Diameter Ratio of twin-screw
MA	Maleic Anhydride
MAS	Magic Angle Spinning
NMR	Nuclear Magnetic Resonance
PHA	Polyhydroxyalkanoate
PLA	Polylactic Acid
scCO2	Supercritical CO_2
SEM	Scanning Electron Microscopy
TBAF	Tetrabutylammonium fluoride
WAXRD	Wide Angle X-Ray Diffraction

Abstract of Dissertation Presented to the Graduate School
of the University of Florida in Partial Fulfillment of the
Requirements for the Degree of Doctor of Philosophy

A STUDY ON PROCESSING OF CELLULOSE AND ITS INTERACTION WITH SUPERCRITICAL CARBON DIOXIDE AND CO-SOLVENT

By

Aniket Selarka

May 2011

Chair: Ronald H. Baney
Major: Materials Science and Engineering

An ecological alternative to reduce plastic waste is to use biodegradable polymer blends and composites using natural polymers. Cellulose is the most abundant natural polymer on earth. However, one of the significant factors that restrict its use at higher levels in blends and composites is high crystallinity. This characteristic comes from extensive inter-chain and intra-chain hydrogen bonds between hydroxyl groups. Supercritical carbon dioxide (CO_2) has been known for efficient plasticizing effect in polymer processing. In this work, the effect of supercritical CO_2 on mechanical properties of a twin-screw extruded Low Density Polyethylene (LDPE)-cellulose blend (70-30) was studied. The supercritical CO_2 assisted LDPE-Cellulose blend showed 300% increase in tensile strain at break compared to non-CO_2 assisted LDPE-Cellulose blend. Moreover, the strain at break of supercritical CO_2 assisted LDPE-Cellulose blend matched with that of LDPE-Starch blend.

An attempt to change the inherent crystallinity of cellulose was performed by exposing it to two systems viz. Dimethyl Sulfoxide (DMSO)-supercritical CO_2 and DMSO-Urea-supercritical CO_2. The change in relative crystallinity was studied by Wide Angle X-Ray Diffraction (WAXD). The samples were characterized by using Diffuse

Reflectance Infrared Fourier Transform Spectroscopy (DRIFT) in order to study the changes in molecular structure preferably hydrogen bonding due to processing under such systems. The samples were also characterized by ^{13}C Nuclear Magnetic Resonance (NMR) technique to acknowledge understanding developed from the DRIFT measurements. The cellulose samples processed in DMSO-supercritical CO_2 system showed a reducing trend of the relative crystallinity with increasing pressure. A maximum 40% reduction was achieved when cellulose was processed with DMSO-supercritical CO_2 at 4500 psi. The reduction in the relative crystallinity occurred due to weakening of inter-chain hydrogen bonds in cellulose. The cellulose samples were processed in DMSO-urea-supercritical system at 2500 psi and 4500 psi. The amount of urea added in cellulose was in the range of 0.25 to 1.00 g per 1.5 g of cellulose. Over 50% reduction in relative crystallinity was found in most of the samples. This reduction in crystallinity was due to the presence of a DMSO-urea complex, which caused weakening of intermolecular hydrogen bond and an intramolecular hydrogen bond.

The supercritical CO_2 assisted extrusion processed LDPE-Cellulose blend (70-30) was proved a suitable alternative of LDPE-Starch blend of the same composition. Batch Processing of microcrystalline cellulose in DMSO-supercritical CO_2 and DMSO-Urea-supercritical CO_2 showed significant reduction in relative crystallinity compared to that of unmodified cellulose. The reduction in crystallinity occurred due to disruption of the molecular structure that was caused by weakening of hydrogen bonds.

CHAPTER 1
MOTIVATION AND APPROACH

1.1 Motivation

There is a growing demand to develop products from bio-based materials and use technologies that can untie the broad dependence on fossil fuels and non-renewable resources. Increasing awareness to minimize plastic waste accumulation in landfills and soil has triggered attempts towards utilizing bio-based materials over conventional polymeric materials. Petroleum based polymers such as polyolefins do not biodegrade for many years even after being buried for a long time. Whereas, bio-based materials degrade easily by enzymatic action of microorganisms like bacteria, fungi etc. in soil. This makes conventional polymers unsuitable to be used to make polymeric products for short term applications but makes natural bio-based materials a better alternative[1]. Usage of non-biodegradable polymers, especially the ones derived from petroleum resources, can be reduced by replacing them completely or the part (by blending) with natural biopolymers such as polysaccharides or natural polypeptides. Among bio-polymers, cellulose and starch are the most important natural polysaccharides[2]. Cellulose, being the most abundant natural polysaccharide and renewable biomass, represents about 1.5×10^{12} tons of the total biomass produced annually[3]. Among the two, starch can be more easily hydrolyzed (first step of disintegration) and processed. Therefore, most of the biodegradable polymer blends and composites are composed of starch as the main filler material. However, the low crystallinity and the very hygroscopic nature of starch affects its mechanical properties, temperature stability and moisture resistance[2,4]. On the other hand, molecular structure and the high crystalline nature of cellulose make it an excellent filler material to impart strength to a polymer blend.

However, the same characteristic not only makes its hydrolysis difficult but also shows poor compatibility with the polymer matrix. As a result, the efficient utilization of cellulose in making fully or partially biodegradable polymer blends is still a challenging task. A good balance of mechanical properties can be achieved if the crystallinity of the cellulose is reduced and/or its compatibility with a base polymer is improved. This can also lead to use of high volume of cellulose in polymer blends, which will not only form a suitable alternative to starch but will also not affect the human food chain unlike the way that the use of starch could potentially do.

This work was performed with a focus on the use of cellulose as a possible alternative to starch in synthetic polymer blends. The emphasis was given on utilizing the advantages of supercritical CO_2 to change the inherent characteristics of cellulose viz. its crystallinity and molecular structure. It was determined that the preliminary groundwork to foresee the benefits of supercritical CO_2 assisted processing on blend properties as well as on the cellulose alone is necessary. Cellulose can be pre-modified for reduced crystallinity by processing in a combination of non-hazardous and environmentally benign solvent systems viz. DMSO- supercritical CO_2 or DMSO-Urea-supercritical CO_2. Modification of cellulose followed by blending with synthetic polymers can be used to make and improve the properties of synthetic polymer-cellulose blends. Thus, the two primary objectives of this research were:

- Investigate the possibility of replacing starch with cellulose as biodegradable filler in LDPE-starch blends.
- Explore DMSO-supercritical CO_2 and DMSO-Urea-supercritical CO_2 as possible solvent systems to disrupt the highly crystalline structure of microcrystalline cellulose and develop understanding of micro-structural changes that occur therein.

1.2 Engineering and Scientific Approach

The high crystallinity of microcrystalline cellulose comes from the glycosidic bond linkages and the intermolecular & intramolecular hydrogen bond network formed between the cellulose chains in the crystallites[5,6,7] (Figure 1-1 and Figure 1-2). Some promising ways to reduce cellulose crystallinity are to alter its molecular structure by breaking and changing[5] its molecular bonds. Usually change in molecular structure by disrupting bonds in cellulose is achieved by processing under high shear, dissolving-regenerating or functionalizing it in a suitable solvent.

The intent of this research was to demonstrate that the high shearing action in a twin-screw extruder with combination of liquid-like density and gas-like viscosity of supercritical CO_2[8] may be used to disrupt the cellulose structure and finely disperse it in the continuous Low Density Polyethylene polymer phase. Supercritical CO_2 can act as a plasticizing agent and its dissolution in blend can further reduce viscosity of the blend over applied shear stress and high temperatures[8]. Blending of cellulose in presence of supercritical CO_2 can also induce change in the chain orientation of cellulose to some extent and so to its crystal structure or crystallinity. Generally, in a polymer blend any considerable change in molecular structure of the blend components is reflected in final properties of the blend. Changes due to supercritical CO_2 assisted processing can be measured by change in thermo-mechanical properties of the blend. Performance of LDPE-Cellulose blend - extruded with and without supercritical CO_2 over LDPE-Starch blend (without supercritical CO_2) was evaluated in order to determine:

a) processibility of high cellulose content LDPE blend compared with LDPE-Starch blends (30/70)

b) advantages of supercritical CO_2 assisted processing of LDPE-Cellulose blend

Dimethyl Sulfoxide (DMSO) is a biodegradable, non-toxic polar solvent. Its high dipole moment[9] and hydrogen bond forming properties with cellulose can be used to expand the micro-fibrillar structure of cellulose. The liquid retention value (a measure of degree of swelling) of DMSO in cotton cellulose is significantly higher among other commonly used organic swelling agents for cellulose[10]. Carbon dioxide is a clean, inexpensive and environmentally benign solvent[11]. In its supercritical state, it displays dual properties – solvating power of liquid and mass transfer properties of a gas[12]. But, a major limitation towards cellulose is its hydrophobic characteristic which prevents swelling of hydrophilic cellulose to any considerable extent[13]. However, its unique physico-chemical characteristics in combination with properties of DMSO can be used to disrupt and re-orient the molecular bonds in cellulose. As depicted in Figure 1-3, the microcrystalline cellulose can first be swollen by solvent DMSO and then pressurized under supercritical CO_2 to improve effectiveness of DMSO towards altering the microstructure. Application of supercritical CO_2 may help the solvent molecules penetrate deeper into crystalline structure, cause disruption of hydrogen bonds, and finally lead to reduction in crystallinity. The high mass-transfer rate in supercritical state can assist the diffusion of solvent molecules. DMSO can later be extracted from cellulose by conducting a supercritical CO_2 drying run, which involves depressurizing CO_2 over a fixed pressure range.

Microcrystalline cellulose does not dissolve in DMSO but only swells. Moreover, there is a possibility to partially reform the disrupted cellulose structure and achieve very small change in crystallinity due to sudden change in pressure during extraction of DMSO. Urea is easily soluble in DMSO but poorly soluble in supercritical CO_2[14,15].

DMSO may act as a carrier for urea molecules in crystalline structure of cellulose. Supercritical CO_2 can assist in diffusing urea deeper into the structure. The poor solubility of urea with supercritical CO_2 can be used to extract only DMSO during the supercritical drying run. This way further reduction in cellulose crystallinity can be achieved by introducing urea. Urea could either interact chemically with cellulose by forming cellulose carbamate[16] or it can physically be entrapped by hydrogen bonds in the cellulose structure. Either way it will increase the free volume of cellulose and so contribute in reducing crystallinity. Table 1-1 shows selective interactions among the components.

1.3 Organization of the Dissertation

Chapter 1 addresses the need and motivation to conduct this research. It defines the specific aims and discusses scientific approach to carry out the research work.

Chapter 2 includes a comprehensive literature study on structure and properties of cellulose and starch. Characterization techniques used to study molecular structure and properties of cellulose are discussed in this chapter. This chapter also includes characteristics and behavior of supercritical fluids with emphasis on supercritical CO_2 and co-solvents used in polymer processing.

Chapter 3 is includes twin-screw extrusion processing of LDPE-Cellulose and LDPE-Starch blends. The effect of processing of LDPE-Cellulose under supercritical CO_2 on thermo-mechanical properties of the blend is discussed. These blend properties are compared with non-CO_2 assisted LDPE-Cellulose and LDPE-Starch blends.

Chapter 4 includes description about materials used, experiment design, batch reactor setup and method followed for batch reactions involving microcrystalline cellulose, DMSO, urea and supercritical CO_2.

Chapters 5, 6 and 7 include methods used to characterize the cellulose samples to study the changes in crystallinity and molecular structure due to batch reaction processing. The change in relative crystallinity was evaluated by the Wide Angle X-Ray Diffraction (WAXRD) method in chapter 5. Changes in molecular structure were explained by using Diffused Reflectance Infrared Fourier Transform Spectroscopy (DRIFT) and solid-state ^{13}C Nuclear Magnetic Resonance (NMR) techniques in chapter 6 and chapter 7 respectively.

Chapter 8 is a summary and a discussion about future work to make cellulose based polymer blends by processing materials directly in a twin-screw extruder with aid of supercritical CO_2.

Table 1-1. Miscibility between components for batch reactions[10,13,17,18,14,15]

	Cellulose-DMSO	Cellulose-supercritical CO_2	DMSO-supercritical CO_2	DMSO-Urea	Urea-supercritical CO_2
Miscibility of Components	Partial	Poor	Good	Good	Poor

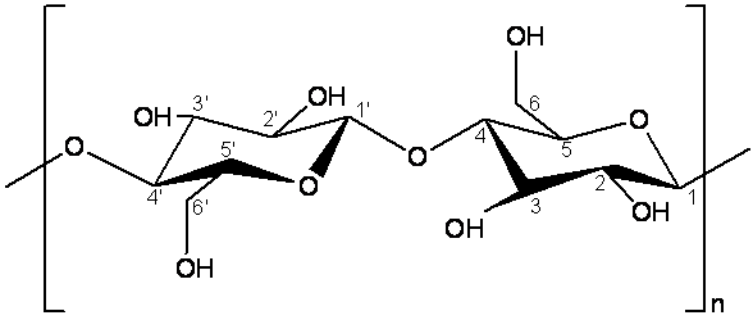

Figure 1-1. Repeat unit of cellulose (Adapted from Kovalenko *et al.*[19])

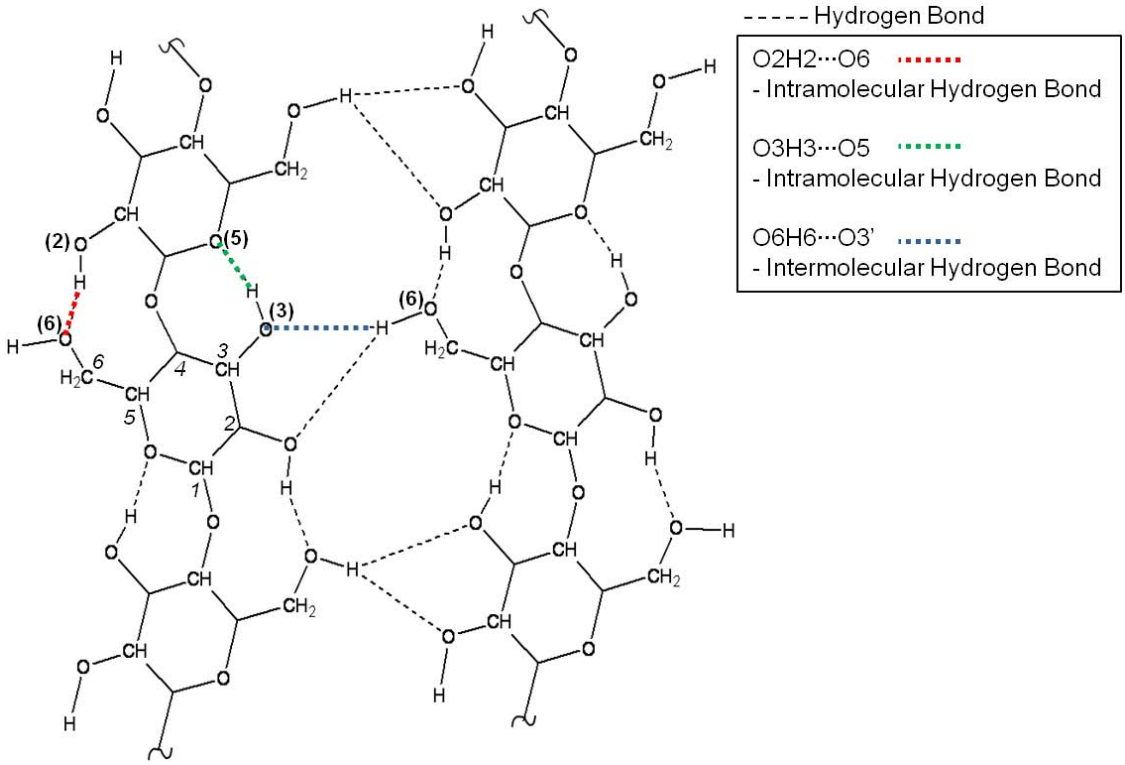

Figure 1-2. Intermolecular and Intramolecular hydrogen bond network in cellulose Iβ (Adapted from Kovalenko *et al.*[19] and Klemm *et al.*[20])

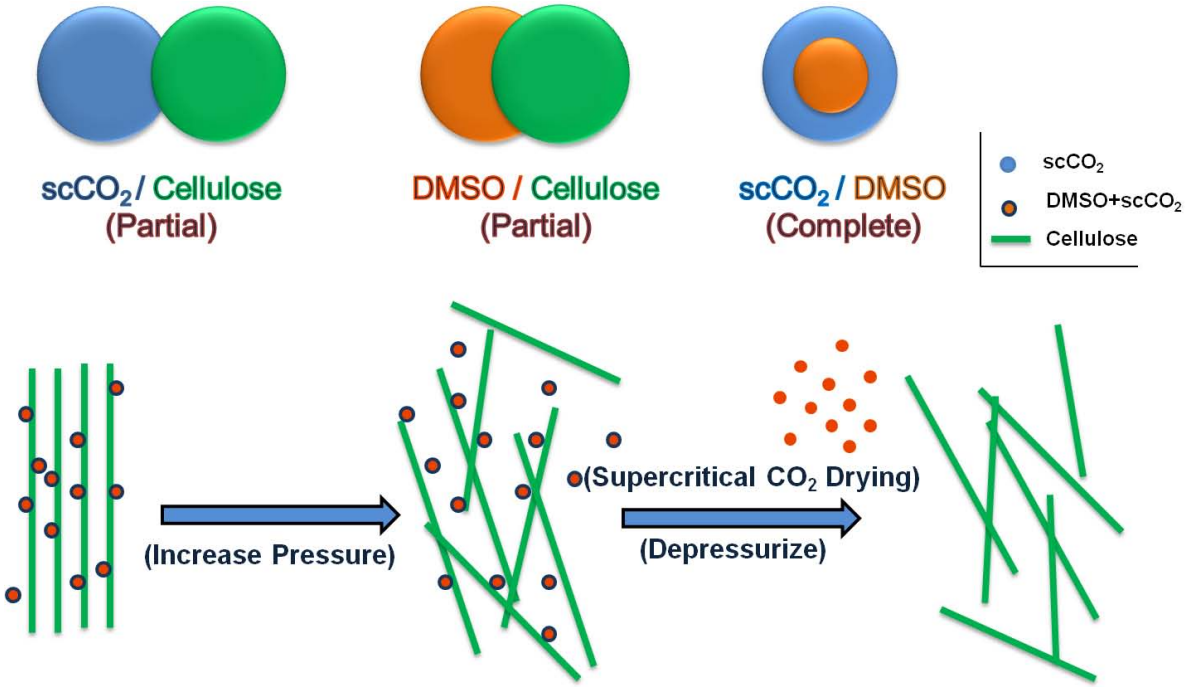

Figure 1-3. Hypothesis for batch reaction involving cellulose, DMSO and supercritical CO_2

CHAPTER 2
BACKGROUND

2.1 Bio-Based Materials

Currently, humankind is confronting two related challenges: finding sustainable solution for increasing energy demand with limited (and diminishing) hydrocarbon fuel resources and, the global warming associated with CO_2 emissions from fossil fuels. A plausible way to resolve this issue is to switch to bio-based renewable resources which can endlessly meet the energy demand as well as reduce the green house gas release compared with petroleum equivalents[21,22]. In simple terms, bio-based materials are agricultural, forestry and marine feed stocks (that include plants, trees, wood waste, grasses, agricultural residues, fungi etc.) and the ones, which are derived from natural renewable resources. All the bio-based materials derived from natural resources are not necessarily biodegradable[23]. For example, polythioesters, which are polymers of mercaptoalkanoic acids found in various microorganisms are not biodegradable[24]. Rudikeet *et al.*[25] showed that Poly lactic acid (PLA), which is a linear aliphatic polyester made from starch, takes a long time to degrade in real environmental conditions. They suggested that the slow rate of degradation of PLA was because of its high glass transition temperature (60°C) and due to slow hydrolysis rate in wastewater conditions at 25-32 °C. Yet, these are important over fossil fuel based polymers from 'carbon neutral' point of view which means carbon emitted at the end of these material's life cycle can be avoided to sequester under the earth's surface and rather be recycled to generate additional biomass via photosynthesis[21-22].

On the basis of production, type of polymer and processing involved, bio-based polymers can be classified in three categories – (a) natural polymers (natural

polysaccharides like starch and cellulose), (b) biosynthetic polymers (extracted from microorganisms, ex. PHA) , and (c) bio-chemosythetic polymers (chemical polymerization of bio-derived monomers, ex.PLA)[4, 23]. Among natural polymers, cellulose is the most abundant polysaccharide and available as the major constituent (35-50%), apart from hemicelluloses (20-35%) and lignin (10-25%), in plant biomass (lignocellulose)[3, 26]. Starch is a natural polymer which is available in principal crops like potatoes, corn and rice[27]. The background study of this research work is focused on natural bio-based materials that include cellulose and starch based materials, blends, and composites.

2.1.1 Cellulose and Starch– Structure and Properties

Organization of elementary fibrils and microfibril in a plant cell wall are shown in Figure 2-1. Hundreds of glucan molecules (polysaccharide made of D-glucose units) aggregate to form elementary fibrils; groups of these elementary units are embedded in a matrix of hemicelluloses which is then surrounded by covalently bonded lignin[28,29]. Cellulose is present in the form of sheets of glucopyranose rings lying in a plane. These sheets successively arrange on top of each other to form a cellulose crystallite. These crystallites arrange together to form the elementary fibril[29] (Figure 2-1). The traditional model for cellulose fibers depicts the microfibrils made of alternating ordered (crystalline) and disordered (amorphous) regions of cellulose[30] (Figure 2-2). A modified model was suggested which was based on the evidence that a number of cellulose chains on the surface of the microfibril can correlate to the amount of amorphous content in cellulose (Figure 2-3). Layers of cellulose chains on the surface of crystallites contributed to amorphous regions. Whereas, chains in the interior were considered to contribute to the crystalline regions[30,31,32]. Numerous studies have been conducted and

various analytical techniques have been applied in order to understand the supermolecular structure of cellulose and determine its degree of crystallinity. The X-ray diffraction method is sensitive to the long-range order of semi-crystalline polymers whereas infrared spectroscopy and solid-state nuclear magnetic resonance techniques are sensitive to immediate environment around nuclei. Thus the values obtained for degree of crystallinity vary according to the technique applied[30].

Cellulose is a polymer which is biogenetically formed by two repeat units of D-glucopyranose molecules that are linked through covalent β-glycosidic bonds between C(1) and C(4) carbon atoms (Figure 1-1). The glucopyranose ring adopts a chair conformation 4C1. Three OH groups per anhydroglucose unit (AGU) are present at C(2), C(3) and C(6) in equatorial positions. Every second AGU ring is rotated by 180° in the plane in order to accommodate preferred bond angles of acetal oxygen bridges. Presence of oxygen atoms on both β-glycosidic bond and pyranose ring, and hydroxyl groups form a three dimensional semi-crystalline supermolecular structure via ordered intra-chain and inter-chain hydrogen bonding[33, 3, 28, 34,20,19]. Equal number of hydroxyl groups on each side of cellulose chain induces extensive intra-chain (2-3 per AGU) and inter-chain hydrogen bonds (2 per AGU) that makes stable and straight fibrils of cellulose. The extensive intermolecular and intramolecular hydrogen bonding between chains results in large lattice forces which causes high crystallinity and water insolubility[33, 35,36]. The highly stable structure so produced cannot be broken by increasing temperature. Cellulose degrades below its theoretical melting temperature[37]. Crystallinity affects mechanical, physical, and chemical properties of the cellulose. For example, the density, tensile strength, and dimensional stability increase whereas

chemical reactivity and swelling decrease with increasing crystallinity of cellulose[38]. On the basis of origin and applied chemical processing, crystalline domains may consist of various polymorphs called I, II, III and IV, V, VI[34,28]. Cellulose lattice types I and II are of most importance and have been most extensively studied. Cellulose I features parallel arrangement of polymer chains by which hydrogen bonds are formed only between the chains on the same sheet whereas in cellulose II the polymer chains are arranged in anti-parallel way which leads to hydrogen bond formation between adjacent sheets[39] (Figure 2-4). Hydrogen bonding patterns in cellulose I and cellulose II are shown in Figure 2-5. Native cellulose (Cellulose I) consists of a crystalline domain with two allomorphs phases Iα and Iβ. The latter is characterized by a monoclinic unit cell in which two polymer chains are in a parallel arrangement. In Iα phase, the polymer chains are shifted along chain axis that forms a triclinic unit cell[40]. Cellulose Iβ is thermodynamically more stable and abundant than Iα form[40, 41]. Cellulose II can be obtained from native cellulose by either regeneration or mercerization. Regeneration is a process of solubilizing cellulose I in a suitable solvent and finally re-precipitating cellulose by water. Mercerization involves swelling of native cellulose fibers using concentrated NaOH and then removing the swelling agent by water. Most of the physical properties of cellulose, swelling, and adsorption are due to its crystallinity and so determination of this physical property (ratio of mass of crystalline regions to total mass of material) is one of the most important structural parameter studied. The dimensions of cellulose crystallites and degree of crystallinity have been extensively studied over years; these parameters vary for different types of native celluloses[3]. The same order of crystallinity for a series of cellulose samples can be found when

crystallinity is calculated by different techniques but the disagreement is usually found for the same sample[28, 34, 42].

Due to its rigid chemical structure formed by hydrogen bond network, and being surrounded by lignin in plant cell wall, cellulose needs to be pretreated prior to use. The pretreatment of cellulose aims toward removal of lignin and disrupting the molecular structure by exposing cellulose to physical or chemical treatments. The common physical and thermal treatments include milling, microwave heating, steam pretreatment, and gamma irradiation. However, these methods are energy-intensive and require high temperatures / pressures[5,43]. Chemical pretreatment methods include dissolution and functionalization of cellulose using various kinds of solvents[44,45,46]. Dissolution of cellulose in various solvents has been reviewed by Heinze *et al.*[44]. They categorized solvents as derivatizing and non-derivatizing. Derivatizing solvents are those in which derivatives like unstable ether, ester or acetal derivatives are formed during the dissolution process. Cellulose is regenerated when its derivatives are decomposed by changing either pH of the solvent medium or changing from non-aqueous to aqueous solvent. A major disadvantage of derivatizing type solvents is the occurrence of side reactions that results into formation of by-products[45,46]. Non-derivatizing solvents dissolve the cellulose by inter-molecular interactions[44]. The current available systems used to dissolve cellulose suffer with drawbacks like volatility, generation of poisonous gas, long reaction times, requirements of fast dissolution rates, difficulty in recycling solvents, sugar degradation, corrosion of instrument by acids, limited to lab-scale, and high capital investments[47].

DMSO is a polar, aprotic, non-derivatizing solvent. The dual functionality, from sulfoxide oxygen and sulfoxide sulfur, as hard and soft bases respectively makes it an excellent solvent for many materials. Although DMSO itself cannot dissolve cellulose, it has been proven as one of the best swelling agents for cellulose[48]. Combinations of DMSO with other compounds, for example DMSO-SO_2-diethylamine or DMSO/TBAF, have been recognized as the most versatile solvent systems for cellulose[44].

Starch is another major storage form of glucose. It is made of two homopolymers of D-glucose: amylase (10-20%) and amylopectin (80-90%). In starch, the glucose units are connected straight by 1,4'-α-D linkages forming a linear homopolymer amylase whereas branching of glucose chains at α-1, 6' branch points forms the amylopectin (Figure)[49,50]. Starch chains contain hydroxyl groups at C2, C3 and a primary hydroxyl group at C6 if it is not linked. These hydroxyl groups can be involved in strong intermolecular associations via hydrogen bonding[50]. The presence of amylopectin as branch polymer chains prevents the inter-molecular association of linear amylase chains[51]. The presence of hydroxyl groups available for hydrogen bonding interactions makes starch susceptible to water molecules. Starch alone has poor processibility, dimensional stability and the final products have poor mechanical properties so direct use of native starch is avoided. However, due to its hydrophilic nature, addition of small amounts of water molecules reduces its glass transition temperature and makes it easy to be processed by using conventional processing techniques like extrusion, injection molding etc.[50]. When compared with cellulose, starch displays poor thermal stability. The glycosidic linkages in starch start to break at 150°C and thermal degradation occurs

at 250°C[52]. In attempts to make biodegradable blends, starch has been blended with polyolefins, aliphatic polyesters, polyvinyl alcohols and other biopolymers[50,53,54] .

2.1.2 Characterization of Cellulose

The crystal lattice formed due to hydrogen bonds and van der Waals dispersion forces in cellulose have been characterized by X-Ray Diffraction, Nuclear Magnetic Resonance[10] and Fourier Transform Infrared techniques[55]. The X-Ray Diffraction method has been the most widely used technique. Characteristic peaks from different crystal planes in the monoclinic unit cell of cellulose I as observed by XRD are shown in Figure 2-8. The peaks were assigned as reported in papers by other authors [56],[57]. Bansal *et al.*[56] have summarized several authors work towards calculation of degree of crystallinity of cellulose by the X-Ray Diffraction Method. According to their report, the degree of crystallinity was mostly calculated by subtracting the background region at around 2 theta = 19.5° (which accounts for the amorphous region) from the crystalline region. If a method by Segal *et al.*[58] was followed, it involved comparing peak intensities at 2 theta = 22.5° (crystalline peak from 002 plane) and 18° (amorphous peak) from the baseline. Authors noted that the Segal's method is comparatively easy and most applied among all methods. It had one drawback - the intensity of presumed amorphous region at 2 theta value 18° was found shifted to a higher 2 theta value of 19.5° for an actual amorphous cellulose sample[56]. On the other hand, the amorphous region subtraction method can also be erroneous if overlapping peaks from crystalline and amorphous regions are not well separated. Thygesen *et al.*[59] applied four different analytical methods viz. Segal method, the Ruland-Vonk method, the Rietveld method, and the Debye method to show that degree of crystallinity of the same microcrystalline cellulose can vary according to the analytical method used. Nevertheless, analytical

methods involving either subtraction of background (as the amorphous region) or the amorphous region from custom-made amorphous cellulose are appropriate to use for estimating the degree of crystallinity but care should be taken while reporting the results as relative crystallinity rather than absolute crystallinity of the sample.

Infrared Spectroscopy has been utilized as one of the most useful techniques to study different conformations of cellulose macromolecules and the hydrogen bonding within. In about past 60 years, various articles have been published where Inter-chain and Intra-chain hydrogen bonding in cellulose is systematically studied by IR spectroscopy. According to Michelle[60], Marinnan & Mann and Liang & Marchessault reported two types of band patterns in OH and CH stretch region of native cellulose (2800-3600 cm^{-1}). Later Marchessault & Liang extended the study for region 640 – 1700 cm^{-1}. An urge to improve the resolution of spectra and the concurrent development of Infrared Spectrometers lead Michelle to obtain Second Derivative FTIR Spectra of cellulose. The advantage of the second derivative mode is that it enhances the fine spectral features of the spectrum by improving the resolution of overlapping bands and suppressing the background signal. The differentiation of spectral signal resolves any component peaks, which are masked by overlapping of other peaks in that region[61]. Michelle's study on cellulose obtained from different sources brought the understanding about molecular bonding and conformation in cellulose to a higher standard by confirming existence of two types of cellulose polymorphs I and II, which differ in hydrogen bonding pattern and crystallite size. Over the years, the complex structure of cellulose has been extensively studied by utilizing the IR spectroscopy method. In order to develop an understanding of the breaking and the formation of inter-chain & intra-

chain hydrogen bonds in cellulose, this technique has been used as a prime substrate for various treatments. The treatments include its addition to aqueous solutions[62]; containing metal complexes[63]; inclusion of alkali[64,65]; adsorption of dye molecules[34]; infusion of urea[66]; dissolution in dilute acids[7]; organic and inorganic solvents[3] etc. Variations in absorbance and shifts in wavenumber in FTIR spectra have been reported to elucidate change in hydrogen bonding due to such reactions.

Cellulose macromolecule has three different hydroxyl groups that participate in inter-chain and intra-chain hydrogen bonding. Combination of these hydrogen bonded OH stretching vibrations show a broad IR peak in 3000-3600 cm^{-1} region [33]. Heavy overlapping of inter-chain and intra-chain hydrogen bonds in OH stretch region makes the interpretation of corresponding bands difficult. Various authors have separated these bands but the assignment of hydrogen bonds corresponding to the peak positions varies not only with author's discretion but also with the source of cellulose. In attempt to distinguish hydrogen bonds formed by three hydroxyl groups in cellulose, Gardener and Blackwell used second derivative FTIR and electron diffraction methods and suggested that two of the hydroxyl groups are involved in intra-chain hydrogen bonding and one hydroxyl group forms inter-chain hydrogen bond. According to these authors the bonds O3H3···O5 and O2H2···O6 (See Figure 2-5) form intra-chain whereas O6H6···O3' form inter-chain hydrogen bond[67]. Later Marechal and Chanzy[68] and Kokot *et al.*[69] also used the second derivative FTIR method to study and assign spectral bands corresponding to these hydrogen bonds. They both suggested that a band around 3446 cm^{-1} corresponds to O2H2···O6 intra-chain hydrogen bond and a band around 3524 cm^{-1} is from the free OH group. Although their analysis for the band around 3270 cm^{-1} did

not match as Marechal and Chanzy assigned this band to O2H2···O6 intra-chain hydrogen bond whereas Kokot *et al.* assigned the band to O6H6···O3' inter-chain hydrogen bond. Oh *et al.*[65] studied change in crystal structure of pulp sheet (Cellunier-F®) when treated with different concentrations of NaOH. Their band assignment by employing FTIR spectroscopy was based on studies by Fengel *et al.*[62, 64]. Recently Watanabe *et al.*[70] studied the drying process of cellulose and used the results from the above authors including Sugiyama's FTIR analysis[71] to understand change in hydrogen bonding when cellulose and water molecules interact.

Solid state ^{13}C cross polarization (CP) Magic Angle Spinning (MAS) Nuclear Magnetic Resonance (NMR) is another commonly used technique to study morphology, and crystalline structure of cellulose[31,41,72,73,74,75,76,77,78]. From their solid state ^{13}C NMR experiments, Attala *et al.*[74] reported that native cellulose is a combination of two allomorphs: Iα (triclinic) and Iβ (monoclinic). They followed the previous studies[73] on crystalline structure of cellulose to verify the presence of two distinct crystalline forms and found that the presence of either of the allomorph depends on the source of cellulose viz. Iα is dominant in algal and bacterial cellulose whereas higher plant celluloses are mainly made of Iβ form. Amounts of Iα and Iβ can be estimated by signals from anomeric carbon atom C1[79]. Usually, the ordered and non-ordered regions in cellulose I are studied by separating the peaks from C4 anhydroglucose unit. The contribution from these regions is determined by either integrating the peak area within fixed limits or signal deconvolution method by utilizing standard Lorentzian and Gaussian curve fit functions[41]. Solid state ^{13}C NMR of apple cell walls by Newman *et al.*[72] provided evidence for the presence of highly ordered cellulose chains on the

surface of crystallites. While studying the molecular conformations of cellulose I and cellulose II at cellulose-water interface by ^{13}C NMR, Newman *et al.*[76] assigned the doublets, from C4 and C6 peaks, to the cellulose chains inside of crystallite and the chains on the surface (Figure 2-9 and Figure 2-10). The chains at the surface are lesser constrained and can adopt more conformations. Moreover, the chains at surface follow a two-dimensional molecular order[80]. Newman *et al.*[31] and Larsson *et al.*[81,82] used the signal deconvolution method to study morphological features of cellulose crystallites and estimate their dimensions. They assigned the deconvoluted peaks from C4 signal as paracrystalline cellulose, cellulose at accessible fibril surfaces, and cellulose at inaccessible fibril surfaces, apart from the usual Iα and Iβ regions (Figure 2-12). Later, Nocanda *et al.*[83] and Zukerstatter *et al.*[41] used such explicitly defined regions to calculate the degree of crystallinity in cellulose.

2.1.3 Cellulose (and Derivatives) Based Polymer Blends

Polymer blending is the process of mixing two or more polymers in a reactive or non-reactive manner. Blending is useful to develop materials with improved properties, such as mechanical strength, rigidity, ductility etc. Generally, polymer blending by non-reactive manner involves mixing two immiscible polymers in the molten state. The blend thus prepared contains a continuous and a disperse phase. Polymer blending by the reactive route involves polymerization of one of the blend components into the host-polymer[8]. Making natural polysaccharide-synthetic (petroleum based) polymer blends is a promising approach to create polymeric products like composite polymer films, membranes, shells for encapsulated drugs etc. Natural abundance and unique properties of cellulose such as biodegradability, non-toxicity, and biocompatibility have been well recognized over the years. Its use over synthetic polymers has also been

openly accepted from the point of saving limited petroleum resources and carbon dioxide neutral combustion[84]. Blending cellulose or its derivatives with synthetic polymers is of interest also because this reduces the recycling issues of synthetic polymers to some extent[85]. There are two possible application aspects for incorporating cellulose in synthetic polymers:

- Develop cellulose-synthetic polymer composites with small amounts of cellulose in order to improve disintegration of petroleum based synthetic polymers in nature,
- Develop cellulose-synthetic polymer composites with largest possible amount of cellulose that can exhibit thermo-mechanical properties, which will be similar to conventional plastics but at reduced CO_2 emissions and a lower price.

Addition of cellulose to synthetic polymers can enhance the degradation of synthetic polymer-cellulose blend by accelerating the disintegration and fragmentation of synthetic polymer chains. This can follow the similar mechanism of disintegration as suggested for LDPE-starch composites by M. Flieger *et al.*[49]. According to these authors, over a time-period microorganisms consume the cellulose, thereby creating pores in the blend, which can deteriorate the molecular structure of the surrounding synthetic polymer along and finally break it apart. From a processing point of view, Simon *et al.*[36] distinguished cellulose-based materials into two groups: cellulose derivatives (ex. esters) which can be extruded and injection molded; and regenerated cellulose for film and fiber production. Making industrial products from cellulose is challenging because it is difficult to process in molten state; thermal processing usually leads to decomposition of its extensively hydrogen bonded structure[37, 86,87]. It is necessary to break the hydrogen bonds in order to obtain melt processable cellulose[37]. Common industrial ways to achieve thermoplasticity in cellulose involves blending with synthetic polymers or derivatizing the hydroxyl groups of cellulose followed by blending

with synthetic polymers of suitable chemical structure[85, 88]. Cellulose derivatives like Cellulose Acetate, Cellulose Acetate Propionate, Cellulose Acetate Butyrate etc. improve the compatibility with synthetic polymer; however, biodegradability of cellulose is affected by derivatization as the number of glucose units for sterical enzyme attack is reduced[37]. Synthetic polymers like polyesters, vinyl polymers and polyamides can form compatible blends with cellulose because of the hydrogen bond forming characteristics of these polymers[85,89]. Due to the presence of high polarity hydroxyl groups, cellulose has a tendency to agglomerate and interact less with synthetic polymer than desired. So blending of cellulose with synthetic polymers is mostly carried out by preparing films from solutions of some common solvent[89,90]. However, finding an appropriate solvent capable of dissolving both blend components without decomposition is challenging. Solid phase blending is another way to make cellulose-synthetic polymer blends in which the blend components undergo plastic flow with unlimited strain under supercritical and shear. This process mixes the blend components very effectively at the molecular scale by increasing the dispersion and specific surface area of the reacting component. Such processing techniques may also induce very low activation energy based chemical reactions between blend components. Solid phase mixing is advantageous over solvent-mixing method from an ecological and an economic outlook as well[89]. In this section, solution based blends and the blends based on solid state mixing are both discussed. Rogovina *et al.*[91] processed polysaccharides cellulose-chitosan blends in a Barbender mixer, a twin-screw extruder, and Bridgman anvils. Their infrared spectroscopic studies indicated broadening of the OH stretch - a result of redistribution of hydrogen bonds. This also suggested that mixing occurred at the

molecular level. With continuing interest in development of polysaccharide based polymer blends, Rogovina *et al.*[92] recently investigated polyethylene blends with cellulose, ethyl cellulose, starch, chitin, and chitosan. They prepared the blends by a rotor disperser and a single screw extruder. They found that, for 20 wt% loading of bio-based materials in LDPE, ethyl cellulose affected the ductility of LDPE by the least extent compared to other materials. Moreover, increase of loading by 30 wt% drastically reduced the elongation at break of LDPE for all types of bio-based materials. At this loading, the corresponding parameter for LDPE-Starch blend was 19 folds of LDPE-Cellulose blend. Their test for fungus resistance over 28 days period showed that starch and chitin containing LDPE blends were considerably affected by fungus whereas morphology of others made their blends with LDPE less accessible to microorganisms. Decrease in XRD peak intensities of blends relative to peak intensities for individual components indicated that shear deformations caused amorphization of blend components and this effect was higher when blends were processed under extruder than in the rotor. Blending of bio-based materials with LDPE reduced enthalpy of melting of LDPE. High shear-temperature blending caused partial deterioration of LDPE crystalline structure[92]. Kondo *et al.*[33] prepared blends of specifically substituted methylcelluloses (O-methylcellulose, 2,3-dimethylcellulose and 6-O-methylcellulose) with Polyethylene Oxide and Polyvinyl Alcohol in order to gain insight of blend miscibility due to hydrogen bond formation between blend components. Their FTIR analysis suggested that, for cellulose-Polyethylene Oxide blend, the inter-chain hydrogen bond formation with hydroxyl group at C6 of cellulose was more favorable. Moreover, for cellulose-Polyvinyl Alcohol system, hydrogen bonding was favored for –OH groups on

Polyvinyl Alcohol with C2, C3 hydroxyl groups and the ring oxygen (O5) of cellulose [33,93]. Zhang *et al.*[84] prepared Cellulose-Polyvinyl Alcohol blends using solution method. In their method, cellulose and Polyvinyl Alcohol were first individually dissolved in Alkali-Urea solution (7.5 wt% NaOH; 11 wt% Urea) to get 4 wt% solutions of Cellulose and Polyvinyl Alcohol each. These solutions were then film cast by passing through a coagulation bath and finally washed with running water for 12 hrs. A series of regenerated cellulose-Polyvinyl Alcohol blend films were prepared and studied for miscibility, structure, and properties. FTIR, SEM, and DSC results indicated cellulose content more than 60 wt% showed miscibility of blend components which was caused by strong hydrogen bonding interactions. Improvement in mechanical properties and thermal stability of Polyvinyl Alcohol was reported[84]. Masson *et al.*[86] studied miscibility of cellulose-polyvinyl pyrrolidone and cellulose-poly(4-vinyl pyridine) blends. They prepared the blends in a solution state by mixing various ratios of separately made homogeneous solutions of cellulose-DMSO; and polyvinyl pyrrolidone-DMSO or poly(4-vinyl pyridine)-DMSO. Their blends were found miscible and the FTIR and NMR studies showed that miscibility was driven by the carbonyl groups on polyvinyl pyrrolidone and poly(4-vinyl pyridine), and hydroxyl groups on cellulose which facilitated hydrogen bonding between blend components[94,90]. Nishioka *et al.*[95] studied thermal decomposition behavior of miscible blends of Cellulose-Poly (N-vinyl-2-pyrrolidone), Cellulose-Polyethylene Glycol and Cellulose-Polyvinyl Alcohol. They found that thermal stability of cellulose was not affected by blending with Polyethylene Glycol or Polyvinyl Alcohol. This observation was explained as an effect of intermolecular interactions occurring between the functional groups of those polymers and hydroxyl groups of

cellulose. However, blending with PVP resulted in reduction in degradation temperature. Kosaka *et al.*[88] studied structure-property relationships for composites of cellulose and its esters with LDPE and Maleic Anhydride grafted LDPE (MA-LDPE). The samples were prepared by compounding using a Hakke Polylab mixer and compression molding press. The MA-LDPE/Cellulose and MA-LDPE/Cellulose Acetate Propionate composites showed superior thermo-mechanical performance than others due to presence of highest number of hydroxyl groups to react with –COOH and –C=O groups on MA-LDPE. The performance was poor in absence of Maleic Anhydride. Oldak *et al.*[96] studied the influence of addition of natural cellulose (5-30 wt%) on bio- and photo-degradation of polyethylene. They blended the components using a PlastiCorder (Barbender) extruder. Samples were UV-irradiated (λ=254nm) using a mercury vapor lamp and biodegraded by composting in wet garden soil up to 28 weeks. They studied the blend properties by Attenuated Total Reflection – Infrared spectroscopy and Raman spectroscopy. It was found that the degradation was dependent on the cellulose content and the blend morphology; blends with higher cellulose content were found to be less bio-resistant but were less efficient for photo-oxidation. According to Bajer *et al.*[97], during a photo-oxidative degradation process of LDPE/waste paper composite, cellulose can undergo cleavage of C-H, C-OH, C-CH_2OH and C-O-C bonds. Then, the free radicals formed can react with atmospheric oxygen to give off oxidized products, which can finally lead to chain scission in the cellulose macromolecule. Degradation of polyethylene involves formation of free radicals, random chain scission, and oxidation to form end functional groups. Polyethylene chains become polar and hydrophilic when oxidized. This can increase the susceptibility to bio-degradation. These authors

prepared blends (5-30wt % paper waste) by twin-screw extrusion and then exposed the samples to UV radiation for up to 100 hrs. They analyzed the test samples by ATR-FTIR spectroscopy, thermo-gravimetric test, and microscopic techniques (SEM). Their ATR-FTIR analysis suggested that blends containing 20-30 wt% paper waste showed more carbonyl and vinyl groups after UV exposure than those with lesser paper waste and thus were more susceptible to photo-oxidative degradation. High shear blending and UV exposure lead to decrease in thermal stability and crystallinity of LDPE. SEM images showed surface destructions (micro-cracks, increased surface roughness) caused by UV irradiation[97].

Mechanical properties of a blend can be improved by better dispersion of the minor blend component in base polymer or increasing the physical/chemical interaction between them. Cellulose is a crystalline material, its compatibility with synthetic polymers is often limited by poor interaction with the polymer unless either the base polymer is functionalized or cellulose is pretreated. From a biodegradation point of view, hydrolysis is the first very basic step required to start degradation. Major factors that affect the susceptibility to hydrolysis of lignocelluloses are association of lignin, accessible surface area and crystallinity of cellulose[98].

2.2 Supercritical Fluids

2.2.1 Properties of Supercritical Fluids

Green chemistry aims to reduce (or even eliminate) use of substances which are hazardous to the environment. It involves environment friendly alternate reaction media in place of conventional organic solvents. Producing chemical products without any solvent can be considered as the ideal case, however practically it is not possible for many chemical processes[99]. A feasible and economical solution is to minimize the use

of such organic solvents and recover those at the end of the process. Supercritical fluids are a clean and versatile alternative to the traditional organic solvents. Supercritical fluids have found successful use in polymer industries for structure modification, particle production, microcellular foaming, blending, composites, and synthesis. They have been used as solvents, anti-solvents and plasticizers in polymer processing[8]. Supercritical fluids can be used to either replace the organic solvents or collect and recycle the organic solvents after their use in many chemical processes. Processing with a combination of supercritical fluids and organic solvents is another way to reduce the solvent waste in the environment. When a liquid-gas mixture is heated, thermal expansion of liquid causes reduction in density of the liquid phase. However, at the same time the density of the gas phase increases due to increase in pressure. When a critical point (critical temperature and pressure) is reached, both liquid and gas phase attain identical densities and cannot be further distinctly identified as two phases. At this point the fluid is referred as a supercritical fluid[100]. Zheng *et al.*[101] defined supercritical fluid as "a fluid that is in a gaseous form but compressed at temperatures above its critical point to a liquid like density". Solvent strength of a fluid depends on its density; by changing temperature and pressure solvent strength of a supercritical fluid can be varied from 'gas-like' to 'liquid-like' and vice versa. Liquid and gaseous states cannot be distinguished in this phase but the physical-chemical properties of this new phase are reminiscent of both states[102]. Supercritical carbon dioxide has high diffusivity, high mass transfer rates, low viscosity, low surface tension and high solvency[102-103]. Transport properties of liquids, gases, and supercritical fluids are compared in Table 2-1. Their ability to tune the density, high diffusion coefficients and low interfacial tension all

together make supercritical fluids an excellent solvent for synthesis and processing of micro to nano-scale substances[104].

Among supercritical fluids, supercritical carbon dioxide meets very well the criteria of ecological and economical constraints. Supercritical carbon dioxide is non-toxic, non-flammable, inexpensive, readily available and has low critical temperature and pressure than other supercritical fluids [101,105,106]. Carbon dioxide doesn't create any chemical waste and is also a green house component[26]. A schematic phase diagram of carbon dioxide is shown in Figure 2-6. Melting, sublimation, and evaporation curves separate the solid, liquid, and gaseous state respectively. The evaporation curve ends at the critical temperature (Tc = 31.1 °C) and critical pressure (Pc = 7.3 MPa) beyond which the supercritical fluid state is formed. The dissolving strength of supercritical CO_2 depends on its density which can be easily adjusted by changing temperature and pressure[107].

2.2.2 Supercritical CO_2 and Co-Solvents

From an industrial and scientific point of view, supercritical carbon dioxide is one of the most attractive media for polymer modification but its solubility is limited for high molecular weight and polar compounds. Primarily there could be two aspects of using co-solvents with supercritical CO_2 – One is to improve solvent strength of supercritical CO_2 to dissolve otherwise non-soluble compounds and the second aspect is to recover solute particles from an aprotic polar solvent by using supercritical CO_2 as an anti-solvent. Supercritical CO_2 is a non-polar solvent with a low solubility parameter, low permittivity, and low polarizability. However, a large quadrupole moment, and electron donor and acceptor sites are available on the CO_2 molecule. When a non-polar solute molecule is introduced in supercritical CO_2, solute-solvent interaction is limited to van

der waals dispersion forces. When a polar solute with zero electric charge is introduced solute-solvent interactions extend to dipole-quadropole[108]. However, these interactions are not strong enough to dissolve polar and high molecular weight molecules in supercritical CO_2. Solubility of such compounds in supercritical carbon dioxide can be improved by adding small amounts of polar co-solvent. Addition of polar co-solvent causes specific intermolecular interactions between polar solute and co-solvent molecules (ex. Hydrogen bonding, charge transfer complex formation) that lead to an increase in the molar density of solvent mixtures and so the solvent strength is increased[109]. Supercritical CO_2 can also be used as an anti-solvent for particle formation and selective extraction of a substance from a multi-component mixture. Supercritical Anti-solvent Precipitation technique involves two simultaneous mechanisms, the supercritical fluid penetrates into the homogeneous solution (solute-solvent mixture) where it works as an anti-solvent for the solute substance and at the same time the organic solvent evaporates on the supercritical fluid which causes precipitation of the solute particles[110]. Miscibility of a supercritical fluid and an organic solvent being an important parameter for such technique, is generally assessed by measuring volumetric expansion of the co-solvent[17]. In this research, preliminary experiments showed insolubility of microcrystalline cellulose in both supercritical carbon dioxide and supercritical carbon dioxide – DMSO system. Thus, the background studies in this section are focused on miscibility of supercritical carbon dioxide - DMSO systems and not on solubility of solute in such systems.

Gonzalez *et al.*[18] collected high-pressure vapor-liquid equilibrium data for CO_2 and DMSO at four different temperatures, ranging from 309 K (36 °C) to 329 K (56 °C), and

pressures up to about 13 MPa (1885 psi). They found that, for 2.5% (mol/mol) DMSO in CO_2, the three phases coexist above 315.6 K (43 °C) and 8.8 MPa (1276 psi). Rajasingam *et al.*[17] collected volumetric expansion data for DMSO with CO_2 at 298 (25 °C), 308 (35 °C), and 318 (45 °C) K. They demonstrated that at a given pressure, increase in temperature caused reduction of CO_2 density and so reduction in miscibility of CO_2 in the liquid phase. Thus, the volume expansion decreased with increase in temperature. They showed that for pressure values less than 5 MPa (725 psi), the solubility of the CO_2 in DMSO was almost linearly dependent on pressure. On moving towards critical point, solubility of CO_2 increased but became much more sensitive to pressure near critical point. They concluded that up to 60 mol % solubility of CO_2 in DMSO was achieved under 10 MPa (1450 psi) over the three temperature values considered.

2.3 Polymer Processing with Supercritical CO_2 (and Co-Solvents)

Supercritical fluids have unique physical-chemical properties that can be used for modification and plasticization of various polymers. Many polymers swell and plasticize in presence of CO_2, which facilitates low temperature processing. CO_2 is soluble in many low molecular weight, amorphous fluoropolymers and silicones. When dissolved, it increases the free volume of molten polymer, which causes reduction in melt viscosity[8,111,112] . Physical properties of polymers like density and diffusivity are also changed[8]. Cooper[113], Tomasko[114] and Nalawade *et al.*[8], and Kazarian *et al.*[111,112] have reviewed developments in the field of application of supercritical CO_2 in polymer synthesis and processing in past two decades. Its solubility in polymers depends on processing temperature, pressure, and interactions with the polymer chains. Kung *et al.* prepared High Density Polyethylene (HDPE) – Polystyrene (PS) composites by

adsorbing supercritical solution of carbon dioxide, styrene and, a thermal radical initiator on HDPE substrate; subsequent polymerization of styrene within the amorphous domain of HDPE lead to formation of a polymer composite. They found that the thus formed polystyrene scaffolds reinforced the polyethylene spherulites which resulted in increased strength and reduced fracture toughness of HDPE[115]. Supercritical fluids can help in polymer extrusion by acting as a molecular lubricant and increase the polymer chain mobility[116]. This can result in increased processability and improved morphology of the end product[103]. In polymer blends, CO_2 can help in reducing viscosity of one of the blend components more than other and ability to vary the viscosity ratio can help to control the blend morphology[117]. Elkovitch *et al.*[118] prepared blends of PMMA-PS with and without supercritical CO_2. They used a high-pressure batch mixer to study solubility of CO_2 in blend components at 20°C and 200°C. It was found that larger amount of CO_2 is soluble at lower temperature. They also used a single screw and a twin-screw extruder to prepare blends and determined effect of supercritical CO_2 assisted processing on melt viscosity and blend morphology. They noted that supercritical CO_2 lowered the viscosity ratio and increased the interfacial tension between the blend components that resulted in reduced size and more even distribution of dispersed phase. Between the two extruders, starve fed twin-screw extruder was advantageous because larger amount of CO_2 was injected in to the extruder barrel to interact with polymer melt. They suggested that intensive mixing in twin-screw extruder continuously exposed the polymer melt to CO_2, which resulted in higher penetration of CO_2. Polymer blends with Ultra High Molecular Weight Polyethylene (UHMWPE) as one of the blend components are very difficult to process because of high melt viscosity of this polymer.

Zhang *et al.*[119] used a batch reactor to synthesize a blend of Poly Methylmethacrylate (PMMA) and UHMWPE in presence of supercritical CO_2. Although supercritical CO_2 did not dissolve the UHMWPE but it penetrated effectively in to UHMWPE and thus found an effective medium for processing.

Lee *et al.*[120] studied morphological and rheological properties of Polyethylene-Polystyrene (PE-PS) blend processed with supercritical CO_2 in a twin-screw extruder. The cell structures of blend components were found similar to pure PE and PS but higher CO_2 content and processing pressures resulted in smaller cell sizes. They found that the viscosity of the blend PE-PS processed with supercritical CO_2 decreased with an increase in the CO_2 content. Sorption of CO_2 in the glassy polymers, generally called plasticization, helps to increase chain mobility and reduce the glass transition temperature[112,121]. Rheological studies on various polymers processed with CO_2 have been done at various shear rates using extruders. Gendron *et al.*[122] studied flow characteristics of PS with CO_2 and found that plasticization caused by CO_2 was equivalent to reduction in glass transition temperature of PS. Similar research by Lee showed that viscosity of PS reduced with increase in CO_2 content but increased with CO_2 pressure[121]. Lan *et al.*[121] studied flow properties of Polypropylene (PP) with CO_2 in a modified injection molding machine at 1/100 (1/s) to very high shear rates of 1/10000 (1/s). They showed that due to plasticized effect of CO_2, viscosity of PP is significantly reduced within low shear rates range but it reduction slows down with increase in shear rate. Li *et al.*[117] worked to gain insight of correlation between interfacial surface tension and viscosity of PP-PS blend. They showed that increase in CO_2 pressure reduced both surface tension and viscosity of the PS-CO_2 and PP-PS blends. Applications of CO_2 in

polymer processing has been reviewed by Tomasko *et al.*[114]. Muljana *et al.*[123] gelatinized starch by treating with supercritical CO_2 in a high-pressure reactor. They observed that degree of gelatinization was increased with increasing temperature and pressure. They achieved a maximum 14% degree of gelatinization at 90° and 25 MPa. They also treated starch with nitrogen at similar conditions and found that degree of gelatinization was not only an effect of high static pressure but CO_2 also played an active role in structural changes. Kim *et al.*[11] treated lignocelluloses with supercritical CO_2 with and without moisture at 165°C and variable pressure of 3100 psi and 4000 psi, in time range of 10-60 minutes. Their subsequent enzymatic hydrolysis showed a significant increase in sugar yield when samples were treated with moisture. Moreover, the sugar yield for lignocelluloses reached to their theoretical maximum when treated with CO_2 at 3100 psi for 30 minutes and 73% (w/w) moisture. Yin *et al.*[66] used supercritical CO_2-ethanol mixture to process cotton cellulose into cellulose carbamate in a high-pressure batch reactor. They utilized supercritical CO_2 to impregnate urea in cotton cellulose, following release of CO_2 and subsequent increase in the reactor temperature resulted in formation of cellulose carbamate by esterification. The amount of urea impregnated was based on the supercritical CO_2 pressure, esterification temperature, and time. They found that urea impregnation at 18 MPa / 50°C for 6 hours and esterification temperature of 140°C for 4 hours yielded highest nitrogen content (8.6%) in cotton cellulose. Catchpole *et al.*[15] studied solubility of urea in supercritical CO_2 and supercritical CO_2-ethanol mixture. They reported that a very small mole fractions of urea (about 3 x 10-5) was soluble in supercritical CO_2 at 353 K (80 °C) and 300 bar (4350 psi). Kiran *et al.*[124] studied solubility of various cellulose derivatives in

supercritical CO_2-acetone and supercritical CO_2-ethanol mixtures each at composition levels of 30-70 and 70-30 (by CO_2 mass). They found that the cellulose derivatives were easily miscible at lower CO_2 levels (30-70) and solutes were easier to dissolve in CO_2-ethanol mixture. Recently Haimer *et al.*[125] precipitated spherical xylan and mannan particles from hemicellulose-DMSO solutions by using CO_2 as an anti-solvent. Cid *et al.*[13] developed a method to improve dyeability of cotton cellulose by treatment with supercritical CO_2 and co-solvents. Cotton cellulose was presoaked in various protic and aprotic co-solvents before incorporating dye molecules in presence of supercritical CO_2. They found that processing with DMSO solvent gave best coloration compared to acetone, ethanol, or methanol. This occurred because of large solvent-solvent polar interactions, hydrogen bond forming ability with cellulose and dye-carrier property of DMSO. Tsai *et al.*[126] showed isothermal solubility of a dye molecule – disperse yellow 54 (structural formula $C_{18}H_{11}NO_3$) in supercritical CO_2 increased with increasing CO_2 pressure. They also showed that addition of a co-solvent ethanol or DMSO significantly improves the dye solubility. However, DMSO was found more effective co-solvent than ethanol. They described the higher solubility with DMSO over ethanol by comparing Kamlet-Taft parameters for both the co-solvents. The Kamlet-Taft solvatochromic parameters are generally used to describe proton acceptor or donor ability of a solvent and individual contribution of polarity to the total solvent effect. Larger dipole moment, higher interaction forces between DMSO-dye molecule and ability of DMSO to act as a hydrogen bond acceptor (ethanol can act both as a proton donor and hydrogen bond acceptor) with the dye molecule, favored to explain better solubility of dye molecule with supercritical CO_2-DMSO system[126].

Table 2-1. Comparison of properties of gas, liquid and supercritical fluids (Adapted from Wypch *et al.*[103])

	Condition	Density g/cm^3	Diffusivity cm^2/s	Viscosity g/cm-s
Gas	1 atm, 25 °C	0.6-2x10^{-3}	1-4x10^{-1}	1-3x10^{-4}
Liquid	1 atm, 25 °C	0.6-1.6	0.2-2x10^{-5}	0.2-3x10^{-2}
Supercritical Fluid	T_c, P_c	0.2-0.5	0.5-4x10^{-3}	1-3x10^{-4}
Supercritical Fluid	T_c, $4P_c$	0.4-0.9	0.1-1x10^{-3}	3-9x10^{-4}

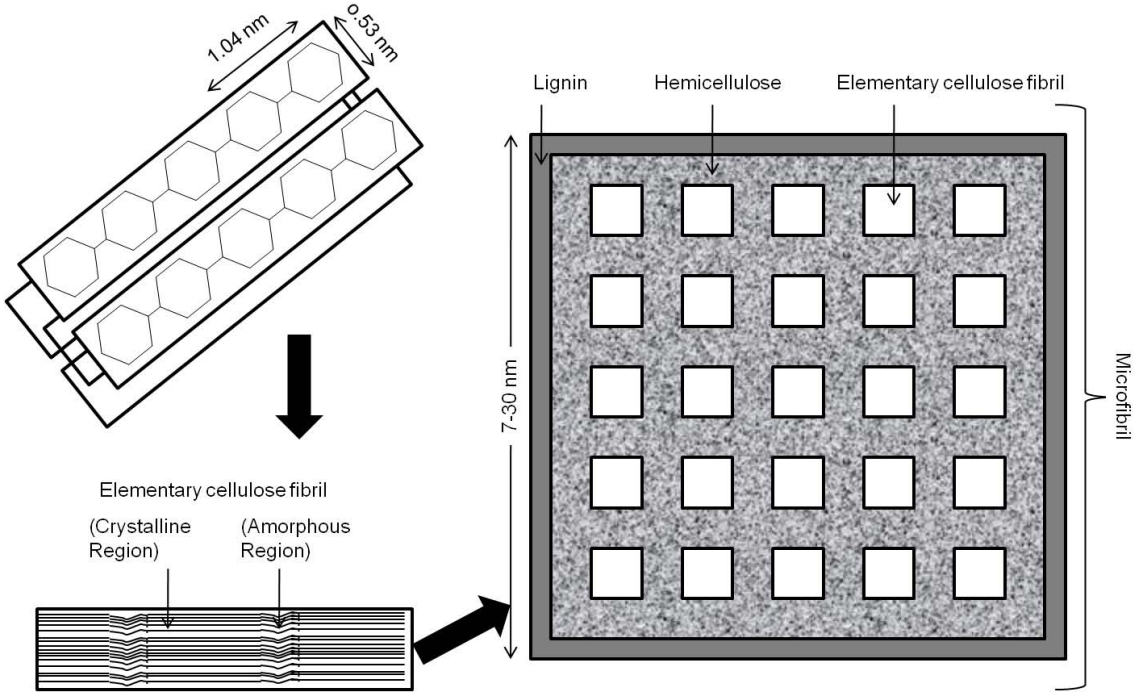

Figure 2-1. Organization of cellulose chains inside a crystal (top-left); stacking of crystals to form an elementary fibril (bottom-left); microfibrills (group of elementary fibrils) in a plant cell wall (right) (Adapted from Zhang *et al.*[29])

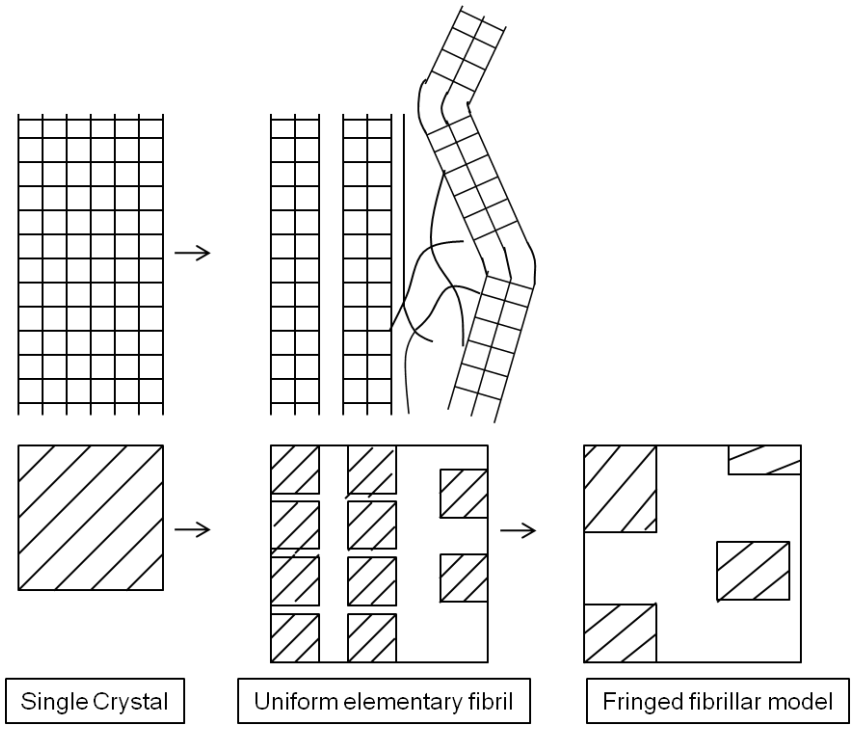

Figure 2-2. Traditional model of molecular structure of cellulose microfibrils (Adapted from Klemm *et al.*[20])

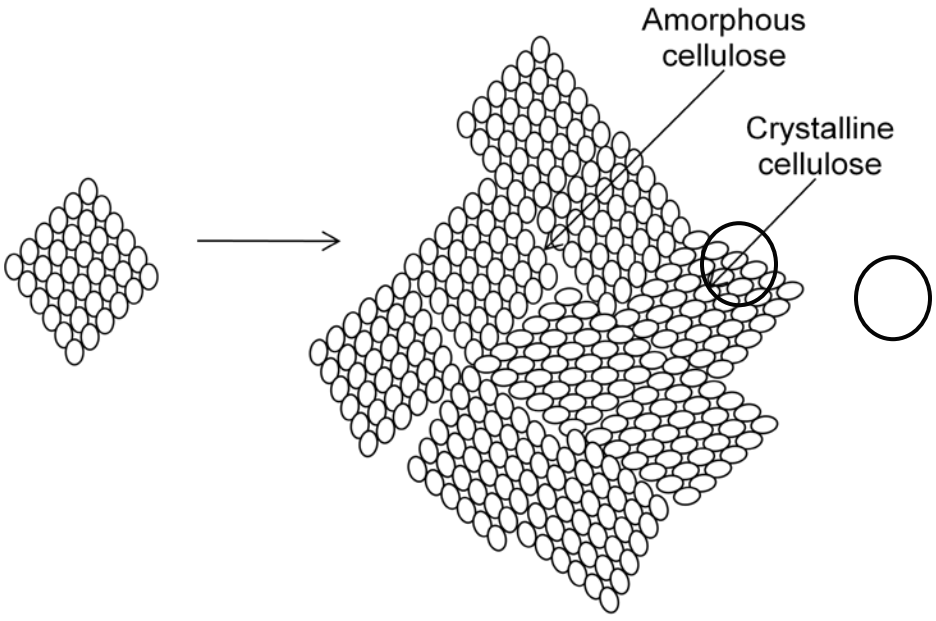

Figure 2-3. Model of arrangement of cellulose crystallites (each ellipse indicate a cellulose chain with its axis normal to the paper (Adapted from Garvey *et al.*[30])

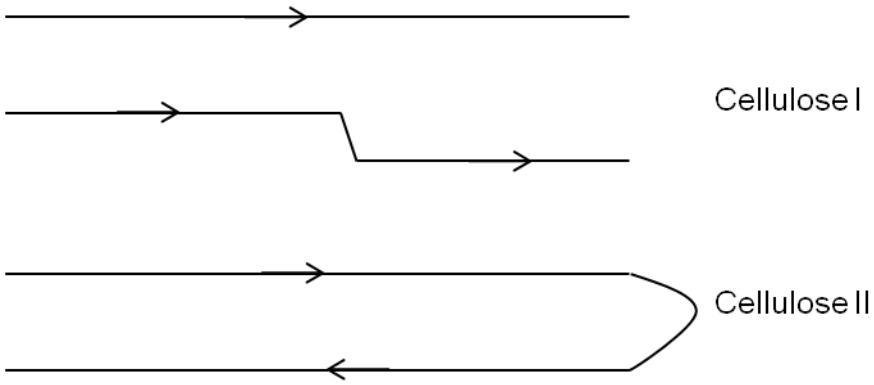

Figure 2-4. Parallel and anti-parallel chain arrangements in cellulose I and cellulose II (Adapted from O'Sullivan *et al.*[127])

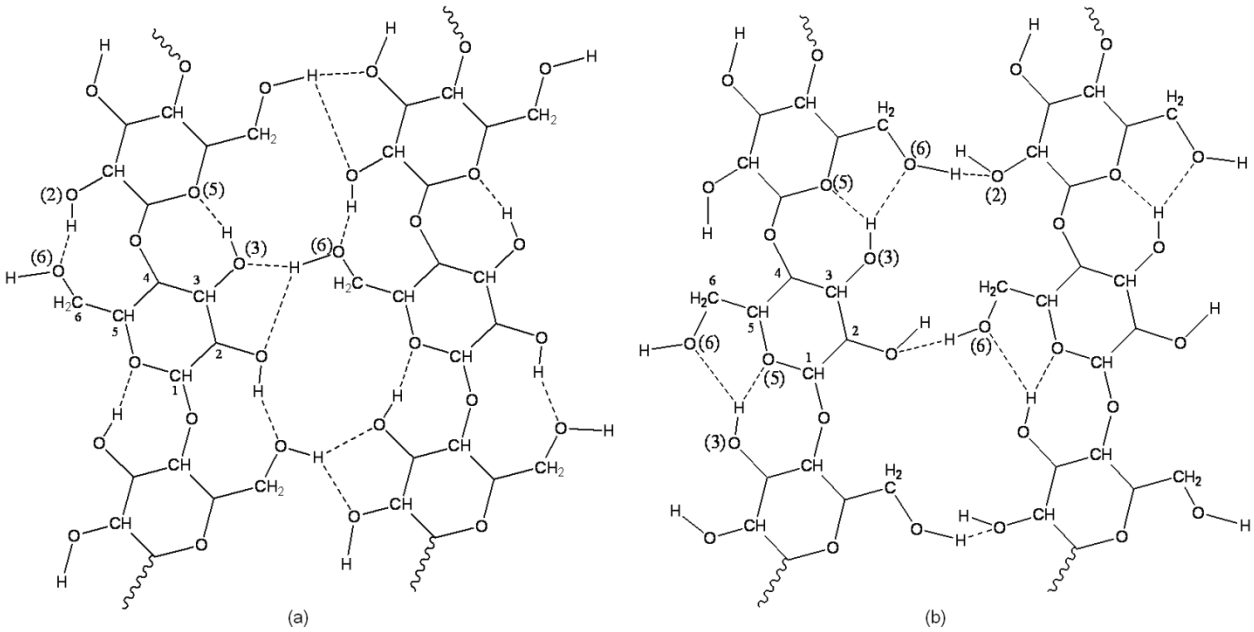

Figure 2-5. Hydrogen bonding patterns in cellulose I (a) and cellulose II (b) (Adapted from Kovalenko[19])

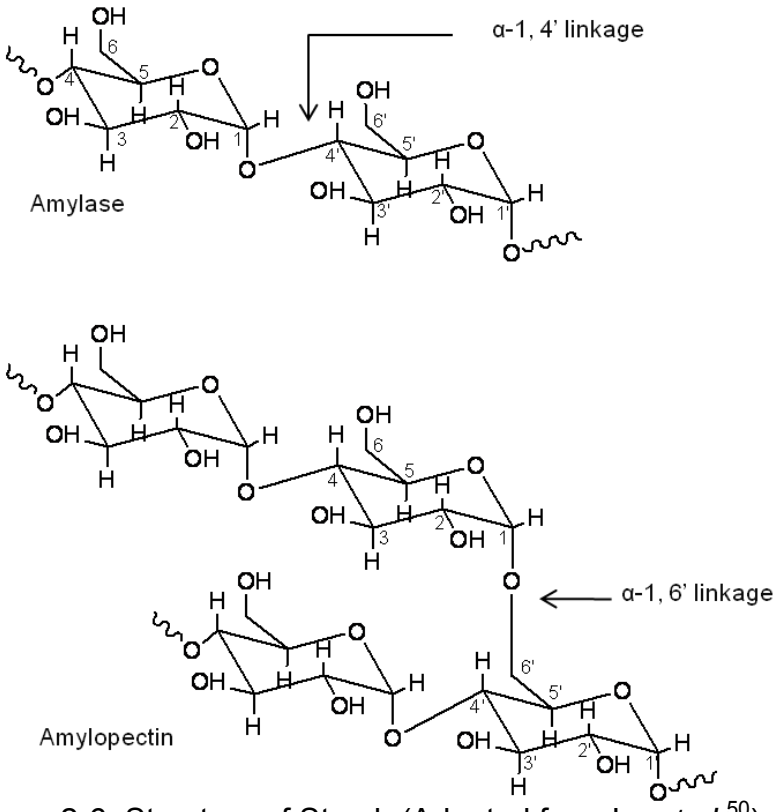

Figure 2-6. Structure of Starch (Adapted from Lu *et al.*[50])

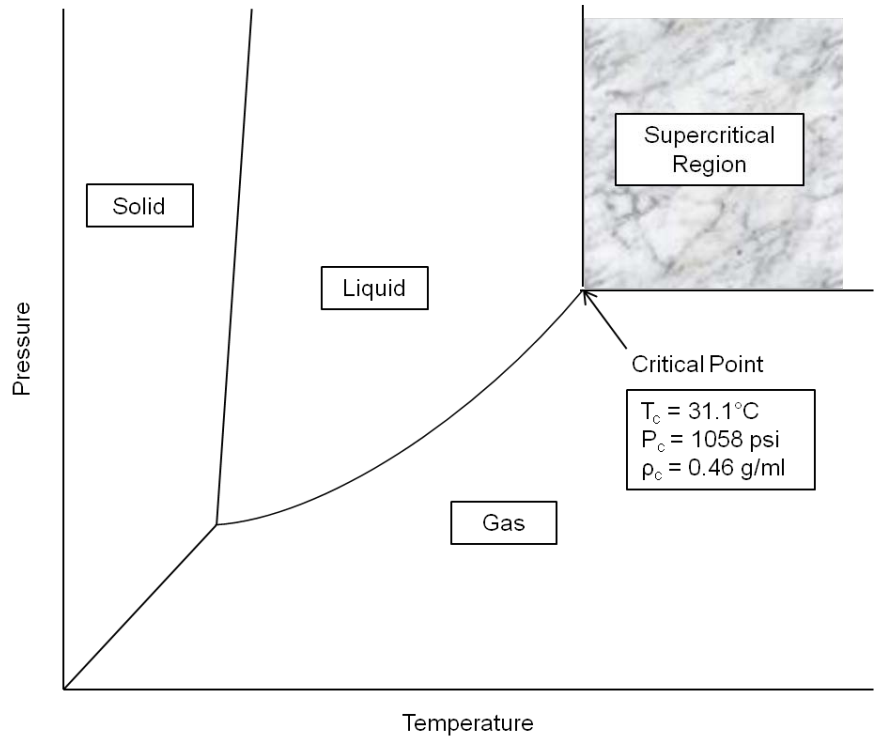

Figure 2-7. Phase Diagram of carbon dioxide (Adapted from Leitner *et al.*[102])

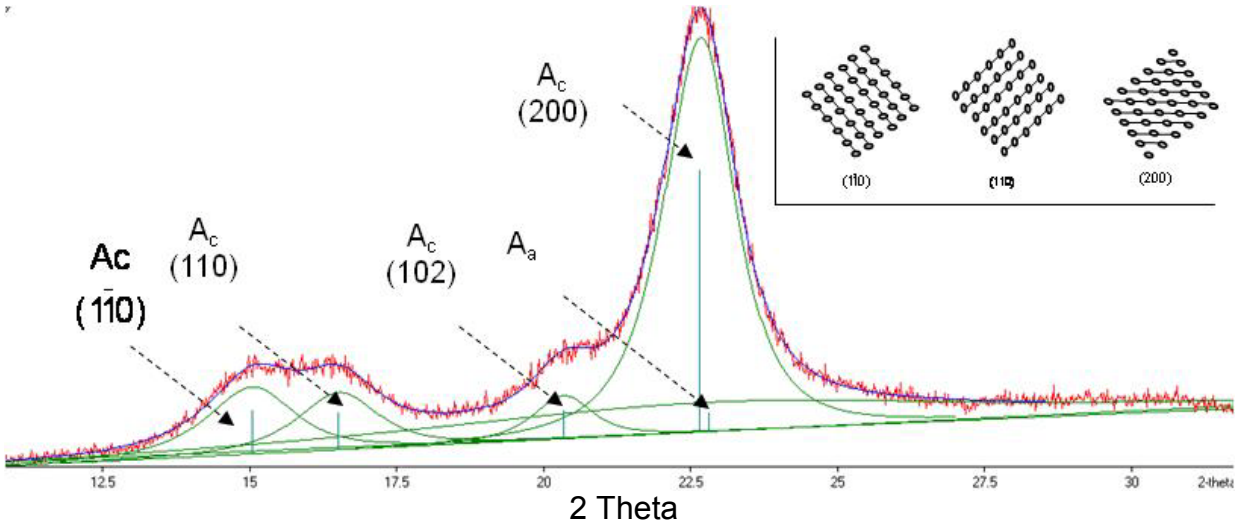

Figure 2-8. X-Ray Diffraction pattern of cellulose. [Inset: cross-sections through a cellulose crystallite containing 36 cellulose chains, circles denote a chain with its axis normal to plane of the paper and the lines represent crystallographic planes of a monoclinic unit cell (Adapted from Newman *et al.*[31])]

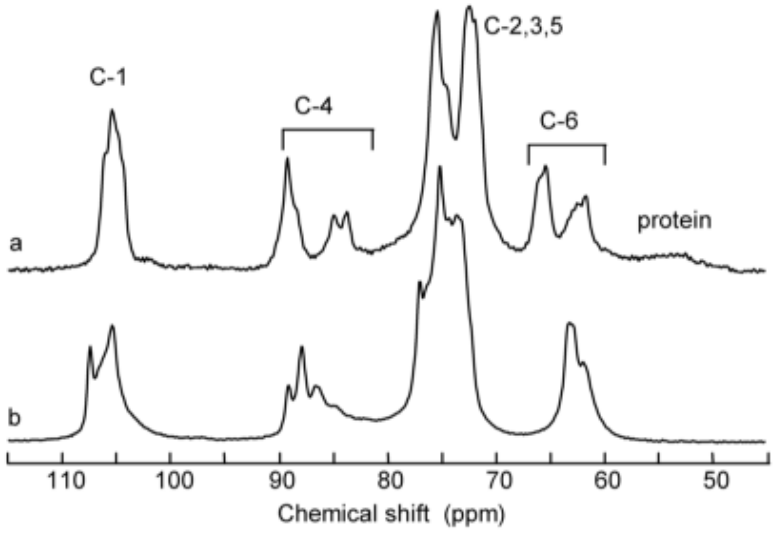

Figure 2-9. ^{13}C NMR spectra of Cellulose I (a) and Cellulose II (b) (Reprinted after permission from Newman *et al.*[76])

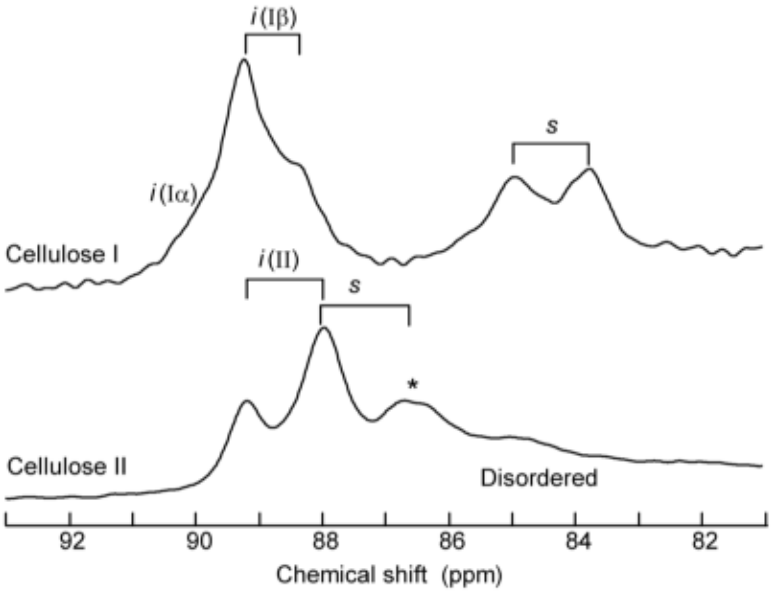

Figure 2-10. Portions of ^{13}C NMR of cellulose, showing signals assigned to C4 in the interiors (i) and on the surface (s) of crystallites (Reprinted after permission from Newman *et al.*[76])

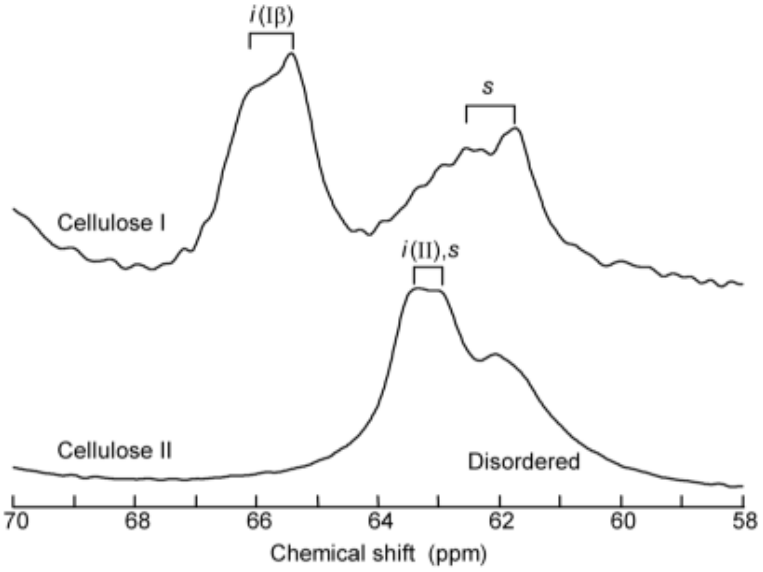

Figure 2-11. Portions of ^{13}C NMR of cellulose, showing signals assigned to C6 in the interiors (i) and on the surface (s) of crystallites (Reprinted after permission from Newman *et al.*[76])

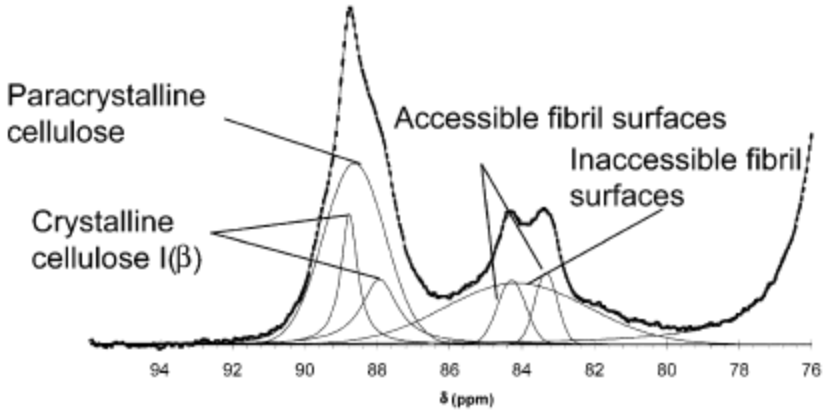

Figure 2-12. Lorentzian and Gaussian spectral fitting of C4 peak (Reprinted after permission from Hult *et al.*[128])

CHAPTER 3
POLYMER BLENDING

Generally, polymer blending of high molecular weight polymers is hindered by high viscosity of the polymer. Twin-screw extruders are the most commonly used equipments to overcome this problem. Twin-screw extrusion processing uses high shear and high temperature to mix polymers in the molten state. The viscosity can be controlled by varying the temperature. However, the polymers subjected to very high temperatures in extruder may degrade, so reduced viscosity at lower processing temperatures is often desired. Supercritical CO_2 has been found to be a successful processing aid to reduce viscosity of the polymer melt at low temperatures. Moreover, supercritical CO_2 has also been utilized for improving the dispersion of one blend component in the other[8,116]. In this section, polymer blending of immiscible polymers LDPE-Cellulose and LDPE-Starch using a twin-screw extruder is discussed. The effect of CO_2 as a processing aid in LDPE-Cellulose blend is also evaluated in terms of final blend properties. Injection molding is a commonly used process to form polymeric products of various shapes. This process involves melting of polymer granules or extrudates and applying supercritical in order to form the desired shape. This section also includes discussion on injection molding, as followed by twin-screw extrusion of the LDPE-Cellulose and LDPE-Starch blends, which was used to form rectangular test specimens.

3.1 Polymer Processing – Twin-screw Extrusion and Injection Molding

In this work, 70/30 blends of LDPE-Cellulose (MC30PE70) and LDPE-Starch (ST30PE70) were prepared by using a twin-screw extruder manufactured by Thermo Prism (L/D 40:1, and screw diameter 24 mm) and provided by SCF Processing Ltd.,

Ireland. In order to determine the effect of supercritical CO_2 on LDPE-Cellulose blend properties, another LDPE-Cellulose (70/30) blend (MC30PE70CO2) was processed under continuous flow of high-pressure CO_2. The CO_2 was injected in the supercritical state between the feed zone and the melting zone of the extruder. However, even though CO_2 was injected in the supercritical state, the basic two-dimensional design of extruder may not contain the CO_2 in the same state throughout the length of the extruder. The interaction of supercritical CO_2 with the matter near feed zone was however sustained by continuously injecting the CO_2 in supercritical state. The blends formulation and amount of material extruded in one minute are listed in Table A-1 of Appendix A. Processing with supercritical CO_2 resulted in higher material yield from the extruder die. Extruded materials were injection molded to form test specimens (rectangular bars of size 100 mm x 11.7 mm x 4 mm) by using a 35 Tonne DeMag Injection Molding machine. The extruded materials were pelletized prior to the injection molding. The extrusion and injection molding parameters used in these experiments are listed in Table A-2, A-3, and A-4 in Appendix A.

3.2 Tests and Analysis

The injection molded test specimens were tested for thermo-mechanical properties and characterized for blend morphology. For tensile properties, the injection molded test bars were cut into dumbbell shaped tensile test specimens using the ASTM cutting die (Type L) according to ASTM D1822-68. The samples were tested in accordance with ASTM D638M at a strain speed of 2 inch/min by using an Instron Universal Testing Instrument (Model 1122). The machine was equipped with TestWorks 3.07 software for analysis. A laser extensometer was used to record Strain at break. Morphological features were analyzed by Scanning Electron Microscopy (SEM) using the instrument

Model JSM-6400 SEM. Samples were sputter coated with a gold-palledium alloy prior to imaging. The thermal analysis of LDPE-Cellulose blends processed with and without supercritical CO_2 was done by Differential Scanning Calorimetric (DSC) method. Samples were heated under nitrogen from room temperature to 425 °C at a heating ramp of 10 °C/ min and air cooled at 50 °C/ min up to room temperature. The Wide Angle X-Ray Diffraction (WAXRD) method was used to analyze changes in cellulose crystallinity and microstructure occurred due to the high shear processing.

The effect of supercritical CO_2 as a processing aid was studied in terms of its effect on mechanical and thermal properties of the LDPE-Cellulose blends. The potential to replace starch with cellulose in LDPE-Starch blend was also studied by comparing the blend properties. The tensile stress-strain curve of the blends is shown in Figure 3-1 and the tensile properties are compared in Figure 3-2 and 3-3. The tensile strength, peak load and peak stress of the cellulose-based blends were greater than the starch-based blend. One the other hand, LDPE-Cellulose blend (MC30PE70) showed significantly lower strain at break than LDPE-Starch (ST30PE70) blend. Higher tensile strength in cellulose based LDPE blends must be due to greater reinforcing nature of cellulose than starch. Starch is formed of a combination of amylose and amylopectin polymers; amylopectin is a branched polymer which prevents high molecular weight linear polymer chains of amylose to interact at molecular level[51]. In contrast, linear arrangements of anhydroglucose linkages in cellulose interact closely via extensive inter-chain and intra-chain hydrogen bonding between hydroxyl groups. This results in a very compact and high strength supermolecular structure of cellulose[28]. As an effect of processing in presence of supercritical CO_2, the strain at break property of LDPE-

Cellulose blend (MC30PE70CO2) was increased fourfold to that of LDPE-Cellulose blend (MC30PE70) (Figure 3-4) whereas other tensile properties remained similar. The plastic strain for LDPE-Cellulose blend processed with CO_2 also increased over LDPE-Starch blend, which was otherwise about three fold shorter for MC30PE70 blend. This shows that processing under supercritical CO_2 significantly improved tensile strength-ductility balance of cellulose-based blends.

From SEM images (Figure 3-5 to Figure 3-10), it was found that cellulose and starch form a heterogeneous blend with LDPE, which is obvious due to absence of any reactive sites on LDPE. MC30PE70CO2 showed intensive flow marks, which are due to the large plastic strain experienced by blend components. However, from SEM images at higher magnification (Figure 3-8 to Figure 3-10), it can be seen that the flow marks in MC30PE70CO2 were limited to the LDPE domain and the LDPE-Cellulose interface or cellulose itself did not show any change in morphology when compared with MC30PE70.

The Wide Angle X-Ray Diffraction (WAXRD) was conducted to study the effect of shear and supercritical CO_2 on crystalline structure of blend components. The blends show combined peaks from LDPE and cellulose (Figure 3-11). The unit cell of polyethylene is orthorhombic, the spectra shows characteristic peaks at 2 theta values of 21.4 (110) and 36.2 (200)[129,130]. Cellulose shows characteristic peaks at 2 theta values of 14.7 (101), 16.5 (10), 22.8 (200), 34.5 (004) and a broad hump at 20.5 (102)[56,57,59]. The peak positions of LDPE or cellulose did not change in the blends, but the peak from the (102) plane of cellulose disappeared and peaks from the (110) and (200) planes of LDPE reduced in intensity. The changes were similar for MC30PE70

and MC30PE70CO2 both. Significant reduction in intensity of the (110) peak of LDPE was due to breaking down of LDPE crystals because of high shear. This effect was more pronounced in the LDPE-starch blend.

Thermal analysis of blends by DSC is shown in Figure 3-12. Effect of processing under supercritical CO_2 on thermal properties of the LDPE-Cellulose blend was determined. The melting temperature and the change in enthalpy of melting of the components of LDPE-Cellulose blend, that was processed with CO_2, were found slightly lower than that of LDPE and cellulose in MC30PE70 (Table 3-1). This shows that supercritical CO_2 caused plasticization of both LDPE and cellulose.

From above discussed results, following can be concluded:

- LDPE-Cellulose blend processed with supercritical CO_2 can successfully replace LDPE-Starch blends
- High shear mixing lead to breaking of LDPE crystallites and amorphization of LDPE
- Supercritical CO_2 acted as a processing aid by inducing large plastic strain to LDPE domain which resulted in increase in tensile strain at break of MC30PE70CO2 compared to that of MC30PE70

Table 3-1. Thermal characteristics of blend components

Sample¥	Melting temperature (°C)		Change in enthalpy of melting (mW)	
	LDPE	Cellulose	LDPE	Cellulose
MC30PE70	105.7	349.8	53.8	55.79
MC30PE70CO2	104.6	348.2	46.5	39.33

¥The denotation used for blend composition:
MC – Microcrystalline Cellulose; PE – Low Density Polyethylene; 30 – 30 wt%; 70 – 70 wt%;
CO2 – Carbon dioxide assisted

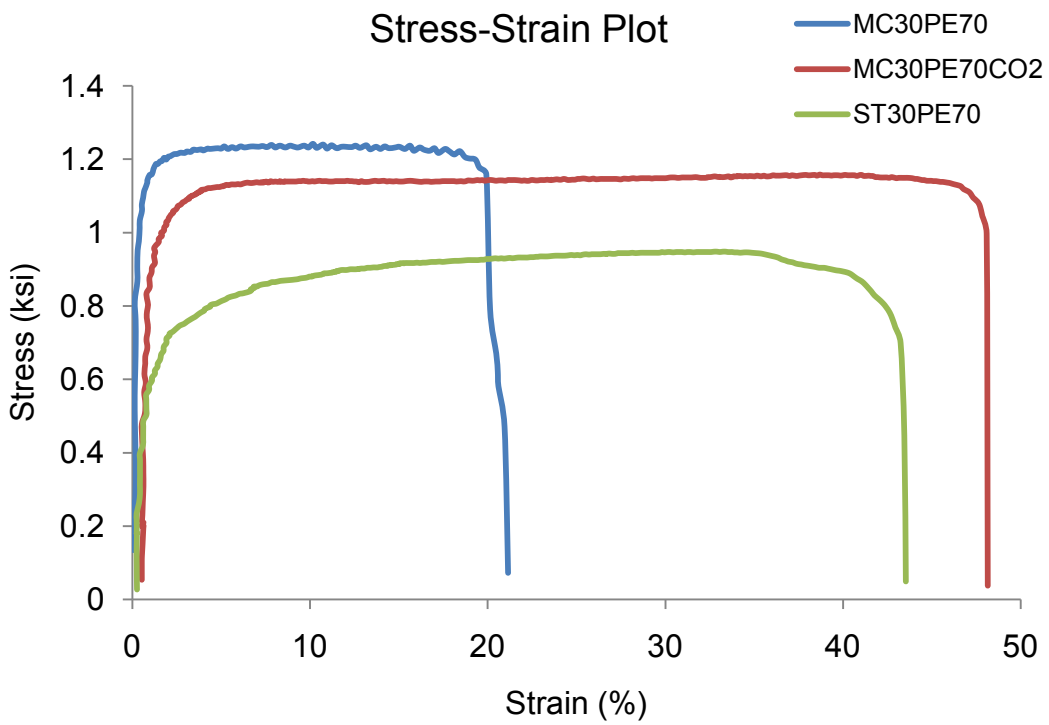

Figure 3-1. Tensile Stress-Strain Plot of LDPE-Cellulose (MC30PE70), LDPE-Cellulose processed with CO_2 (MC30PE70CO2) and LDPE-Starch (ST30PE70) blends

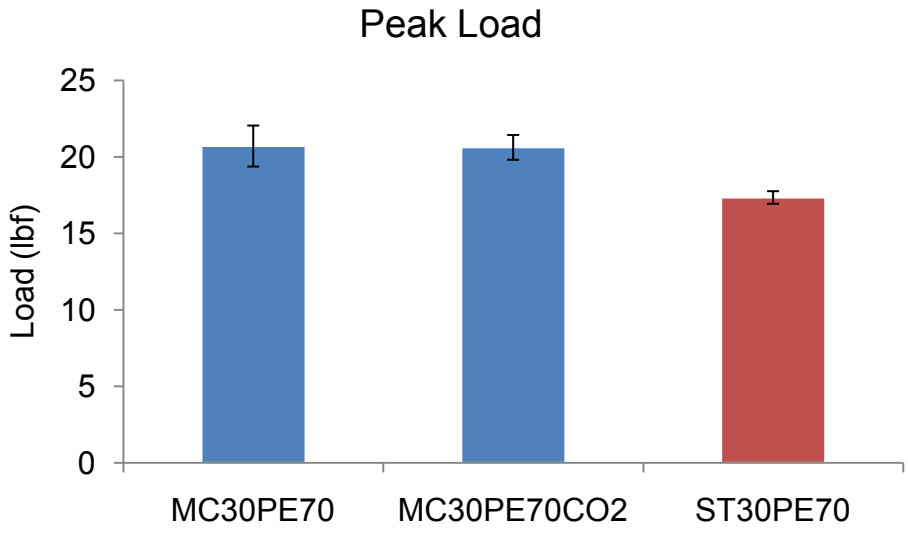

Figure 3-2. Peak Load of blends of LDPE-Cellulose (MC30PE70), LDPE-Cellulose processed with CO_2 (MC30PE70CO2) and LDPE-Starch (ST30PE70)

¥The denotation used for blend composition:
MC – Microcrystalline Cellulose; ST – Starch; PE – Low Density Polyethylene; 30 – 30 wt%; 70 – 70 wt%; CO2 – Carbon dioxide assisted

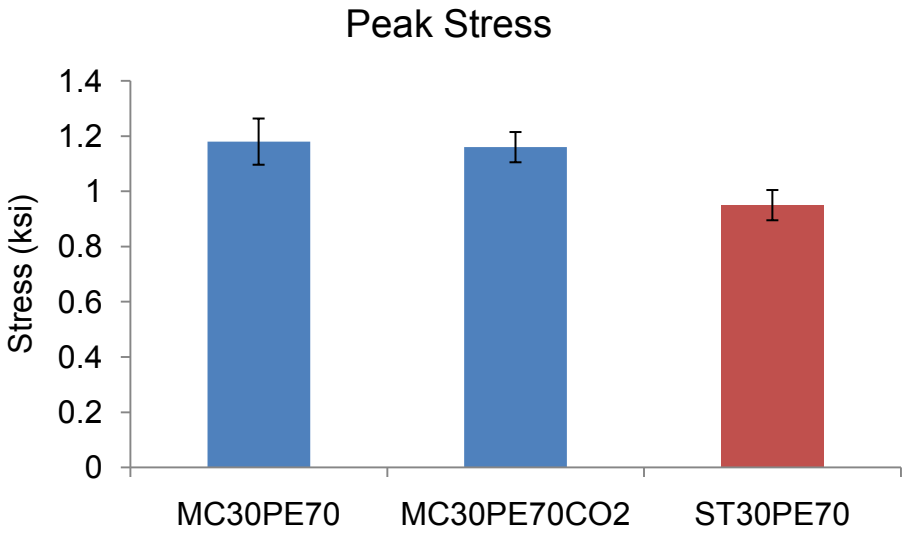

Figure 3-3. Peak Stress of blends of LDPE-Cellulose (MC30PE70), LDPE-Cellulose processed with CO_2 (MC30PE70CO2) and LDPE-Starch (ST30PE70)

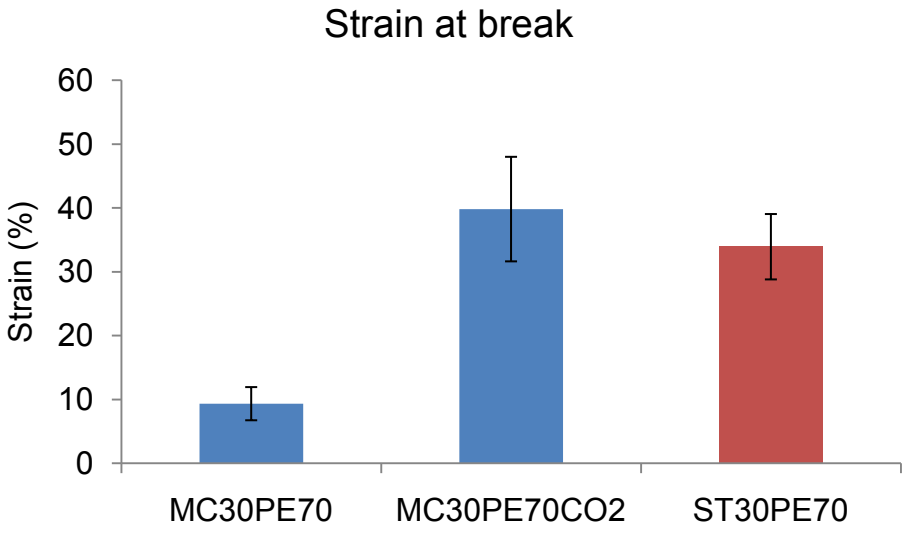

Figure 3-4. Strain at Break of blends of LDPE-Cellulose (MC30PE70), LDPE-Cellulose processed with CO_2 (MC30PE70CO2) and LDPE-Starch (ST30PE70)

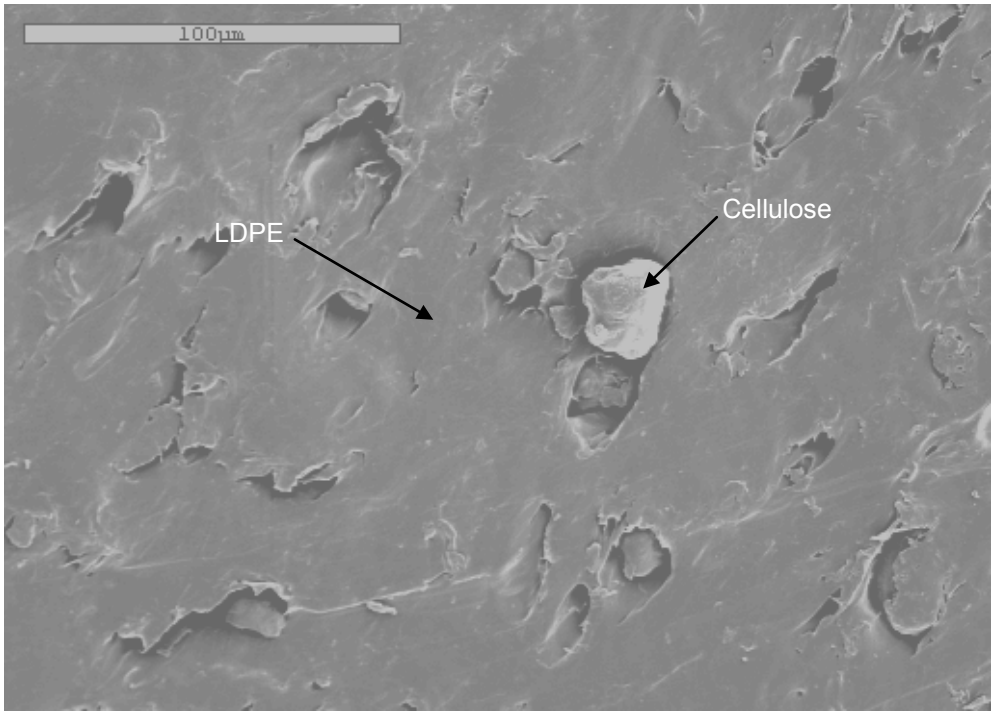

Figure 3-5. SEM image of LDPE-Cellulose blend (MC30PE70), magnification 500X

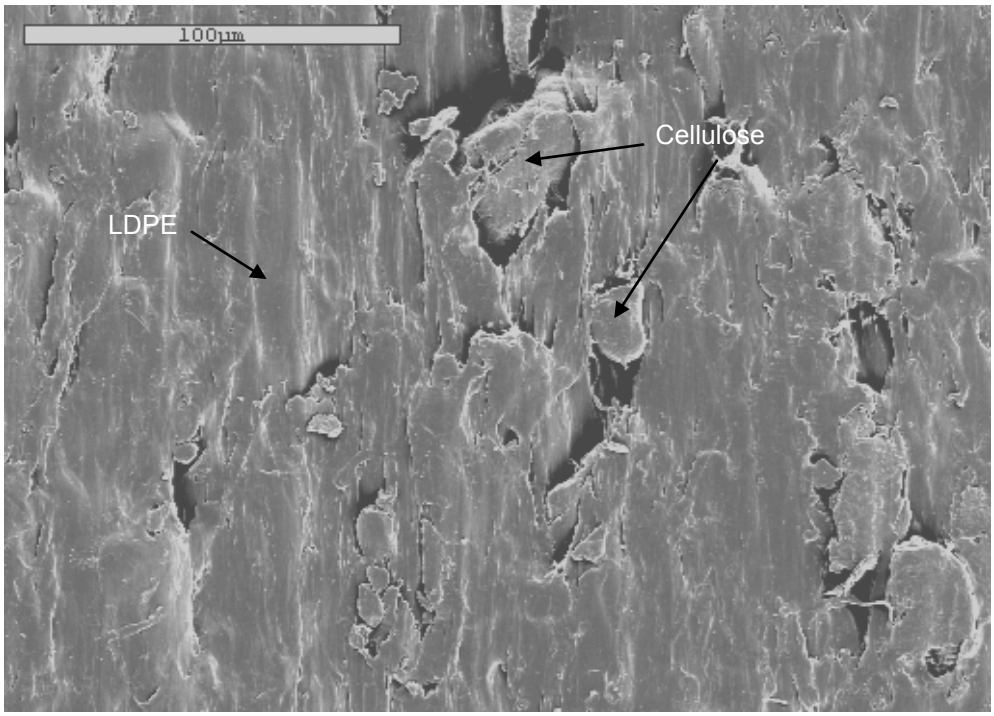

Figure 3-6. SEM image of blend of LDPE-Cellulose blend processed with CO_2 (MC30PE70CO2), magnification 500X

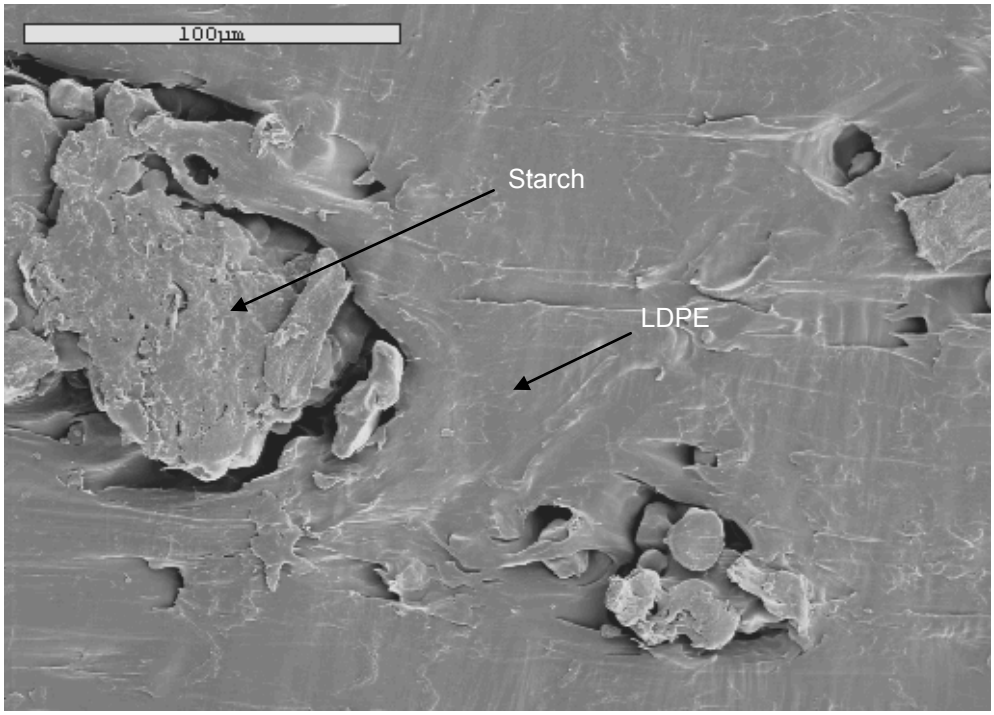

Figure 3-7. SEM image of LDPE-Starch blend (ST30PE70), magnification 500X

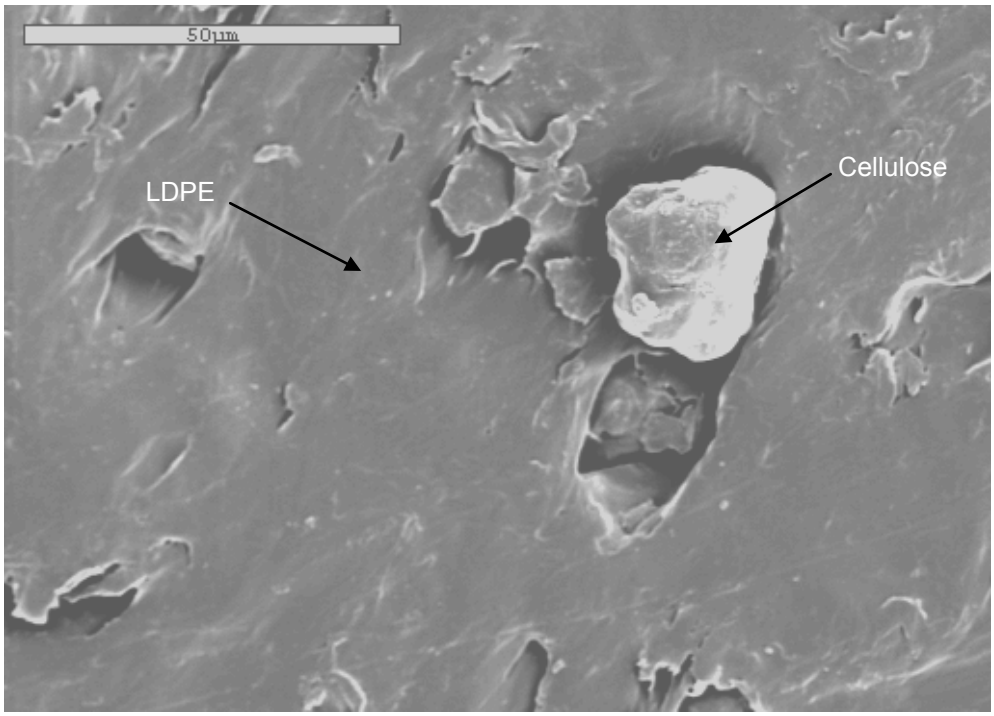

Figure 3-8. SEM image of blend of LDPE-Cellulose (MC30PE70), magnification 1000X

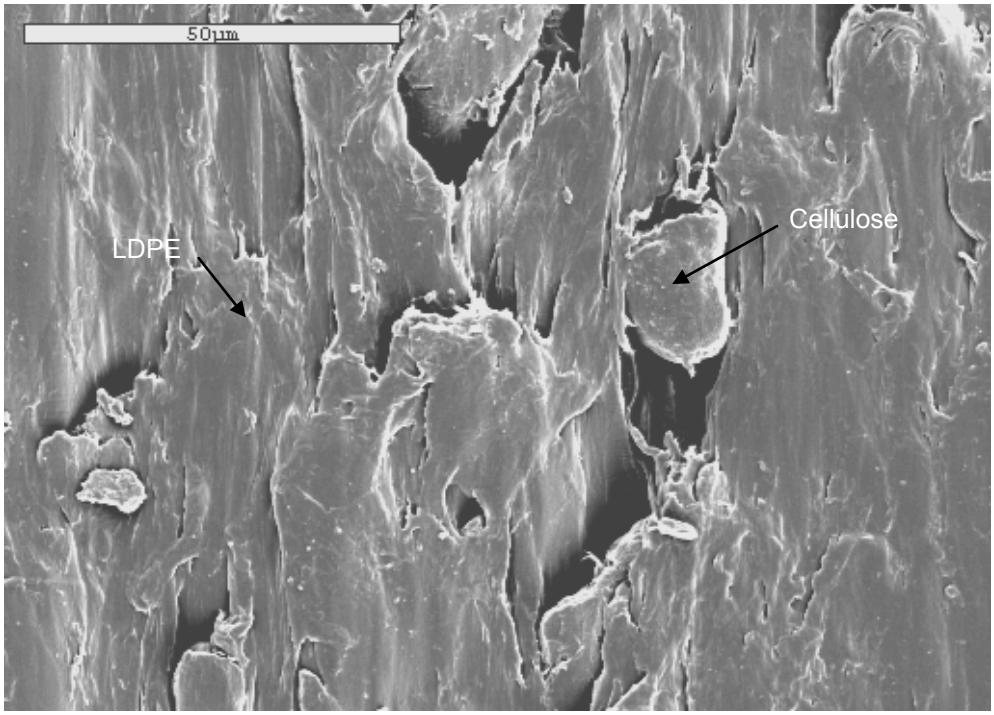

Figure 3-9. SEM image of LDPE-Cellulose blend processed with CO_2 (MC30PE70CO2), magnification 1000X

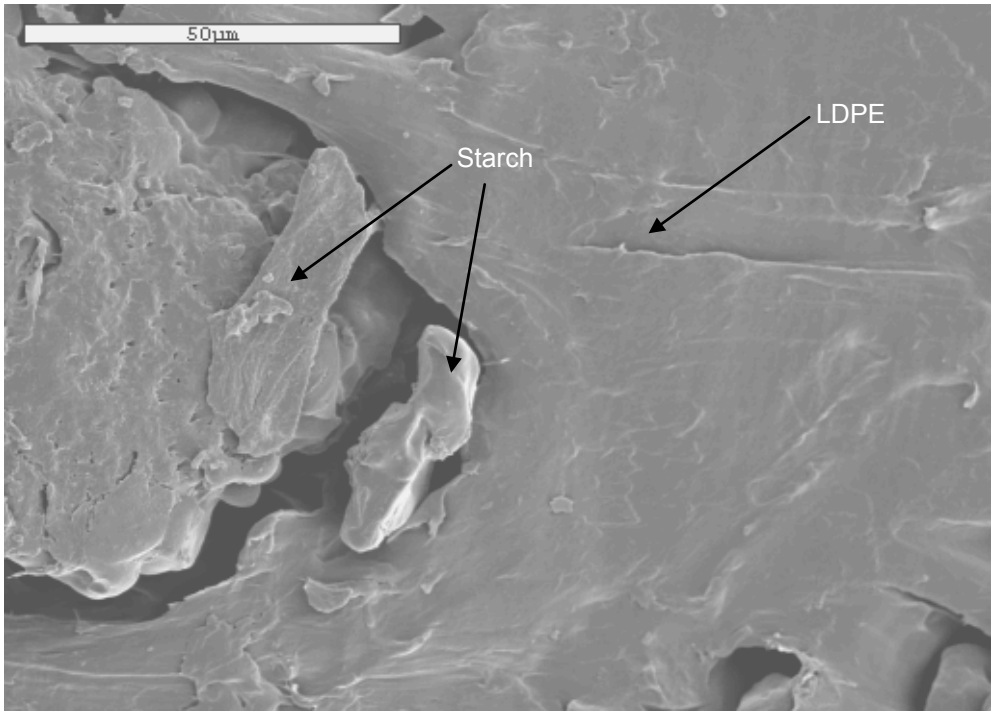

Figure 3-10. SEM image of LDPE-Starch blend (ST30PE70), magnification 1000X

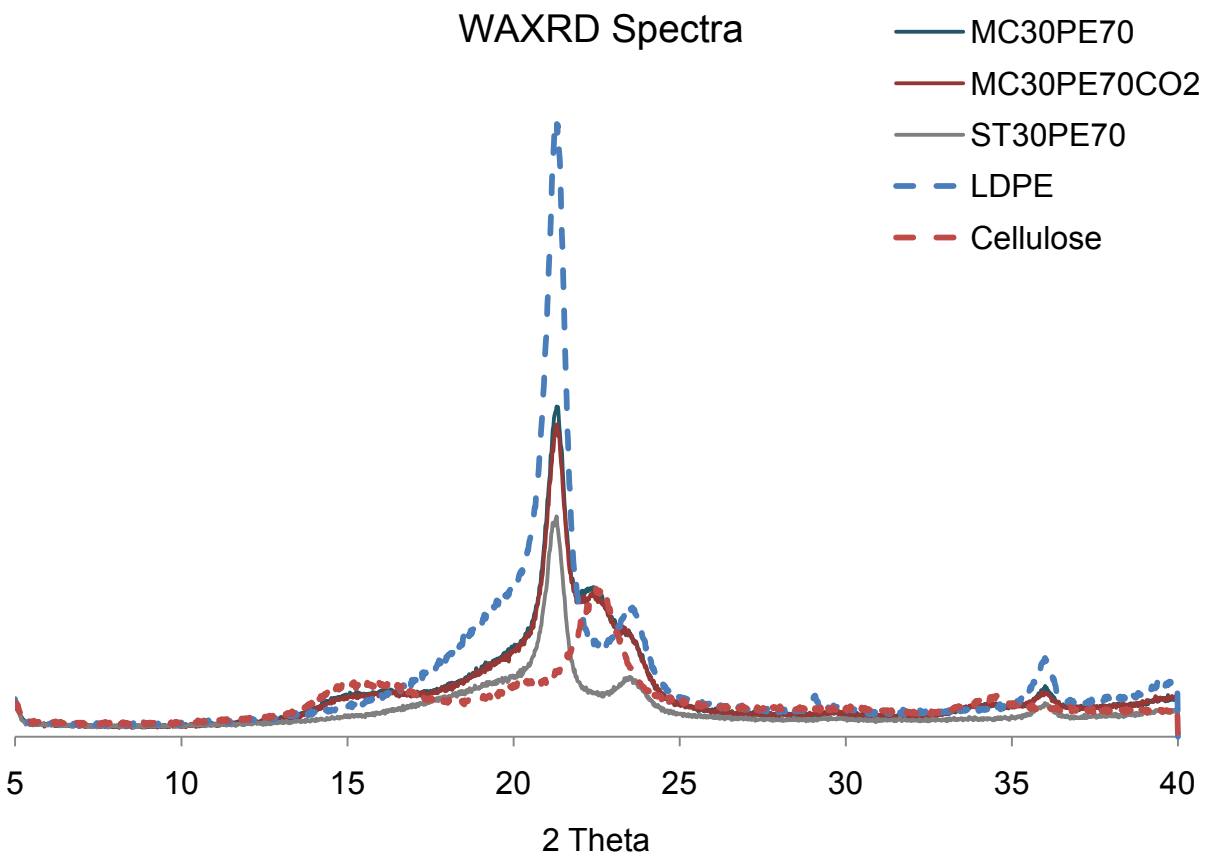

Figure 3-11. Wide Angle X-Ray Diffraction spectra of LDPE-Starch blend (ST30PE70), LDPE-Cellulose blend (MC30PE70), LDPE-Cellulose blend processed with CO_2 (MC30PE70CO2) and blend components LDPE and Cellulose

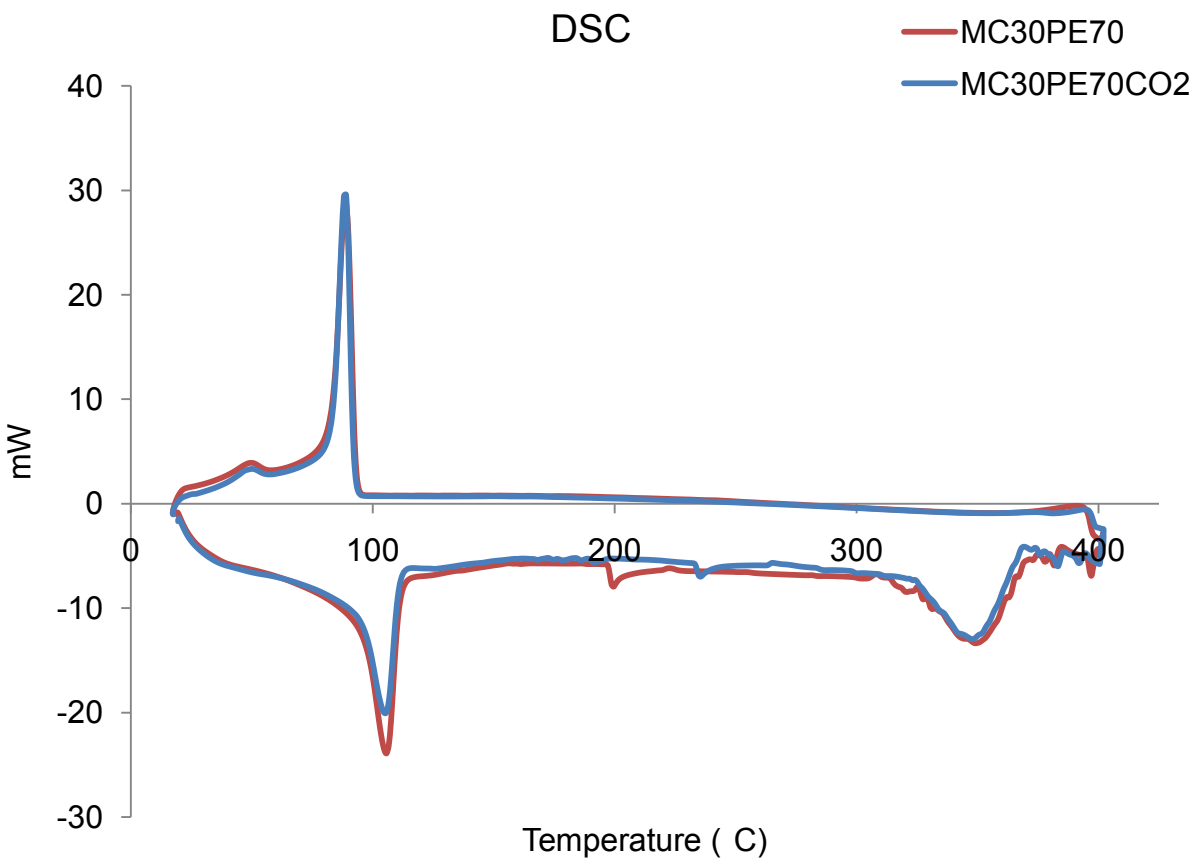

Figure 3-12. DSC curves of LDPE-Cellulose blend (MC30PE70) and LDPE-Cellulose blend processed with CO2 (MC30PE70CO2)

CHAPTER 4
BATCH PROCESSING

In Chapter 3, it was found that the supercritical CO_2 assisted extrusion of LDPE-Cellulose blends resulted in improved blend properties. However, on characterizing the processed samples, it was found that the effect of supercritical CO_2 was more pronounced on LDPE than cellulose. In order to investigate whether the structure of microcrystalline structure can be further affected (disrupted) by using supercritical CO_2, a batch process method was followed. Batch processing is an efficient way to modify materials by exposing them to supercritical CO_2 and other organic solvents in a temperature-pressure controlled environment. Batch processing is useful to study the changes in material's property that occur when process parameters like temperature and pressure are changed in a systematic manner. In order to reduce the inherent high-crystallinity of microcrystalline cellulose, the cellulose was processed in a combination of supercritical CO_2 and a solvent medium inside a batch reactor. This chapter describes the materials and experimental procedure used for the batch processing of microcrystalline cellulose.

4.1 Materials

Microcrystalline cellulose, Avicel® FD100 provided by FMC Corporations, Philadelphia, PA was, used as the starting material. The molecular weight was about 36,000 g/mol and degree of polymerization was approximately 140. The crystallinity index is approximately 82% and the particle size falls in the range of 6-12 microns. Dimethyl Sulfoxide (DMSO) A.C.S. grade was purchased from Fisher Scientific, Atlanta, GA and used as received. Urea A.C.S. grade (U-15) was also received from Fisher Scientific Co. CO_2 gas cylinder was purchased from Airgas South Inc., Gainesville, FL.

4.2 Experiment Setup

.A schematic of the experimental setup used is shown in Figure 4-1. The three main components of the experimental setup - CO_2 gas cylinder (1), syringe pump (2), and view cell (batch reactor) (6) were connected in series. Two sizes of stainless steel tubes, 1/8” and 1/16” were used for all the connections. Flow of CO_2 from gas cylinder to the syringe pump was controlled by a valve on the cylinder. Two hundred and sixty ml ISCO syringe pump was used to control flow rate of CO_2 into the view cell and to pressurize it to the desired pressure values. Gas flow into the view cell was controlled by a one-way regulating valve (3). The view cell used has three ports – inlet, outlet (vent) and one port for thermocouple to maintain close contact with inside. The view cell was supported horizontally by using a stir plate (5). A reducing union (4) was used to bridge 1/8” to 1/16” tubes between the syringe pump and view cell. Band Heater (7) and temperature controller with precision ± 2 °C (9) from Omega® were used to heat and control temperature of the view cell. The pressure inside the view cell was measured by a digital pressure gauge (12) which was connected to outlet port of the view cell via a 0.5 micrometer filter (10). CO_2 depressurization runs were conducted by operating a one-way regulating valve (13) which lead the gas out inside a fume hood (14). The experimental setup is also shown in Figure 4-2.

4.3 Experiment Procedure

For each batch reaction, 1.5 g microcrystalline cellulose was added into 5 ml DMSO and the mixture was stirred at 80 rpm at 30 °C for 2 minutes inside the fume hood. The white heterogeneous solution, as formed, was immediately transferred into the view cell before it turned into a gel form. For batch reactions with urea, known quantity of urea was first added into 5 ml DMSO, stirred at 80 rpm at 30 °C until a clear

homogeneous solution was formed. Cellulose was added consequently. The view cell was held horizontally using a Stir-Plate support and purged with CO_2 between 50-80 psi for about 1 min. The view cell was heated to 80 °C. During the heating process, outlet port of the view cell was closed and it was filled with CO_2 (about 850 psi) when the temperature reached to about 40 °C. The inlet port of the view cell was closed and CO_2 was pressurized to the desired pressure values (2500 psi or 4500 psi) by syringe pump. Once the temperature reached to set value, inlet port of the view cell was opened and pressurized CO_2 was transferred into it at gas flow rate of 80 ml/min. The inlet valve for view cell was closed when syringe pump and view cell reached to pressure equilibrium. The solution was kept inside view cell under this temperature and pressure condition for 30 minutes. The solution was stirred at about 500 rpm using a stirring bar inside the view cell. The stirring speed was controlled by a Stir-Plate. After 30 minute reaction time, DMSO was removed along with CO_2 by depressurizing CO_2. Depressurization process was conducted in multiple steps of 2500 psi to 2000 psi. If the batch reaction was conducted at CO_2 pressures higher than 2500 psi, then the depressurization process included first a step down from maximum pressure to 2500 psi and 2500 psi to 2000 psi in subsequent multiple pressure steps. Depressurization was stopped when sample under view cell was observed as a free flowing powder. Finally, the pressure and temperature were brought down to room conditions. The sample was removed from view cell and transferred in a vacuum sealable container. A close-up of cellulose being processed inside the view cell with DMSO-supercritical CO_2 at 2500 psi is shown in Figure 4-3.

It is worth noting that the batch reactions involving both microcrystalline cellulose and urea required longer depressurization times to obtain dry powder samples compared to reactions in absence of urea. Compositions and processing conditions used are listed in Table 4-1 and Table 4-2. Cellulose samples recovered after completion of batch processing are shown in Figure 4-4.

Table 4-1. Compositions and processing conditions for cellulose-DMSO-supercritical CO_2 batch reactions

Sample¥	Cellulose (g)	DMSO (ml)	Temperature (°C)	CO_2 Pressure (psi)
Unmodified Cellulose	1.5	N/A	N/A	N/A
D2500	1.5	5	80	2500
D3500	1.5	5	80	3500
D4500	1.5	5	80	4500

¥ The letter D denotes DMSO and the succeeding number denotes the CO_2 pressure (psi) at which cellulose was processed.

Table 4-2. Compositions and processing conditions for cellulose-DMSO-Urea-supercritical CO_2 batch reactions

Sample¥	Cellulose (g)	DMSO (ml)	Urea (g)	Temperature (°C)	CO_2 Pressure (psi)
UD25025	1.5	5	0.25	80	2500
UD25050	1.5	5	0.50	80	2500
UD25075	1.5	5	0.75	80	2500
UD25010	1.5	5	1.0	80	2500
UD45025	1.5	5	0.25	80	4500
UD45050	1.5	5	0.50	80	4500
UD45075	1.5	5	0.75	80	4500
UD45010	1.5	5	1.0	80	4500

¥ The letter UD denotes DMSO-Urea mixture. The first two digits of the numeric figure denote the CO_2 pressure (psi) at which cellulose was processed (e.g. 25 for 2500 psi and 45 for 4500 psi). The last three digits correspond to the urea content (g) (025 for 0.25 g, 050 for 0.50 g, 075 for 0.75 g and 010 for 1.00 g).

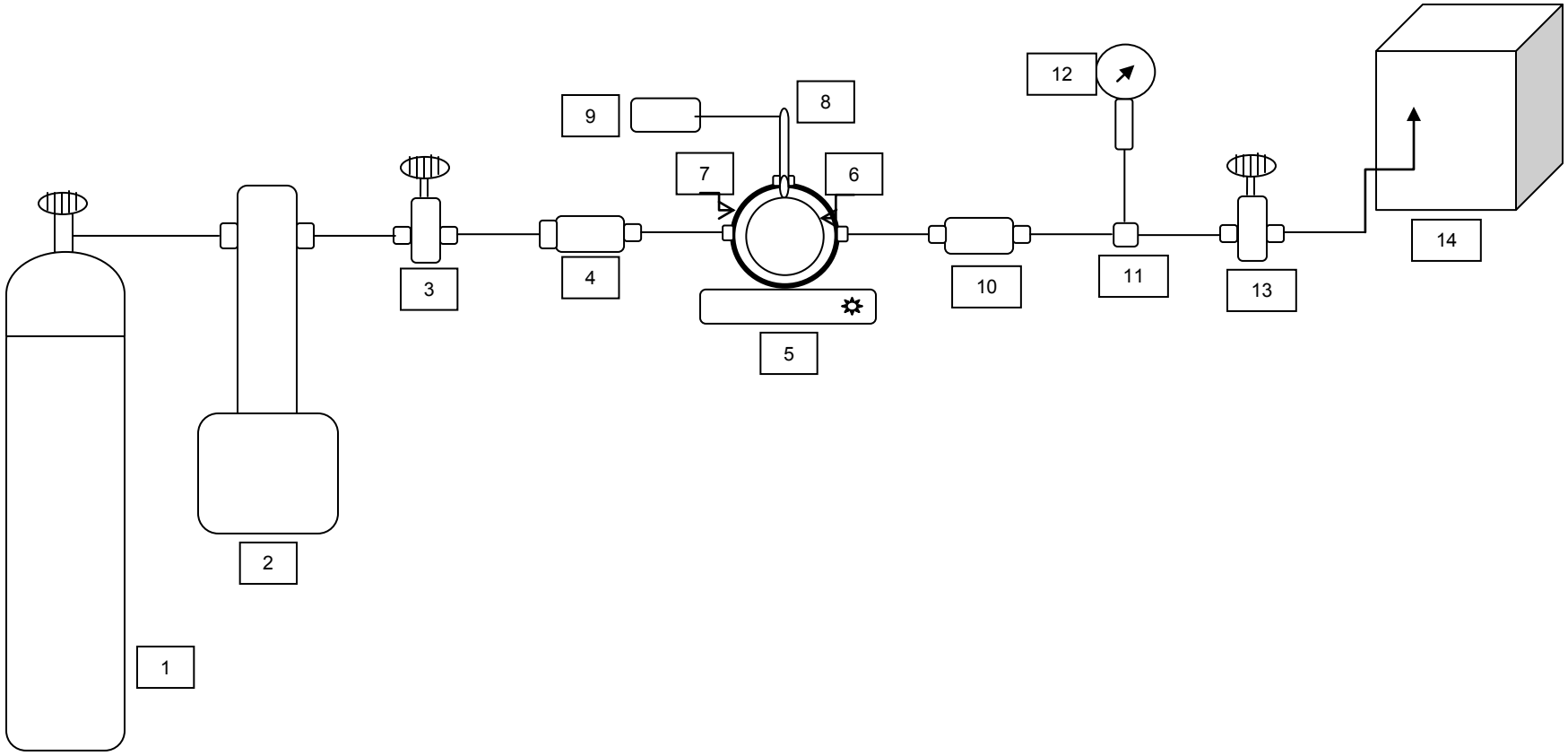

Figure 4-1. Schematic of experimental setup for batch processing

1. CO_2 cylinder,
2. Syringe Pump,
3. One way Pressure Regulating Valve,
4. Reducing Union,
5. Stir-Plate,
6. View Cell,
7. Band Heater
8. Thermocouple
9. Temperature Controller
10. Filter (0.5 micrometer)
11. T-Joint
12. Pressure Gauge
13. One-way Pressure Regulating Valve
14. Fume Hood

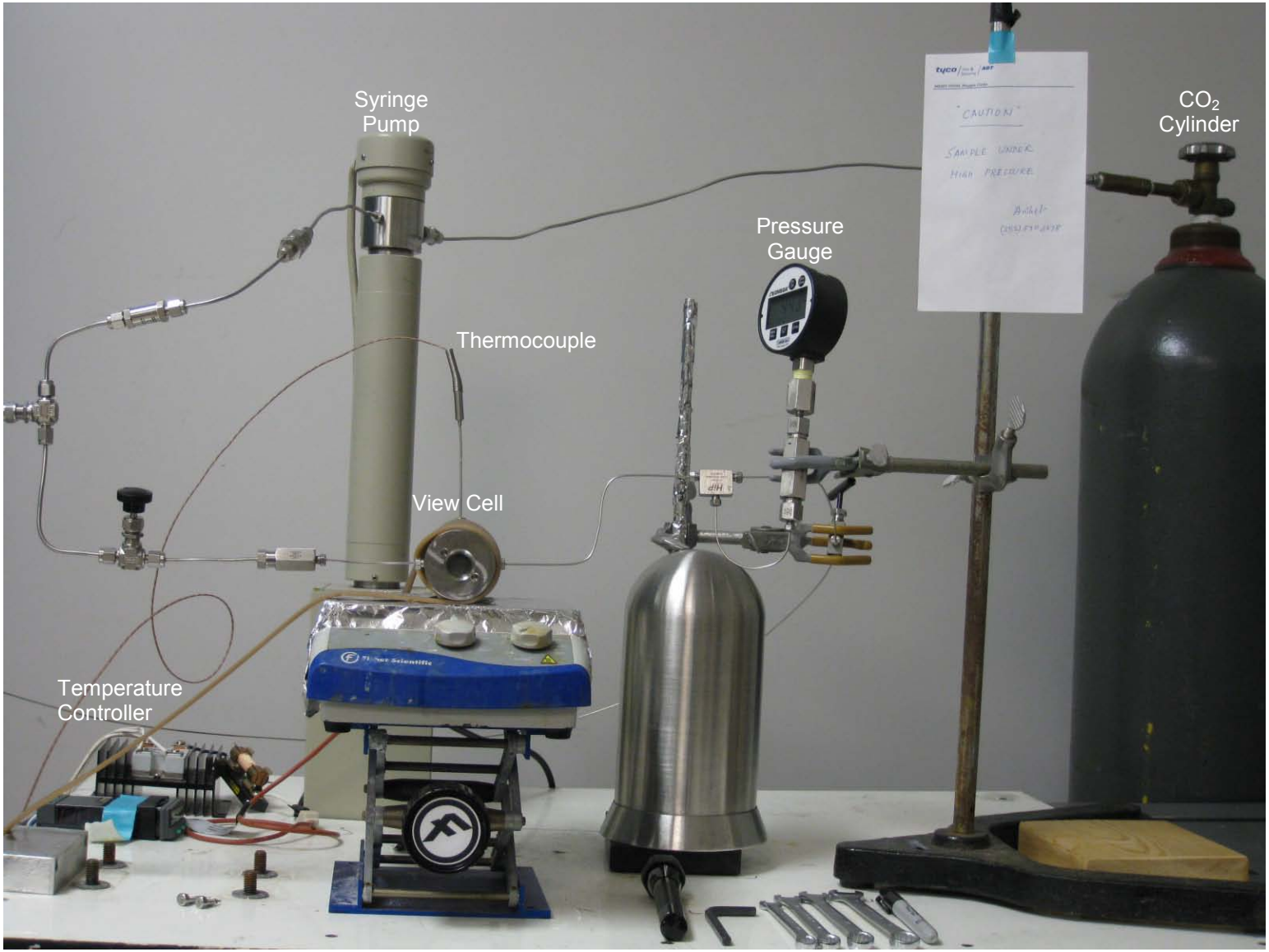

Figure 4-2. Experimental setup for batch processing

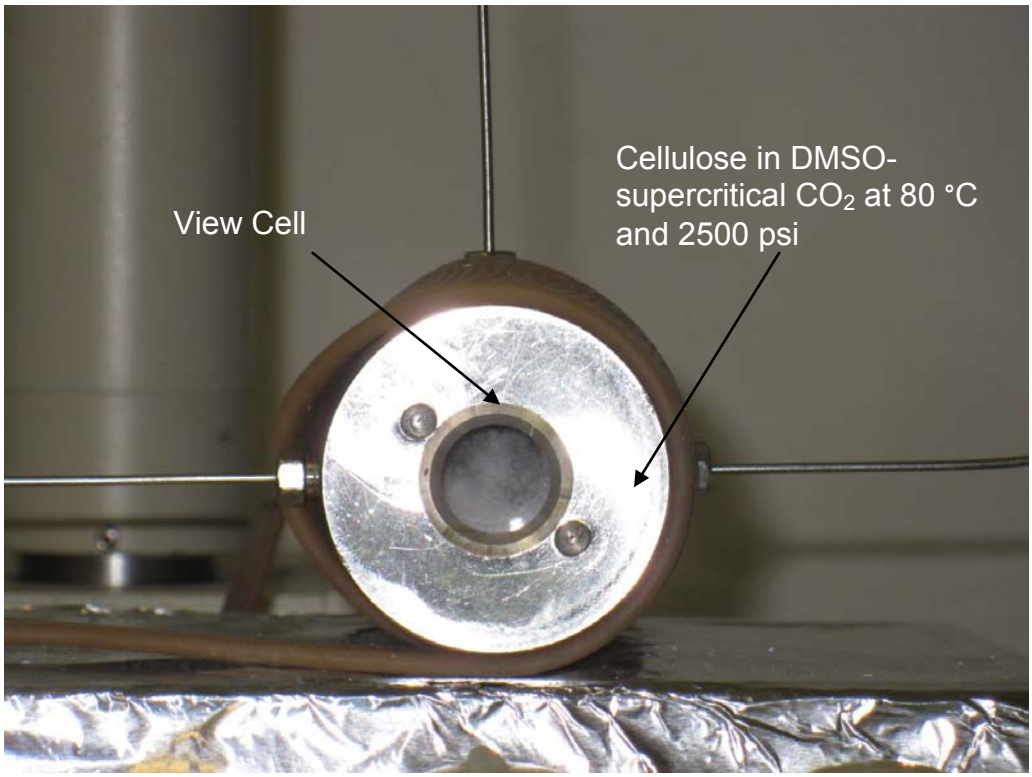

Figure 4-3. Cellulose under DMSO-supercritical CO_2 system at 2500 psi

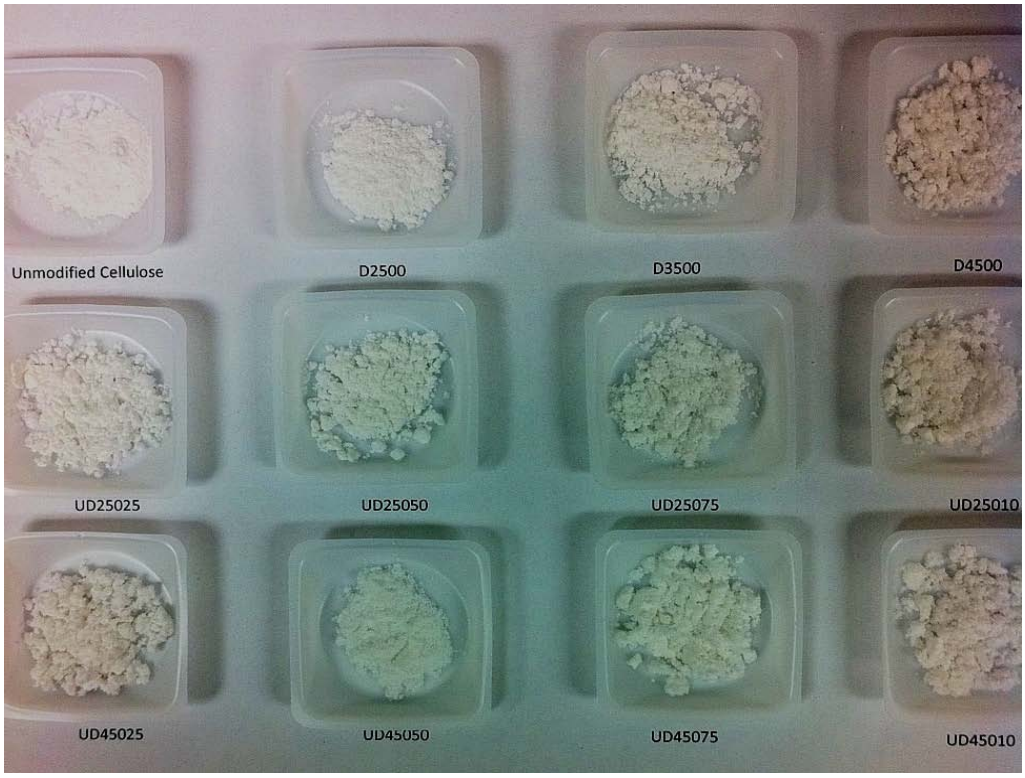

Figure 4-4. Cellulose samples processed under DMSO-supercritical CO_2 and DMSO-Urea-supercritical CO_2 systems

CHAPTER 5
CHARACTERIZATION OF CELLULOSE BY WIDE ANGLE X-RAY DIFFRACTION

Wide Angle X-Ray Diffraction (WAXRD) is the most extensively used technique to study crystal structure and estimate the crystallinity of cellulose[38]. This chapter describes use of this technique to calculate the relative crystallinity of batch-processed cellulose samples and study the changes in their crystal structure as affected by the processing.

5.1 Wide Angle X-Ray Diffraction Measurement

The changes in crystallinity and crystal structure of microcrystalline cellulose were studied by X-Ray Diffractometry (XRD, Philips APD 3720). The WAXRD was conducted using CuKα radiation at 40 KV and 20 mA. The wavelength of x-ray was 1.54 Å. Diffraction patterns were collected in the range of 5° to 40° at step size of 0.02. The diffraction results were treated using in-built ProFit^{TM} software by deconvoluting the spectra into 4 crystalline peaks and one amorphous peak in the 2-theta range of 10.77° to 31.77°. Pearson VII profile fit was applied until the best fit was obtained. A broad peak with highest intensity at 2-theta value of about 22.8° was selected to represent the amorphous region. It was generated by first selecting a peak at 2-theta value of 19°, and then applying Pearson VII profile fit until best fit was obtained. The relative degree of crystallinity was calculated by separating the amorphous region from the diffraction pattern and subtracting it from the crystalline region.

Degree of crystallinity of cellulose can be defined as the mass fractions of crystalline domains in cellulose[38]. The following formula was used to calculate the relative degree of crystallinity of each sample[7,123,131,132]:

Relative Crystallinity (%) = $\left(\frac{A_c}{A_a + A_c}\right) \times 100$ where, A_c is the sum of integral area of peaks assigned to crystalline regions (110), (110), (102), (200) and A_a is the integral area of amorphous region as shown by broad curve joining the end points of the spectrum with maximum intensity at 2-theta value of 22.5° (Figure 5-1).

5.2 Effect of DMSO and Supercritical CO_2 on Crystallinity of Cellulose

The X-Ray diffraction spectra of cellulose samples processed under DMSO and supercritical CO_2 at pressures ranging from 2500 psi to 4500 psi were compared with unmodified cellulose (Figure B-1 to B-3 in Appendix B). It was found that the crystal structure of cellulose did not change due to processing but the (200) peak intensity was reduced and the amorphous region was increased with increasing processing pressure of the supercritical CO_2. This could be due to breaking down of cellulose crystallites. Quantitative comparison of the relative degree of crystallinity is shown in Figure 5-2. It was found that the relative degree of crystallinity of samples followed a decreasing trend with increase in processing pressure. Cellulose processed with DMSO at 2500 psi (D2500) was only marginally affected but relative crystallinity of cellulose processed with DMSO at 4500 psi (D4500) was reduced by about 40% from that of unmodified cellulose. From these results, it can be suggested that the increase in processing pressures of supercritical CO_2 must have resulted in deeper penetration of DMSO into micro-fibrils of cellulose without affecting the original crystal structure. Crystalline peaks in cellulose diffraction spectra arise from crystal lattices formed due to glycosidic bonds, hydrogen bonds and van der Waals dispersion forces in the macromolecule[56]. Crystal structure of cellulose did not change from I to II (as of regenerated cellulose) which is also obvious from insoluble nature of cellulose seen during batch reactions at various

processing pressures. The change in relative crystallinity in spite of unmodified crystal structure suggests that the DMSO molecules affected the cellulose by interacting with intermolecular bonds in the amorphous region of cellulose.

5.3 Effect of Urea on Crystallinity of Cellulose

As discussed in section 5.2, the reduction in relative crystallinity of cellulose in DMSO-supercritical CO_2 system was found to be limited to about 40% at CO_2 processing pressure of 4500 psi. In order to find whether the limited reduction is due to process of CO_2 depressurization, which might have caused collapse of some structural features that were otherwise separated in presence of DMSO, and to further reduce the relative crystallinity, a variable amount of urea was incorporated into cellulose at processing pressures of 2500 psi and 4500 psi.

The X-Ray Diffraction spectra of cellulose samples with 0.45 to 1.80 mole fractions of urea in cellulose, processed with DMSO and supercritical CO_2 at 2500 psi are shown in Figure B-4 to Figure B-7 in Appendix B. It was found that the crystal structure of cellulose did not change in the presence of urea. When supercritical CO_2 processing pressure was increased from 2500 psi to 4500 psi, while keeping the same range of urea-cellulose molar ratios, the crystal structure of cellulose was affected at the highest urea content (Figure B-8 to B-11 in Appendix B). However, the amorphous region (broad peak at around 2 theta = 22.5°) in all the urea containing cellulose samples was similar except even larger in the UD25010 that contained highest urea molar fraction at 2500 psi processing pressures.

Quantitative comparison of the relative crystallinity of urea containing cellulose samples is shown in Figure 5-3. The samples processed at 2500 psi followed a marginal decreasing trend while the least degree of crystallinity (32%) was calculated

for the UD25010 sample. Samples processed at 4500 psi did not show any significant reduction in the relative crystallinity with increasing urea content. However, the relative crystallinity of the cellulose samples processed at this pressure showed about 45% reduction in crystallinity from that of unmodified cellulose. Mostly, the relative degree of crystallinity did not change significantly as a function of urea content or pressure.

In comparison to samples of cellulose without urea and processed at 2500 psi to 4500 psi supercritical CO_2 pressures, urea containing samples formed a plateau at about 45% relative crystallinity. Effective reduction in relative crystallinity followed an order: UD25010>D4500>D3500>D2500.

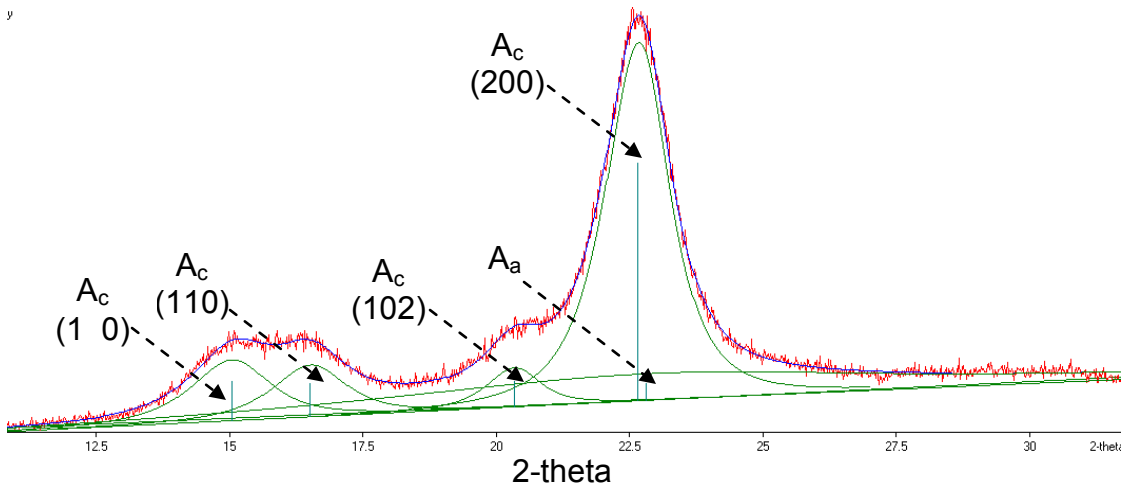

Figure 5-1. X-Ray Diffraction of unmodified microcrystalline cellulose; crystalline (A_c) and amorphous (A_a) regions are separated.

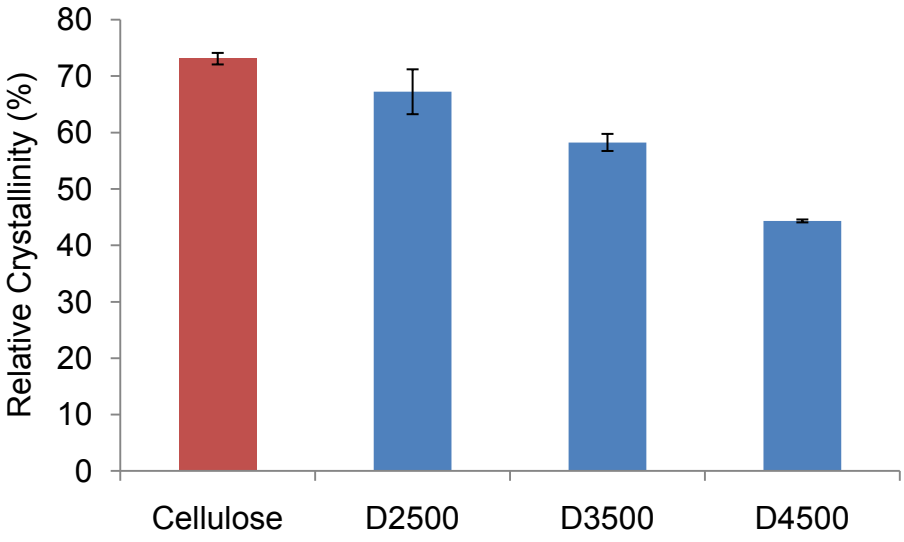

Figure 5-2. Relative crystallinity (%) of cellulose samples processed in DMSO and supercritical CO_2 at processing pressures 2500 psi (D2500), 3500 psi (D3500) and 4500 psi (D4500)

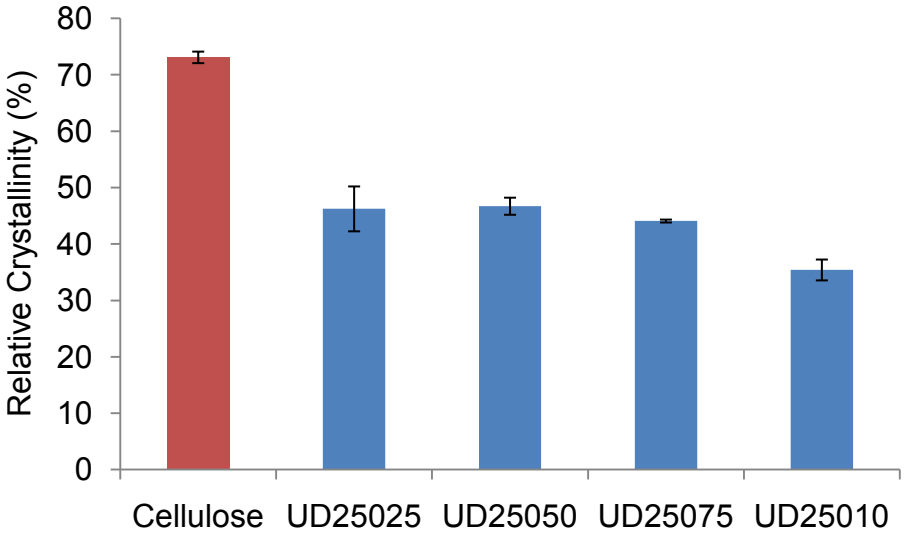

Figure 5-3. Relative crystallinity (%) of cellulose samples processed in DMSO-urea-supercritical CO_2 at 2500 psi. Amount of urea in cellulose was varied as 0.25 g (UD25025), 0.50 g (UD25050), 0.75 g (UD25075), and 1.00 g (UD25010).

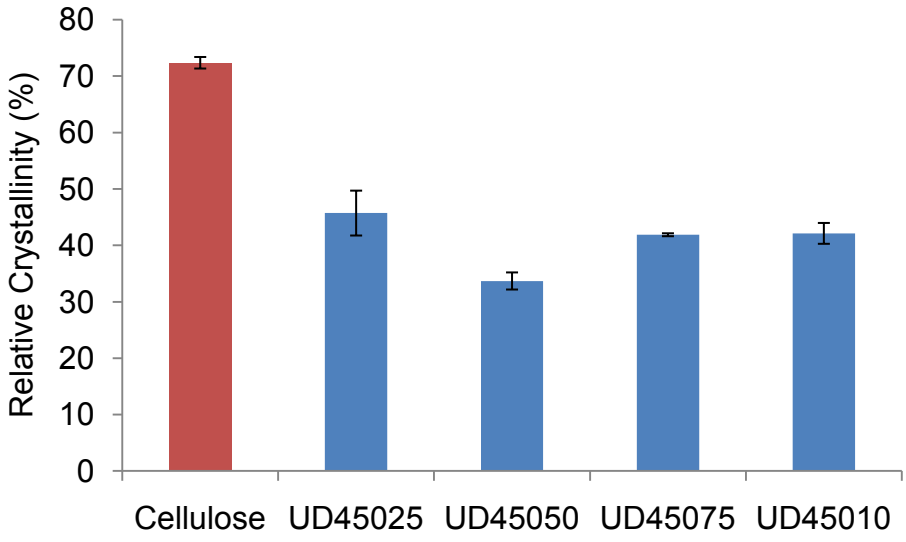

Figure 5-4. Relative crystallinity (%) of cellulose samples processed in DMSO-urea-supercritical CO_2 at 4500 psi. Amount of urea in cellulose was varied as 0.25 g (UD45025), 0.50 g (UD45050), 0.75 g (UD45075) and 1.00 g (UD45010).

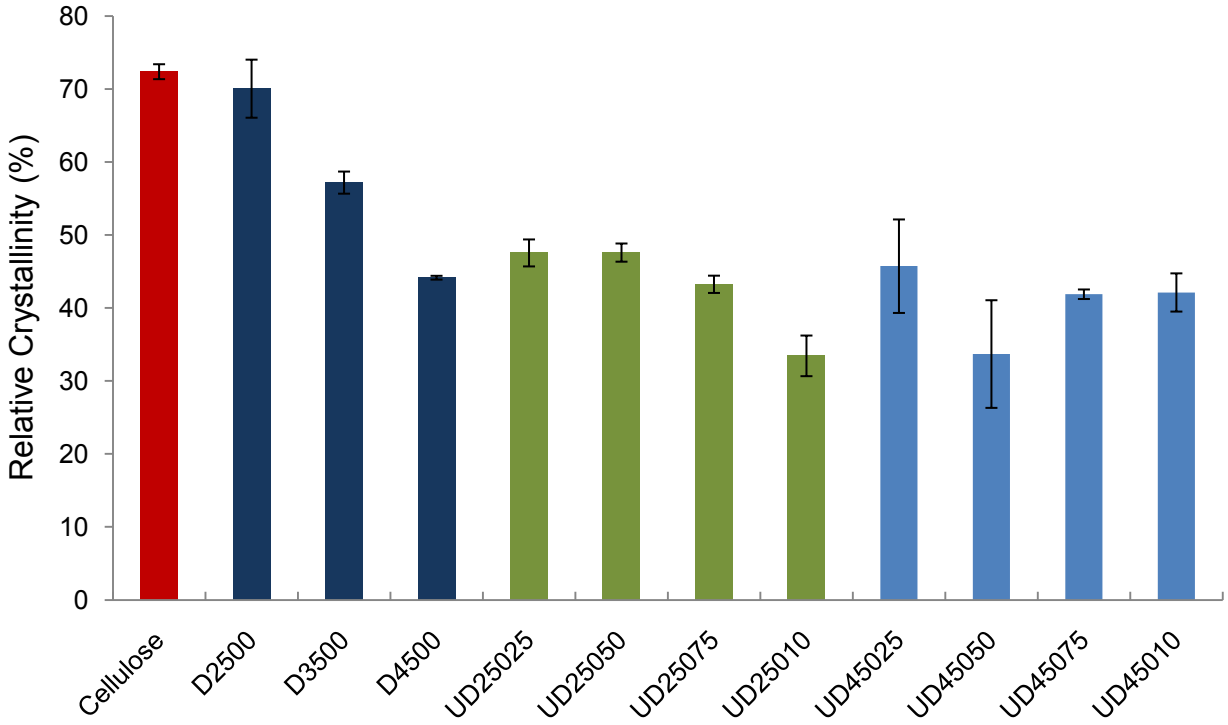

Figure 5-5. Quantitative comparison of the relative crystallinity(%) of cellulose samples processed in DMSO-supercritical CO_2 and DMSO-Urea-supercritical CO_2 systems at variable pressures and variable urea content

CHAPTER 6
CHARACTERIZATION OF CELLULOSE BY DIFFUSED REFLECTANCE INFRARED FOURIER-TRANSFORM SPECTROSCOPY (DRIFT)

Infrared Spectroscopy has been utilized as one of the most useful techniques to study different conformations of cellulose macromolecules and the hydrogen bonding within. It is the most sensitive for detecting the hydrogen bonds[14]. It can provide useful information about change in hydrogen bonds of cellulose during crystal transformations[65]. In Diffused Reflectance FT-IR technique, the diffusively reflected energy is collected to create a spectrum. Simpler sample preparation, increased spectral resolution and reduced interference from water bands compared to transmission FT-IR makes this technique suitable for powdered, non-transparent and rough surfaced samples[133,134]. A study that utilized DRIFT technique to investigate the structural changes that occurred in the batch-processed cellulose samples, is discussed in this chapter.

6.1 DRIFT Measurement

Diffused Reflectance Infrared Spectroscopy was conducted with a Thermo Electron Magna 760, Thermo Scientific Inc., MA. Approximately 0.0030 g of sample was first mixed 0.30 g of Potassium Bromide (KBr) in a high speed shaker for 1 min. Microcrystalline Cellulose Avicel® FD100 was kept in oven for 24 hrs at 75 °C before preparing the sample for spectroscopy. The spectra were recorded at 4cm^{-1} resolution in the range of 400 cm^{-1} to 4000 cm^{-1}. The number of scans for each sample was set at 64. The spectra were further analyzed by performing curve-fitting simulations using the open source – peak fitting software 'fityk 0.9.4'[135,136,137]. The bands for the hydrogen bonding region (3000 to 3800 cm-1) were deconvoluted assuming peaks as Gaussian shaped with a number of iterations to get the best fit[138]. Although there are

disagreements about interpretation of band assignments by different authors[65,68,69,70,71] an attempt to indicate the most probable band assignments was performed. Table 6-1 comprehensively covers FTIR spectral band assignments from the above-mentioned authors in hydrogen bond region 3000-3600 cm^{-1}. Table 6-2 covers spectral band assignments for lower wavenumber regions in the spectra. This information is used as the basis to understand the changes in molecular bonding of cellulose caused due to processing under 'DMSO-supercritical CO_2' and 'DMSO-Urea-supercritical CO_2' solvent system in this research.

6.2 Effect of DMSO - Supercritical CO_2 on Cellulose

Figure 6-1 compares Infrared spectra of microcrystalline cellulose - as received, and microcrystalline cellulose processed in DMSO and supercritical CO_2 at 2500 psi (D2500), 3500 psi (D3500), and 4500 psi (D4500) CO_2 pressures. The hydrogen-bonding region (3000-3600 cm^{-1}) became narrow with increasing supercritical CO_2 pressure. This change can be attributed to disruption in hydrogen bonding either due to fewer hydroxyl groups to form hydrogen bond [33] or change in the inter-chain and intra-chain hydrogen bonding networks due to hydrogen bonding with the DMSO molecules. On deconvoluting the OH stretch region by the fityk tool, four bands were observed. Most of the earlier studies by other authors reported three major bands under the OH stretch region. In our study, better peak fitting was observed with four individual bands under OH stretch region. Based on previous reports by various authors[68,69, 71,139,65], the spectral bands in this study are assigned as follows: O2H2···O6 intra-chain hydrogen bond, O3H3···O5 intra-chain hydrogen bond, O6H6···O3' inter-chain hydrogen bond and OH stretch in Iβ crystalline phase (See Figure 1-2, Figure 6-2 and Table 6-2). The comparison of position and intensity of these bonds relative to those in unmodified

cellulose is shown in Table 6-3 and Table 6-4 respectively. The deconvoluted hydrogen-bonding regions for these samples are shown in Figure C-1 and Figure C-2 in Appendix C. When compared with intra-chain and inter-chain hydrogen bonds in unmodified cellulose, it was found that the peak position of intra-chain hydrogen bond O2H2···O6 moved to lower wavenumbers with an increase in the processing pressure. The intensity of this bond increased with pressure. In contrast, the peak for the inter-chain hydrogen bond O6H6···O3' moved to higher wavenumber by about 70-90 cm^{-1} but its absorption intensity remained unchanged with variation in processing pressure. Peak positions for the strongest intra-chain hydrogen bond O3H3···O5[19] and the valence hydrogen bond in Iβ crystalline phase remained the same albeit absorption intensity of former decreased and that of latter increased with increase in processing pressures. It is known that among different hydrogen bonded hydroxyl groups, the one with stronger hydrogen bond is shifted more towards lower wavenumber in the spectrum[68]. This suggests that the intra-chain hydrogen bond O2H2···O6 became stronger whereas inter-chain hydrogen bond became weaker with increase in processing pressure. Moreover, among the three samples, O2H2···O6 intra-chain hydrogen bond strength was found to follow the trend: Unmodified cellulose < D2500 < D3500 < D4500 whereas inter-chain hydrogen bond followed a reverse trend. The processing under combination of DMSO and supercritical CO_2 partially re-structured the hydrogen bonding in cellulose such that processing pressures higher than 2500 psi caused significant reduction in O3H3···O5 bond intensity whereas O6H6···O3' bond intensity increased over unmodified cellulose. The increase in absorption intensity was caused by an increase in the dipole moment due to interaction of DMSO molecules. This suggests that DMSO-supercritical CO_2

preferentially interact with the inter-chain hydrogen bonds O6H6···O3' and intra-chain hydrogen bonds O2H2···O6 but the interaction changes for the intra-chain hydrogen bond at different levels of processing pressures whereas it remains the same for inter-chain hydrogen bond for any level of pressures above 2500 psi.

DMSO molecules have a tendency to self-associate. The S=O stretching vibrations of monomers, dimers and trimers of DMSO molecules are usually overlapped in the 850-1150 cm^{-1} region of the IR spectra[140]. The skeletal vibration modes in this region can also interact with the rocking modes of methyl groups[141]. Figure 6-3 shows spectral changes at around 1035 cm^{-1} and 957 cm^{-1} for the cellulose samples processed in DMSO at different CO_2 pressures. The band at 1035 cm^{-1} is assigned to CH3 rocking mode in DMSO[141] which is overlapped with stretching vibrations of C(6)-O(6) bond in cellulose[65]. This band is found to match the intensity of stretching vibrations of C(3)-O(3) (1058 cm^{-1}) in cellulose for D4500. This suggests that DMSO molecules sterically interact with C(6)-O(6) bond and change the environment around C(6) carbon atom of cellulose to make this bond more polar. Cellulose processed under DMSO and supercritical CO_2 also shows two spectral bands at 957 cm^{-1} and 700 cm^{-1} from S=O stretching, CH_3 rocking combination, and asymmetric stretching vibrations of DMSO dimers respectively[140-141,142]. The increase in peak intensity at 957 cm^{-1} and narrowing of the peak at 700 cm^{-1} with increase in the CO_2 processing pressures suggest that DMSO molecules penetrated deeper into the crystalline structure of cellulose. Depressurization process at approximate pressure range of 2500-1500 psi was not enough to extract all DMSO after cellulose was processed at pressures 2500 psi and above.

From the above observations, it can be suggested that the processing of cellulose under DMSO-supercritical CO_2 system at two different pressure values caused weakening of the O6H6···O3' intermolecular hydrogen bonds. Yet, all of the hydroxyl groups still participate in forming hydrogen bond network such that overall hydrogen bond strength becomes and remains smaller than unmodified cellulose. Higher CO_2 pressure caused DMSO molecules break in crystalline structure of cellulose deeper and interact mainly with O6H6···O3' inter-chain hydrogen bond while remaining trapped inside the macromolecule.

6.3 Effect of DMSO-Urea with Supercritical CO_2 on Cellulose

Figures 6-4 and 6-7 shows change in IR spectra of cellulose due to the addition of different amounts of urea in cellulose by supercritical CO_2 batch processing route. 0.06 to 0.24 mole fractions of urea was first dissolved in DMSO and then incorporated in cellulose at 2500 psi and 4500 psi supercritical CO_2 pressures to get 0.45, 0.9, 1.35, and 1.8 mole fractions of urea in cellulose. With comparison to IR spectra of unmodified cellulose, one can conclude that the hydrogen bonding region (3000-3600 cm^{-1}) in processed samples includes an additional peak at around 3200 cm^{-1} which is formed due to presence of NH stretching vibrations[138]. On deconvolution of hydrogen bonding region, two additional peaks were identified other than the two intra-chains and one inter-chain hydrogen bond in cellulose. The sample with the highest molar ratio of urea to cellulose i.e. UD25010 was chosen to assign the peaks to respective molecular bond vibrations (Figure 6-5). Spectral bands around 3450 cm^{-1}, 3370 cm^{-1} and 3245 cm^{-1} were assigned to two intra-chain bonds O2H2···O6, O3H3···O5 and inter-chain hydrogen bond O6H6···O3' respectively. DMSO-Urea complex is formed when urea is dissolved in DMSO; peaks at around 3340 cm^{-1} and 3200 cm^{-1} are assigned to these

compounds[14]. It is worth to note that the peaks around these wavenumbers were assigned to the intra-chain and inter-chain hydrogen bonds in unmodified cellulose. However, significant change in the intensity and small shift of wavenumber corresponding to CH_2 bending (1430 cm^{-1}) suggests that DMSO-Urea complex affected the environment around O6H6 bond; this resulted in spectral shift of band associated to inter-chain hydrogen bond O6H6···O3'. This observation formed a good reason to change the assignment for O6H6···O3' from 3200 cm^{-1} to 3245 cm^{-1} for cellulose processed in DMSO-urea-supercritical CO_2. On comparison with the IR spectra of the unmodified cellulose, cellulose processed under DMSO-urea-supercritical CO_2 shows obvious new peaks in the range of 1600-1800 cm^{-1} which arise from C=O stretching vibrations of amide I[138]. The bands at 1620 cm^{-1} and 1670 cm^{-1} are assigned to ordered and disordered hydrogen bonded carbonyl groups respectively[143,144]. The peak at 1470 cm^{-1} was assigned to the asymmetric stretch of C-H-N group in Urea[145]. This band was shifted to lower wavenumbers for processed samples due to the weakening of its strength because of hydrogen bond formation with DMSO.

6.3.1 Effect of Urea Concentration at Processing Pressure of 2500 Psi

The FTIR spectra for cellulose samples containing 0.25 to 1.0 g urea viz. UD25025 (0.25 g), UD25050 (0.50 g), UD25075 (0.75 g), and UD25010 (1.0 g) are shown in Figure 6-4 and Figure 6-6. The hydrogen- bonding region (3200 cm^{-1} to 3600 cm^{-1}) in samples was deconvoluted by fityk software as shown in Figure C-3 and Figure C-4 in Appendix C. The changes in wavenumber and peak intensities relative to corresponding peaks in unmodified cellulose are listed in Table 6-6 and Table 6-7 respectively. Intra-chain hydrogen bond O2H2···O6 shifted from 3478 cm^{-1} (unmodified cellulose) to around 3455 cm^{-1} for processed samples. However, it did not vary

significantly among processed samples. On the other hand, the spectral band of intra-chain hydrogen bond O3H3···O5 shifted to higher wavenumbers with an increase in urea concentration. The spectral band for inter-chain hydrogen bond O6H6···O3' also shifted to a higher wavenumber for all the processed samples. The intensities of Urea-DMSO complex was increased with increase in urea concentration. These observations suggest that processing caused reduction in the hydrogen bond strength of O3H3···O5 and O6H6···O3' but increased the strength of O2H2···O6 in cellulose; this effect was more prominent in sample with highest urea content. Moreover, the spectral band at 1035 cm^{-1} was broadened and its ratio with the spectral band at 1058 cm^{-1} increased with increase in the urea content (Figure 6-6). As mentioned earlier, these bands are assigned to CH_3 rocking mode of DMSO (which is overlapped with C6H6···O6 of cellulose) and C3O3 of cellulose respectively. This shows incremental interaction of DMSO with C6H6···O6 of cellulose and more DMSO being trapped in cellulose with increase in urea content.

6.3.2 Effect of Urea Concentration at Processing Pressure of 4500 Psi

The FTIR spectra for cellulose samples containing urea in quantities of 0.25 g (UD45025), 0.50 g (UD45050), 0.75 g (UD45075), and 1.0 g (UD45010) are shown in Figure 6-7. These samples were processed in DMSO-Urea-supercritical CO_2 at 4500 psi. Hydrogen bonding region in samples was deconvoluted by fityk software as shown in Figure C-5 and Figure C-6 in Appendix C. The changes in wavenumber and intensity of peaks relative to corresponding peaks in unmodified cellulose are listed in Table 6-8 and Table 6-9 respectively. When compared to the position of the corresponding bands in unmodified cellulose, it was found that the spectral band for intra-chain hydrogen bond O2H2···O6 moved to lower wavenumbers and the band for O3H3···O5 was shifted

to higher wavenumbers for UD45025 and UD45010 respectively. Moreover, the spectral band for inter-chain hydrogen bond O6H6···O3' shifted to a higher wavenumber compared to that in unmodified cellulose. These observations suggest that the processing resulted in weakening of hydrogen bonds O3H3···O5 and O6H6···O3' whereas the bond O2H2···O6 was strengthened. Strengthening of O2H2···O6 can also be explained by reduction in its absorption intensity, which might be due to interaction of Urea-DMSO complex preferentially with other two hydrogen bonds. However, the increase in urea content didn't bring any significant difference in O6H6···O3' inter-chain and O3H3···O5 intra-chain bond strengths for UD45025 and UD45010 samples. The intensities for Urea-DMSO complex increased for the sample containing higher amounts of urea. Also, the spectral band at 1035 cm^{-1} was broadened and its ratio with spectral band at 1058 cm^{-1} matched by increase in urea content (Figure 6-8). This shows that interaction of DMSO with C6H6···O6 of cellulose increased and more DMSO was trapped in cellulose when urea content was increased.

From the above analysis, it can be concluded that addition of urea caused weakening of O3H3···O5 intra-chain hydrogen bond in addition to weakening of the inter-chain hydrogen bond unlike non-urea containing systems in which only the inter-chain hydrogen bond was weakened. This could imply slightly lower crystallinity of cellulose samples that contains urea. However, change in hydrogen bonding was also due to the presence of Urea-DMSO complex that was entrapped in cellulose after processing. The DMSO-Urea complex reduced the solubility of DMSO in supercritical CO_2 and retained more DMSO-Urea complex trapped inside microfibrils of cellulose after depressurization process. Dissolution of urea in DMSO prevented the direct

interaction with cellulose. Therefore, increase in urea content did not bring any considerable change in molecular bond strength and hence the crystallinity of cellulose samples did not show a significant change by varying the urea content.

Table 6-1. Peak assignments used in current study[36, 40, 65, 68, 69, 71, 143, 144,146,147]

Wavenumber (cm^{-1})	Peak Assignment
3000-3600	OH Stretching
2900	CH Stretching
1430	CH_2 Bending
1316	CH_2 Wagging
1280	CH Bending
1200	C-OH in plane bending at C6
1158	Asymmetric C-O-C Stretching
1058	C3-O3 Stretching
1035	CH_3 Rocking in DMSO
957	S=O Stretching and CH_3 Rocking in DMSO
900	β-linkages
700	DMSO dimers

Table 6-2. Peak assignments for intra-chain and inter-chain hydrogen bonds in cellulose

Wavenumber	Peak assignment in this work	Hydrogen bond type	References
3478	O2H2··O6	Intra-chain	Marechal *et al.*[68]
3345	O3H3··O5	Intra-chain	Marechal *et al.*[68], Kokot *et al.*[69]
3208	O6H6··O3’	Inter-chain	Oh *et al.*[65]
3274	Iβ	Hydrogen Bond	Sugiyama *et al.*[71]

Table 6-3. Wavenumber shift relative to unmodified cellulose

Hydrogen Bond	Unmodified Cellulose	D2500	D3500	D4500
O2H2··O6	3478	3451	3426	3417
Wavenumber shift	N/A	(-27)	(-52)	(-61)
O3H3··O5	3345	3353	3345	3345
Wavenumber shift	N/A	(+8)	(0)	(0)
O6H6··O3’	3208	3278	3298	3292
Wavenumber shift	N/A	(+70)	(+90)	(+90)
Iβ	3274	3274	3278	3274
Wavenumber shift	N/A	(0)	(+4)	(0)

Table 6-4. Peak intensity of hydrogen bonds relative to those in unmodified cellulose

Hydrogen bond	Peak Height			
	Unmodified Cellulose	D2500	D3500	D4500
O2H2··O6	0.01	0.03	0.03	0.05
O3H3··O5	0.04	0.02	0.03	0.03
O6H6··O3’	0.02	0.03	0.03	0.07

Table 6-5. Peak assignments for intra-chain, inter-chain hydrogen bonds, and DMSO-urea complex in cellulose samples processed in DMSO-urea-supercritical CO_2 at 2500 psi

Wavenumber (cm^{-1})	Peak assignment in this work	Hydrogen bond type
3454	O2H2··O6	Intra-chain
3371	O3H3··O5	Intra-chain
3248	O6H6··O3’	Inter-chain
3339	DMSO-Urea complex	N/A
3200	DMSO-Urea complex	N/A

Table 6-6. Wavenumber shift in cellulose samples processed in DMSO-urea-supercritical CO_2 at 2500 psi

Hydrogen Bond	Unmodified Cellulose	UD25025	UD25050	UD25075	UD25010
O2H2··O6	3478	3447	3454	3457	3454
Wavenumber shift	N/A	(-31)	(-24)	(-21)	(-24)
O3H3··O5	3345	3352	3360	3375	3371
Wavenumber shift	N/A	(+7)	(+15)	(+30)	(+26)
O6H6··O3’	3208	3255	3233	3235	3248
Wavenumber shift	N/A	(+47)	(+25)	(+27)	(+30)

Table 6-7. Comparison of peak intensities of hydrogen bonds in cellulose samples processed in DMSO-urea-supercritical CO_2 at 2500 psi and intensities in unmodified cellulose

Hydrogen bond	Peak Height				
	Unmodified Cellulose	UD25025	UD25050	UD25075	UD25010
O2H2··O6	0.01	0.02	0.16	0.20	0.21
O3H3··O5	0.04	0.02	0.27	0.11	0.26
O6H6··O3’	0.02	0.07	0.14	0.18	0.17

Table 6-8. Wavenumber shift in cellulose samples processed in DMSO-urea-supercritical CO_2 at 4500 psi

Hydrogen Bond	Unmodified Cellulose	UD45025	UD45050	UD45075	UD45010
O2H2··O6	3478	3454	3444	3461	3460
Wavenumber shift	N/A	(-24)	(-34)	(-17)	(-18)
O3H3··O5	3345	3357	3343	3389	3387
Wavenumber shift	N/A	(+12)	(-2)	(+44)	(+42)
O6H6··O3’	3208	3245	3211	3242	3244
Wavenumber shift	N/A	(+37)	(+3)	(+34)	(+36)

Table 6-9. Comparison of peak intensities of hydrogen bonds in cellulose samples processed in DMSO-urea-supercritical CO_2 at 4500 psi and intensities in unmodified cellulose

Hydrogen bond	Peak Height				
	Unmodified Cellulose	UD45025	UD45050	UD45075	UD45010
O2H2··O6	0.01	0.03	0.08	0.12	0.16
O3H3··O5	0.04	0.05	0.19	0.22	0.24
O6H6··O3’	0.02	0.03	0.12	0.06	0.10

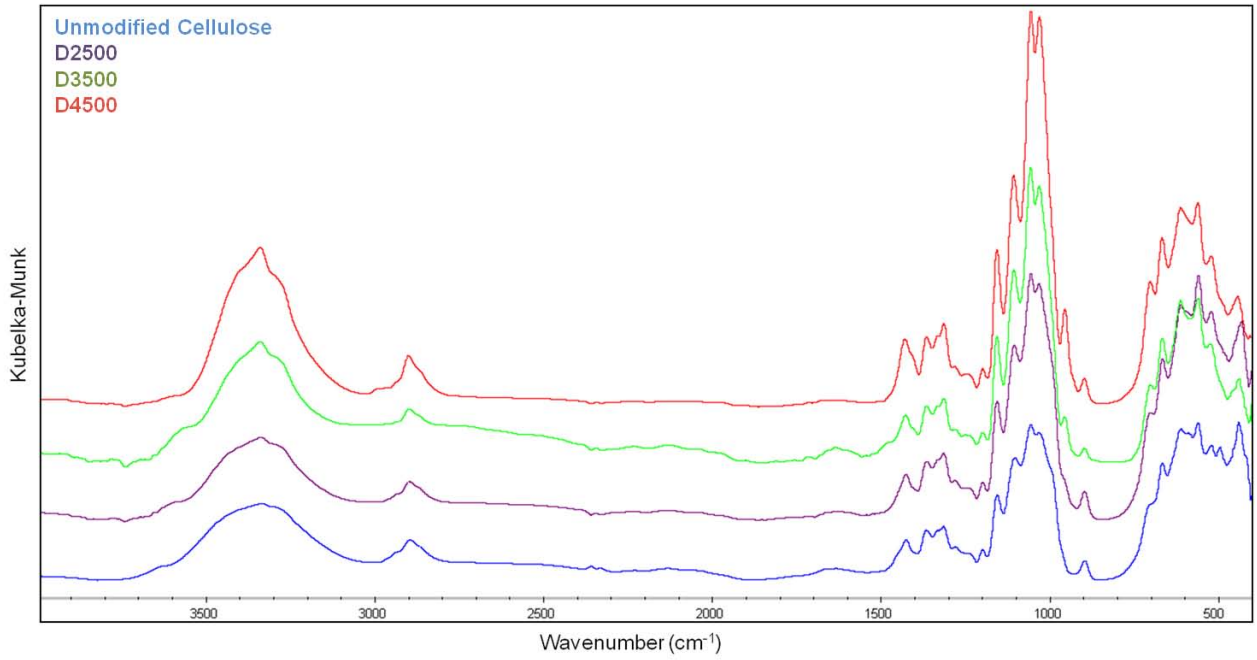

Figure 6-1. DRIFT spectra of unmodified cellulose, cellulose processed in DMSO-supercritical CO_2 at 2500 psi (D2500), 3500 psi (D3500), and 4500 psi (D4500)

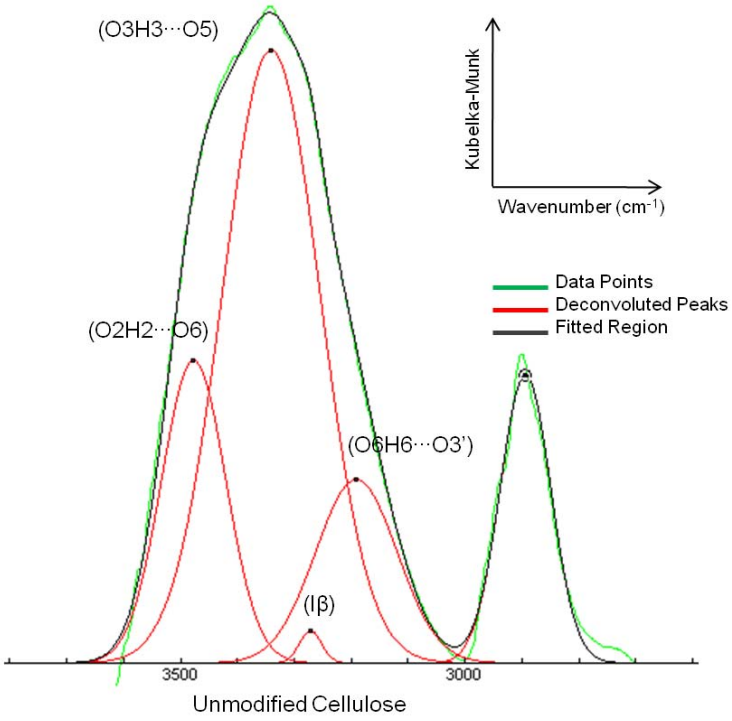

Figure 6-2. Peak deconvolution and assignment of intra-chain and inter-chain hydrogen bonds in unmodified cellulose

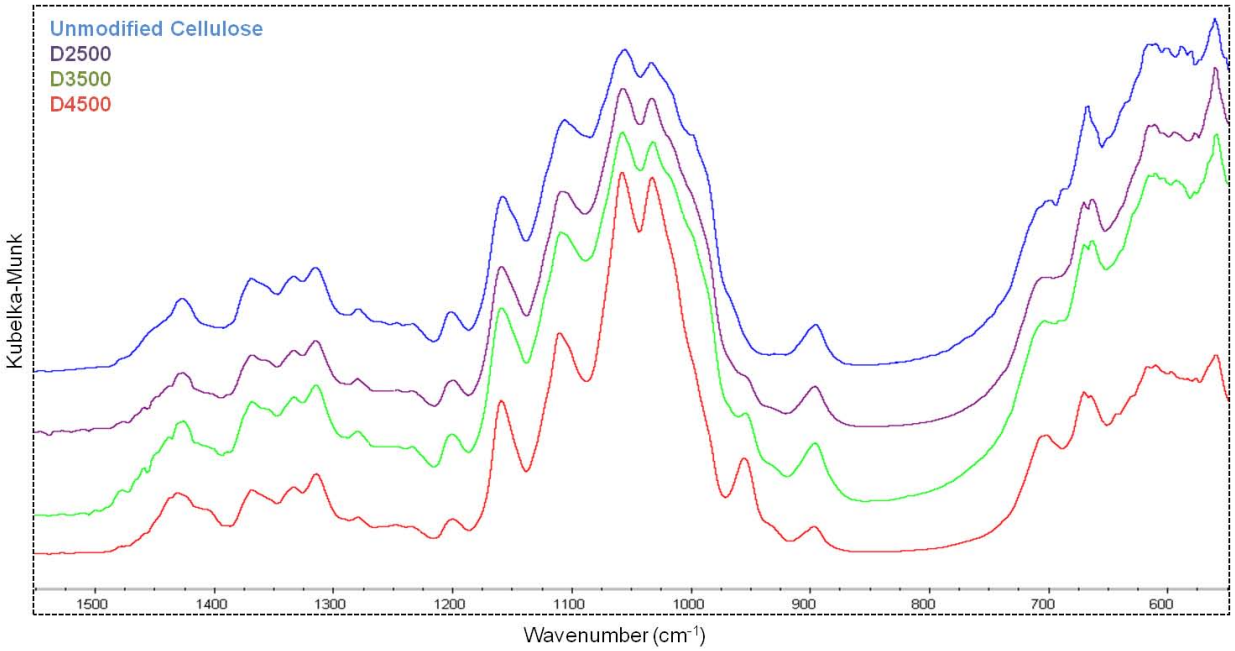

Figure 6-3. DRIFT Spectra (lower wavenumber region) of unmodified cellulose, cellulose processed in DMSO-supercritical CO_2 at 2500 psi (D2500), 3500 psi (D3500), and 4500 psi (D4500)

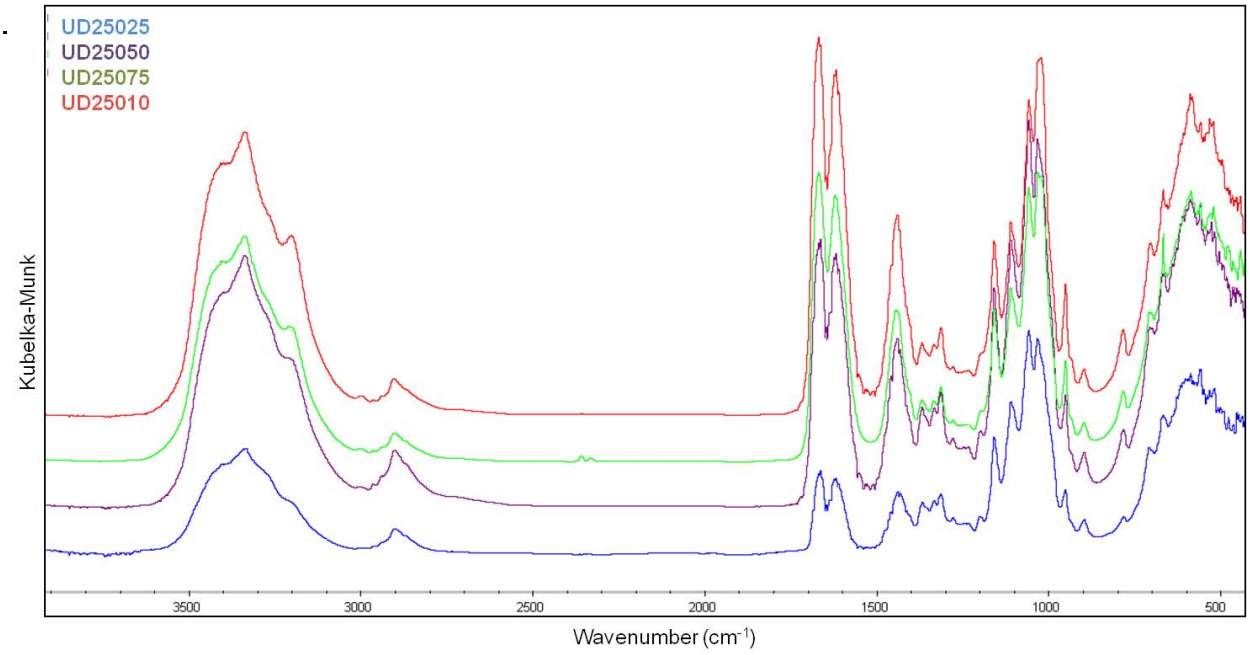

Figure 6-4. DRIFT Spectra of cellulose processed in DMSO-Urea-supercritical CO_2 at 2500 psi with urea content 0.25 g (UD25025), 0.50 g (UD25050), 0.75 g (UD25075), and 1.00 g (UD25010)

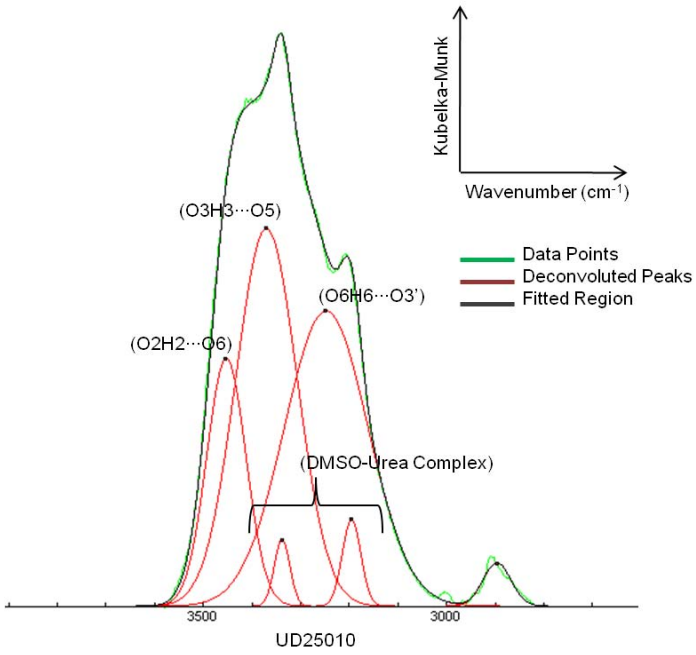

Figure 6-5. Peak deconvolution and assignment of intra-chain and inter-chain hydrogen bonds in cellulose processed in DMSO-Urea-supercritical CO_2 system at 2500 psi with 1.00 g urea content (UD25010)

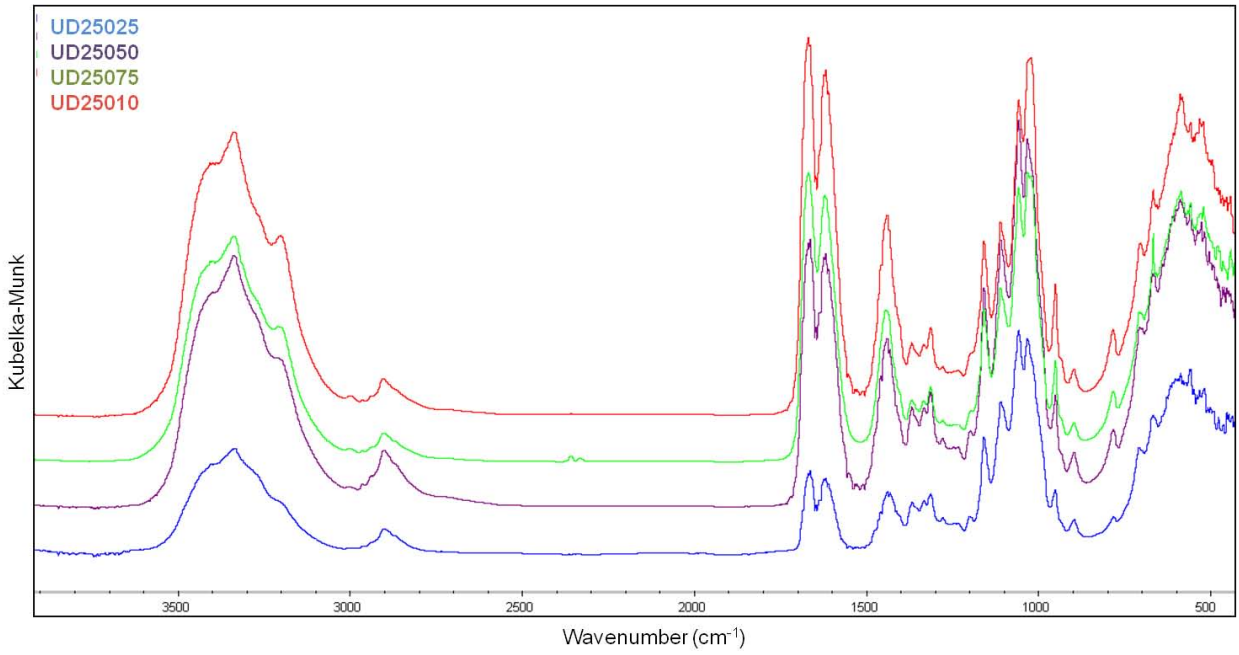

Figure 6-6. DRIFT Spectra (lower wavenumber region) of cellulose processed in DMSO-Urea-supercritical CO_2 at 2500 psi with urea content 0.25 g (UD25025), 0.50 g (UD25050), 0.75 g (UD25075), and 1.00 g (UD25010)

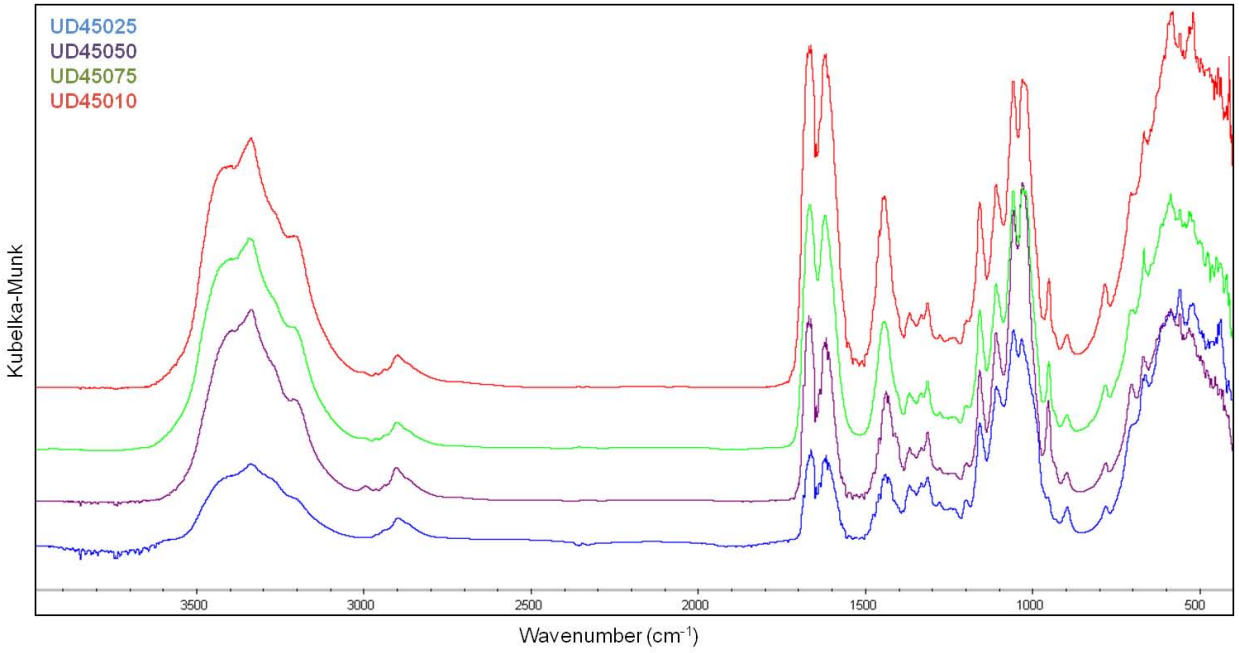

Figure 6-7. DRIFT Spectra of cellulose processed in DMSO-Urea-supercritical CO_2 at 4500 psi with urea content 0.25 g (UD45025), 0.50 g (UD45050), 0.75 g (UD45075), and 1.00 g (UD45010)

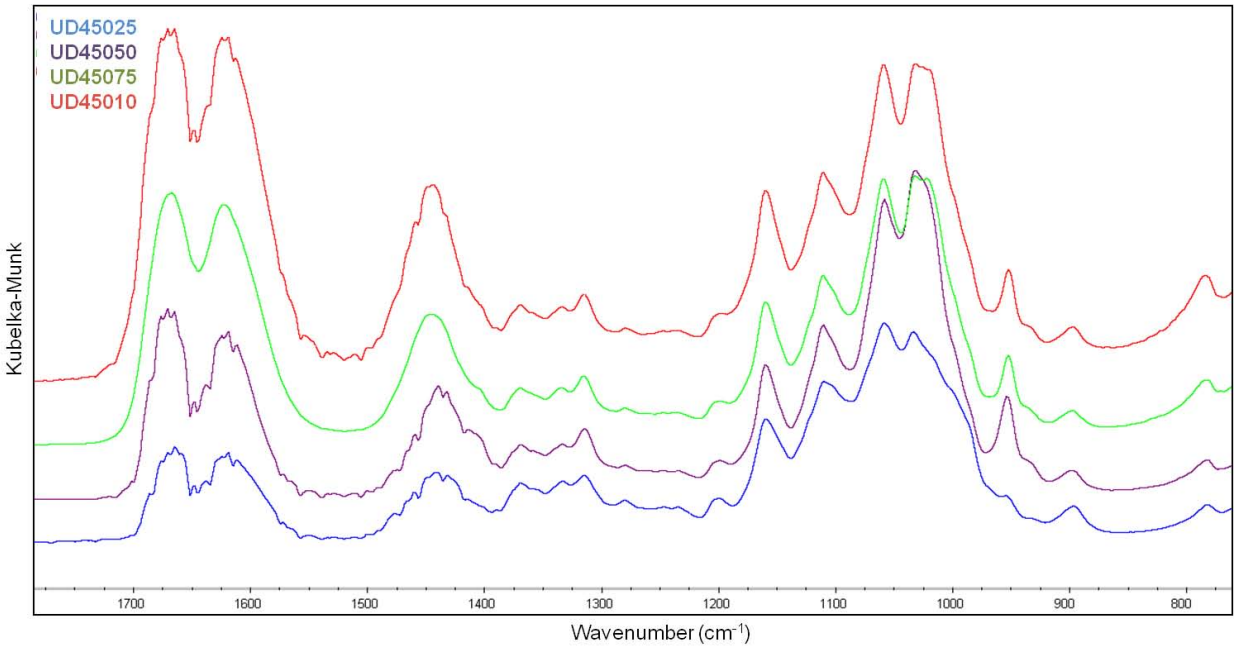

Figure 6-8. DRIFT Spectra (lower wavenumber region) of cellulose processed in DMSO-Urea-supercritical CO_2 at 4500 psi with urea content 0.25 g (UD45025), 0.50 g (UD45050), 0.75 g (UD45075), and 1.00 g (UD45010)

CHAPTER 7
CHARACTERIZATION OF CELLULOSE BY SOLID-STATE ^{13}C NUCLEAR MAGNETIC RESONANCE (NMR)

Solid state ^{13}C cross polarization (CP) Magic Angle Spinning (MAS) Nuclear Magnetic Resonance (NMR) is another commonly used technique to study morphology, and crystalline structure of cellulose[31,41,72,73]. This technique has been found useful to separate the ordered and disordered domains in cellulose[41]. This chapter includes a discussion on the structural changes occurred in batch-processed cellulose samples as measured by solid-state 13C CP MAS NMR technique.

7.1 Nuclear Magnetic Resonance Measurements

The cellulose samples were characterized by conducting solid-state ^{13}C CP MAS NMR experiments. The experiments were performed on a Bruker AVANCE 600 MHz spectrometer operating at field strength of 14 T. A 4.0 mm zircomium oxide rotor was packed with approximately 20 mg of sample. The rotor was spun at 10 kHz and a total 2048 number of scans were taken. Hartmann-Hahn cross polarization and proton decoupling was applied to most of the samples. Samples UD25010 and UD45025 were additionally ran under direct polarization mode. The pulse sequence was timed with a 3 μs proton π/2 pulse, 2 ms proton and carbon contact pulses, 26 ms acquisition time and 3 s relaxation delay. The proton field strength was 80 kHz for proton decoupling. Solid-state MAS ^{13}C NMR was also conducted in direct polarization mode for samples UD25010 and UD45025. In direct polarization mode, all the parameters were kept the same as for cross-polarization mode but the pulse sequence was timed with an 8.5 μs proton π/2 pulse and 10 s relaxation delay. In order to measure the chemical shifts, sample UD25010 was at first internally referenced with signal from DMSO at 39.5 ppm

and then rest of the samples were referenced with the anomeric C1 carbon signal of UD25010.

7.2 Results and Discussion

To identify any measureable changes in molecular interactions of the processed cellulose it is useful to compare its spectra with native cellulose. The experimental solid-state CP MAS NMR spectra of unmodified cellulose, D2500, and D4500 psi are shown in Figure 7-1. On comparison with work by VanderHart and Attala[148], it is verified that the cellulose used was type I and with abundant of the Iβ form. The signals between 60-70 ppm are attributed to C6, between 70-80 ppm to C2, C3, and C5, between 80-90 ppm to C4, and from 98 to 110 ppm to C1 carbon atom of cellulose [148,73,40,149,80,76]. It is found that the chemical shifts of DMSO-supercritical CO_2 processed cellulose did not change relative to the chemical shifts from unmodified cellulose (Table 7-1). The signals at 87 ppm and 64 ppm are assigned to the highly ordered regions of cellulose whereas 82 ppm and 60 ppm are from the disordered regions of C4 and C6 respectively[76,150](Refer Figure 2-10 and Figure 2-11). The disordered region of C4 did not show any effect due to processing. The ratio of ordered to disordered region from the C6 signals in sample D4500 was decreased compared to other samples including unmodified cellulose (Table 7-2). This means that the environment around C6 was changed due to processing in DMSO-CO_2 at 4500 psi. The Anhydroglucose unit C6 can either involved in an inter-chain hydrogen bonding or remains at the surface with lesser constraint. This suggests that the significant increase in amorphous region observed in D4500 by WAXRD (Refer Figure B-3 in Appendix B) was due to the increased number of cellulose chains at the crystallite surface which was caused due to breaking of inter-chain hydrogen bonds O6H6···O3'. The processing effect was not enough to break open

the crystalline structure completely but the cellulose chains at and closer to the surface of cellulose crystallites were affected.

Cellulose samples with urea did not show any change in chemical shifts from unmodified cellulose. This means urea molecules did not interact with cellulose. The ^{13}C NMR spectra of samples D2500 and UD25025 were compared to determine effect of presence of urea on cellulose structure (Figure 7-2). There was no considerable difference found between the two spectra. There is no significant effect on chemical structure of cellulose due to varying amount of urea in cellulose, at fixed CO_2 processing pressure (2500 psi), as shown in Figure 7-3. Effect of the CO_2 processing pressure at fixed quantity of urea is shown in Figure 7-4. In this figure, the disordered region from C4 peak is the same for both the samples whereas the ordered regions from C4 and C6 are larger for the UD45010. From this observation, it can be suggested that the UD25010 is lesser crystalline than UD45010. From calculations for amount of DMSO extracted during depressurization (Appendix D), it was found that samples containing urea retained higher quantities of DMSO than cellulose samples without any urea (Table 7-3). Most of the DMSO was extracted from cellulose samples processed under DMSO and supercritical CO_2. This indicates that DMSO-urea complex formation lowered solubility of DMSO in supercritical CO_2.

The solid-state MAS ^{13}C NMR experiments for UD25010 and UD 45025 were also performed in direct polarization mode (Figure 7-5). The C=O peak from urea was observed in this method which was not found when experiments were conducted in cross-polarization mode. This means that, after processing, urea was still solvated by DMSO and is not interacting directly with the cellulose. Moreover, the DMSO to

carbonyl peak ratio seemed similar in both the samples. This means that the entrapment of DMSO molecules was similarly favored by both the high CO_2 processing pressure and the large urea content.

Table 7-1. ^{13}C NMR – Chemical Shifts of carbon atoms

Sample	C1 (ppm)	C2,3,5 (ppm)	C4 (ppm)		C6 (ppm)	
			Interior	Surface	Interior	Surface
Unmodified Cellulose	104	71	88	84	64	60
D2500	104	71	87	82	62	60
D4500	104	71	87	82	62	60
UD25025	105	71	87	82	62	59
UD25010	104	71	87	82	63	60
UD45010	103	71	87	82	63	60

Table 7-2. C4 and C6 interior to surface height ratio

Sample	C4 Interior to Surface Height Ratio	C6 Interior to Surface Height Ratio
Unmodified Cellulose	2.0	1.8
D2500	2.3	1.8
D4500	1.7	1.5
UD25025	2.6	1.9
UD25010	2.2	1.9
UD45010	2.5	1.8

Table 7-3. Amount of DMSO extracted after batch processing¥

Sample	DMSO Area	Amount of DMSO Extracted** (ml)	DMSO / C=O Area Ratio	Amount of DMSO Extracted*** (ml)
D2500	1.90	4.99	N/A	N/A
D4500	2.60	4.98	N/A	N/A
UD25010*	229.74	3.49	0.50	4.41
UD45025*	195.51	3.71	0.14	4.96

* Direct polarized spectra
**Assuming homogeneous mixing and no cellulose loss during process
***Assuming homogeneous mixing and no urea loss during process
¥ See Appendix D for calculations

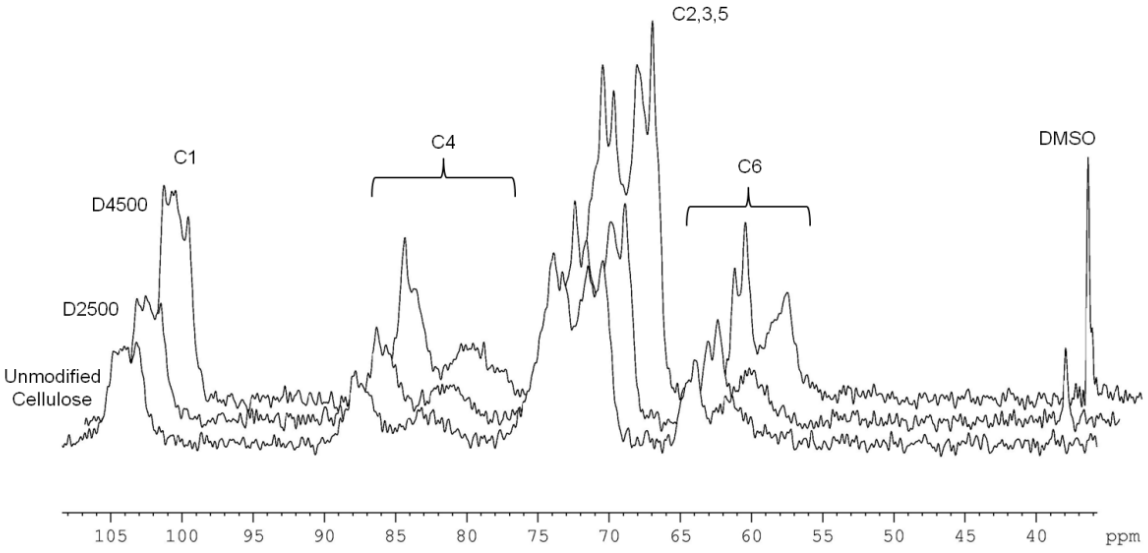

Figure 7-1. ^{13}C CP MAS NMR spectra of unmodified cellulose, cellulose processed in DMSO-supercritical CO_2 at 2500 psi (D2500), and 4500 psi (D4500)

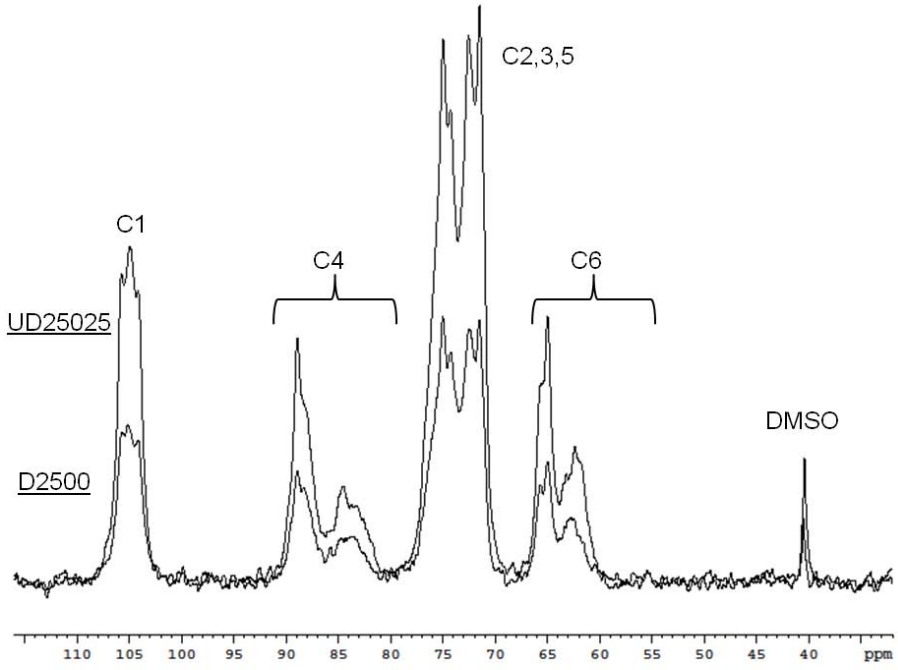

Figure 7-2. ^{13}C CP MAS NMR spectra of cellulose processed in DMSO-supercritical CO_2 at 2500 psi (D2500) and cellulose processed in DMSO-Urea-supercritical CO_2 at 2500 psi and 0.25 g urea (UD25025)

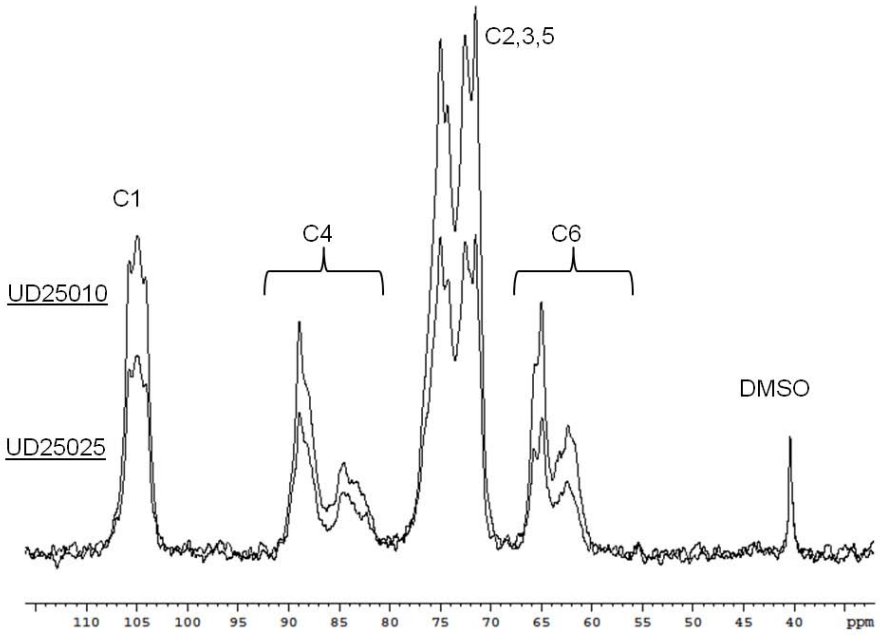

Figure 7-3. ^{13}C CP MAS NMR spectra of cellulose processed in DMSO-Urea-supercritical CO_2 at 2500 psi with urea content of 0.25 g (UD25025) and 1.00 g (UD25010)

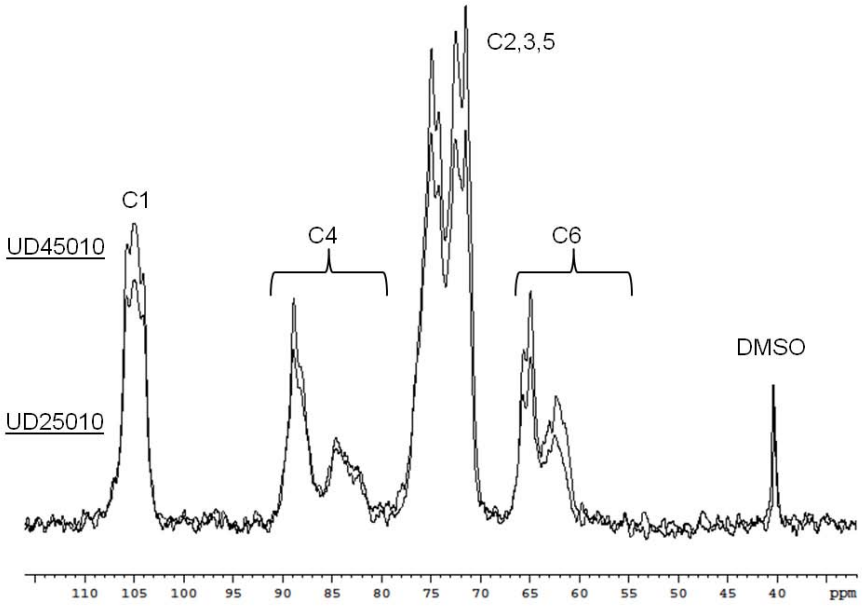

Figure 7-4. ^{13}C CP MAS NMR spectra of cellulose with urea content of 1.00 g after processed in DMSO-Urea-supercritical CO_2 at 2500 psi (UD25010) and 4500 psi (UD45010)

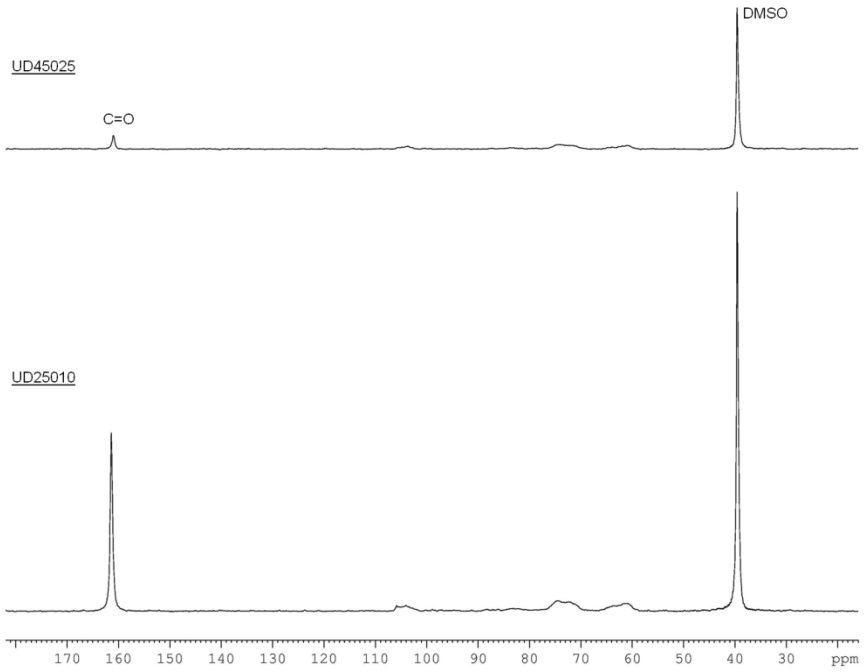

Figure 7-5. Direct Polarized ^{13}C MAS NMR spectra of cellulose with 1.00 g urea processed in DMSO-Urea-supercritical CO_2 at 2500 psi (UD25010) and cellulose with 0.25 g urea processed in DMSO-Urea-supercritical CO_2 at 4500 psi (UD45025)

CHAPTER 8
CONCLUSION AND FUTURE WORK

8.1 Conclusion

Extrusion processing of LDPE-Cellulose blend (70-30) with supercritical CO_2 resulted in improved blend property like 'tensile strength – strain at break' balance compared to a blend processed without supercritical CO_2. Also, strain at break of LDPE-Cellulose blend processed with CO_2 matched to generally more ductile LDPE-Starch blend. Higher strain at break in LDPE-Cellulose blend was caused by plasticization effect of CO_2 mainly on LDPE crystallites. High shear processing resulted in breaking of LDPE crystallites whereas crystalline structure of cellulose was less affected. Thermal analysis showed plasticization of LDPE and cellulose by supercritical CO_2. With these results, it can be concluded that LDPE-Cellulose blends (70/30) processed with supercritical CO_2 can successfully replace LDPE-Starch blends (70/30). In addition, supercritical CO_2 assisted extrusion processing of LDPE-Cellulose blend results in improved blend properties than the blend processed without supercritical CO_2.

An environmentally benign pretreatment method to reduce the relative crystallinity of cellulose by using a combination of solvents viz. DMSO and DMSO-Urea mixture with supercritical CO_2 through a batch reaction was developed. The reason for structural and molecular changes occurred due to batch processing was understood by using powerful characterization techniques viz. WAXRD, DRIFT, and solid-state ^{13}C NMR spectroscopy. Processing under DMSO (and urea) with supercritical CO_2 did not break the crystalline regions of microcrystalline cellulose completely, yet the experiments resulted in significant reduction of the relative crystallinity. A maximum of 40% reduction in relative crystallinity was found when cellulose was processed in DMSO-supercritical

CO_2 system at 4500 psi. The changes in relative crystallinity were caused by plasticization of short-range order – near crystallite surface regions and changes in the hydrogen bonds in cellulose. Processing of microcrystalline cellulose with DMSO (or DMSO-Urea mixture) with supercritical CO_2 caused restructuring of inter-chain and intra-chain hydrogen bonding in cellulose. For cellulose without urea, DMSO molecules primarily interacted around the O2H2···O6 intra-chain hydrogen bond which, in presence of supercritical CO_2, resulted in stretching and weakening of the O6H6···O3' inter-chain hydrogen bond. Over 50% reduction in relative crystallinity was found when cellulose was processed in DMSO-Urea-supercritical CO_2 system. In samples of cellulose with urea, the DMSO-urea complex with supercritical CO_2 caused weakening of O3H3···O5 intra-chain as well as O6H6···O3' inter-chain hydrogen bond. Increase in supercritical CO_2 pressure resulted in deeper penetration of DMSO in cellulose. For urea containing cellulose samples, extraction of DMSO during CO_2 depressurization was affected by the presence of urea and considerable quantities of DMSO was left after completion of the batch process.

8.2 Future Work

Based on above stated results, high shear blending with supercritical CO_2 and batch reactions with DMSO and supercritical CO_2 look promising techniques to make synthetic polymer-cellulose blends and composites. In future, microcrystalline cellulose modified with DMSO (and urea) and supercritical CO_2 can be scaled-up. A two-stage process can be developed – the first stage will involve pretreatment of cellulose by batch processing and the second stage will be supercritical CO_2 assisted twin-screw extrusion of the pretreated cellulose with LDPE and other polymers. Pretreated cellulose samples will have overall reduced crystallinity that, in combination with

supercritical CO_2, are expected to show improved compatibility with the polymer matrix when high shear processing be applied. Biodegradation studies shall also be conducted to determine change in biodegradation rate of LDPE-cellulose blend as an effect of processing. Finally, similar processing experiments can be carried on with higher amount of cellulose (more than 30 wt%) in LDPE-Cellulose blends to expand the envelope to utilize cellulose in making polymer blends.

APPENDIX A
TWIN SCREW EXTRUSION AND INJECTION MOLDING PARAMETERS

Table A-1. Blend composition and extrusion output (g/min)

Sample ID	MC30PE70	MC30PE70CO2	ST30PE70
Blend Composition	LDPE (70 wt%)-Cellulose (30 wt%)	LDPE (70 wt%)-Cellulose (30 wt%)-Supercritical CO_2	LDPE (70 wt%)-Starch (30 wt%)
Output (g/min)	31	41	35

Table A-2. Twin-screw extrusion processing parameters

	Temperature Profile (°C) and Torque (%)											
Sample ID	Zone 1	Zone 2	Zone 3	Zone 4	Zone 5	Zone 6	Zone 7	Zone 8	Zone 9	Zone 10	Die Zone	Torque
MC30PE70	30	90	120	145	180	200	175	145	130	120	120	65-75
MC30PE70CO2	30	90	120	145	180	200	175	145	130	120	120	65-75
ST30PE70	30	90	110	135	165	165	155	145	130	120	120	55-65

Table A-3. Injection molding parameters

Sample ID	LDPE	MC30PE70	MC30PE70CO2	ST30PE70
Injection Time (s)	0.9	1.1	1.1	1.6
Injection Pressure (bar)	70	80	80	75
Injection Speed (mm/s)	75	85	85	75
Holding Time (s)	10	10	10	10
Holding Pressure (bar)	20	20	20	20
Cooling Time (s)	20	20	20	20
Screw Rotation Speed (rpm)	150	150	150	150
Screw Retraction (mm)	53	58	58	58
Dosing Stop (mm)	50	55	55	55
Cushion (mm)	15	15	15.5	13
Switch Over Time (s)	0.9	1.1	1.1	1.6

Table A-4. Temperature profile for injection molding (°C)

Zone 1	Zone 2	Zone 3	Zone 4	Nozzle	Sprue	Mold
20	90	140	155	160	65	30

APPENDIX B
X-RAY DIFFRACTION SPECTRA

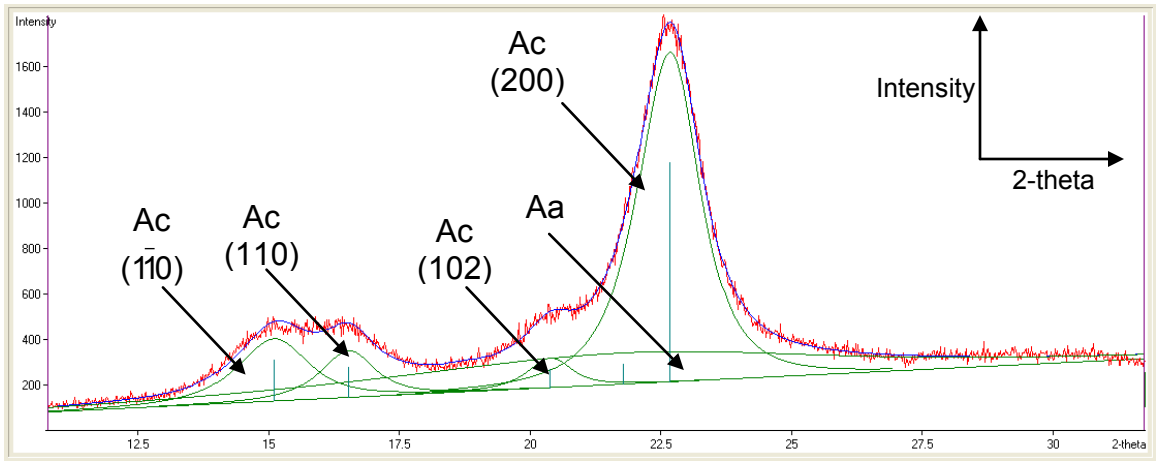

Figure B-1. XRD spectrum of unmodified cellulose

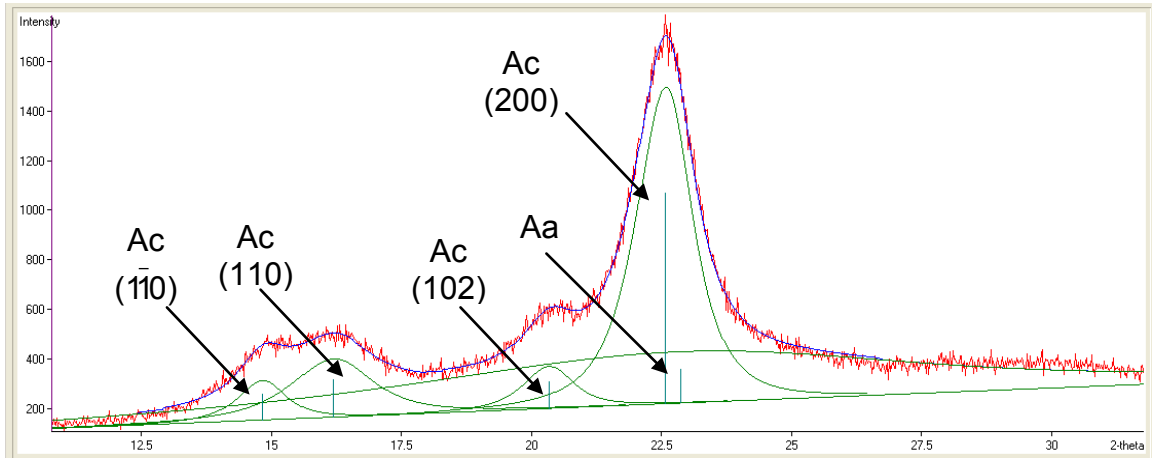

Figure B-2. XRD spectrum of cellulose processed in DMSO-supercritical CO_2 at 2500 psi (D2500)

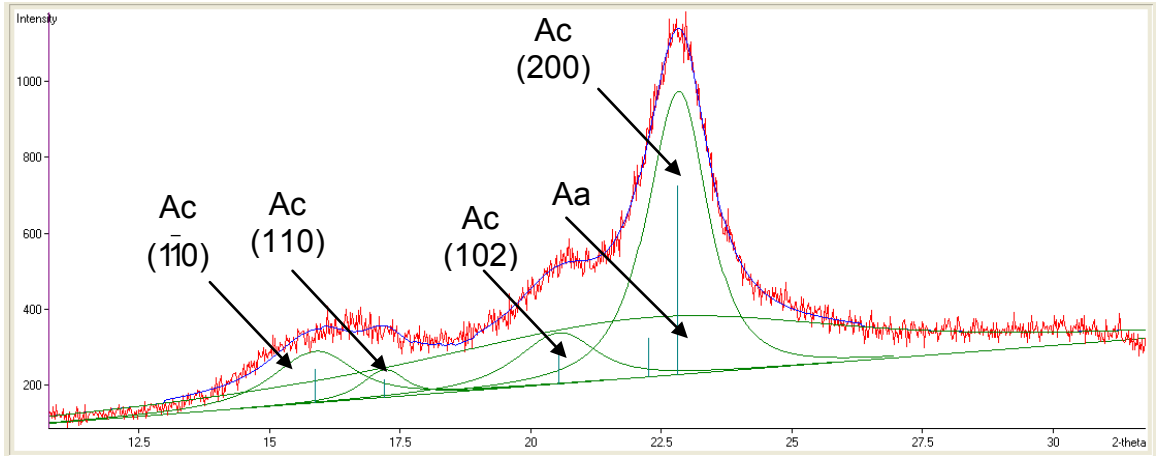

Figure B-3. XRD spectrum of cellulose processed in DMSO-supercritical CO_2 at 4500 psi (D4500)

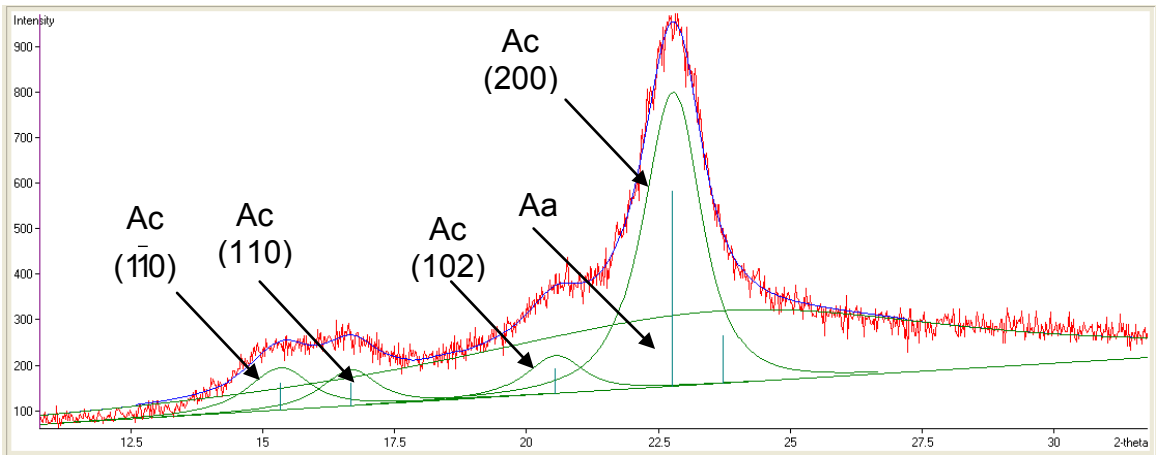

Figure B-4. XRD spectrum of cellulose processed in DMSO-Urea-supercritical CO_2 at 2500 psi and 0.25 g urea (UD25025)

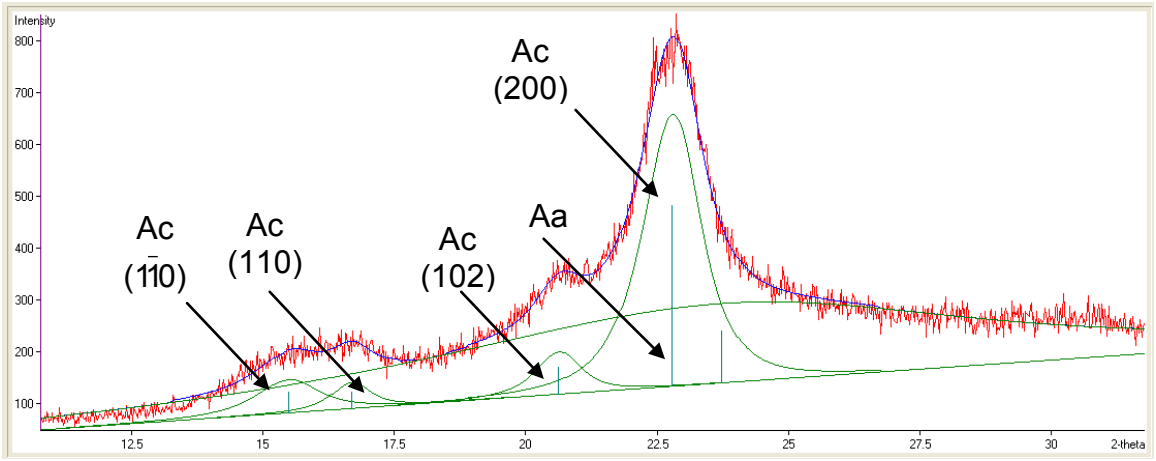

Figure B-5. XRD spectrum of cellulose processed in DMSO-Urea-supercritical CO_2 at 2500 psi and 0.50 g urea (UD25050)

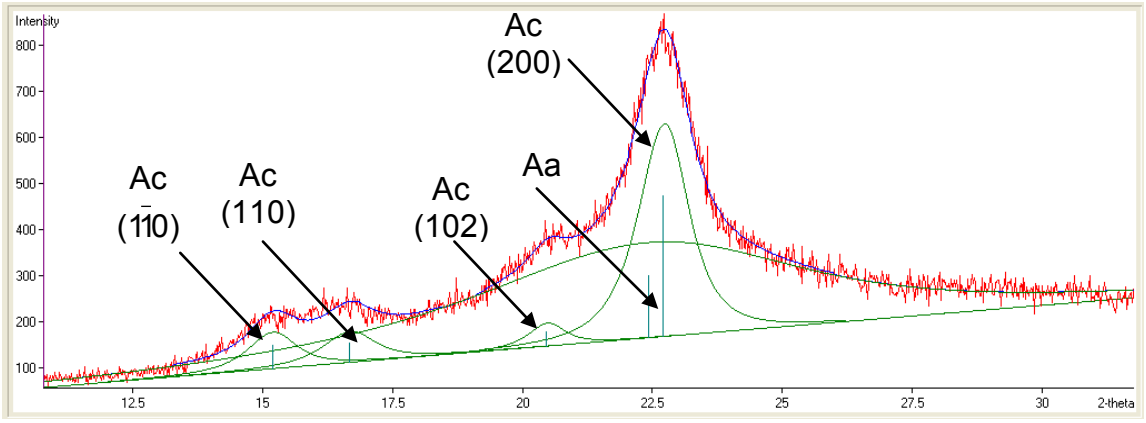

Figure B-6. XRD spectrum of cellulose processed in DMSO-Urea-supercritical CO_2 at 2500 psi and 0.75 g urea (UD25075)

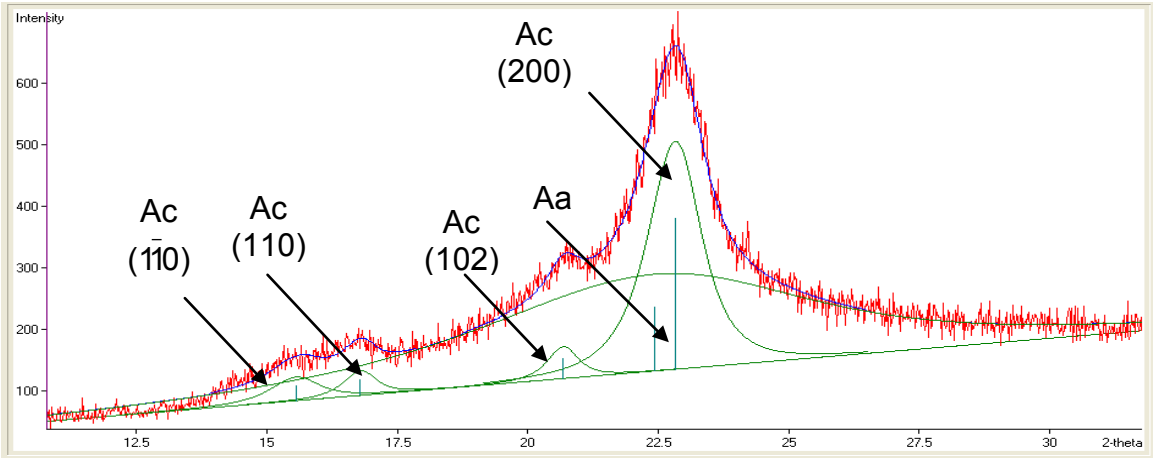

Figure B-7. XRD spectrum of cellulose processed in DMSO-Urea-supercritical CO_2 at 2500 psi and 1.00 g urea (UD25010)

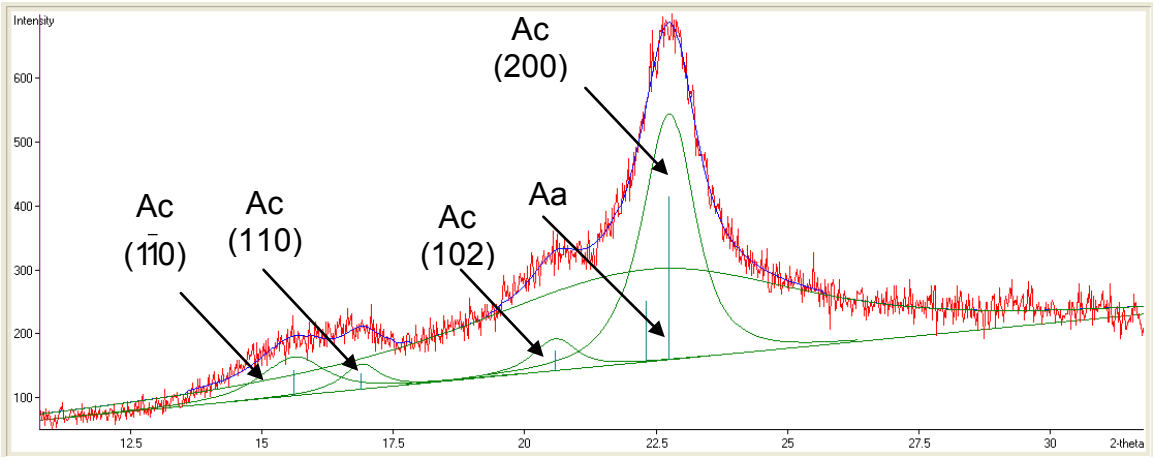

Figure B-8. XRD spectrum of cellulose processed in DMSO-Urea-supercritical CO_2 at 4500 psi and 0.25 g urea (UD45025)

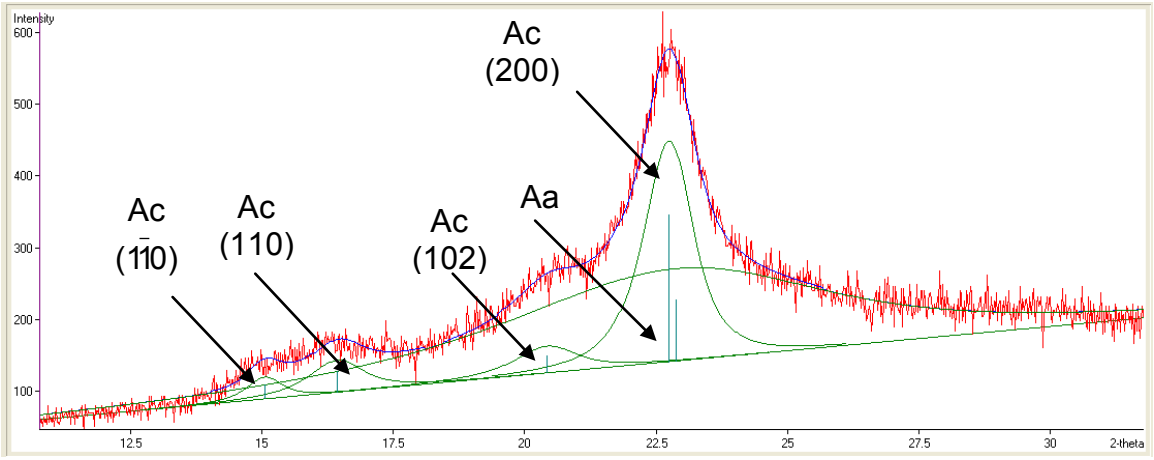

Figure B-9. XRD spectrum of cellulose processed in DMSO-Urea-supercritical CO_2 at 4500 psi and 0.50 g urea (UD45050)

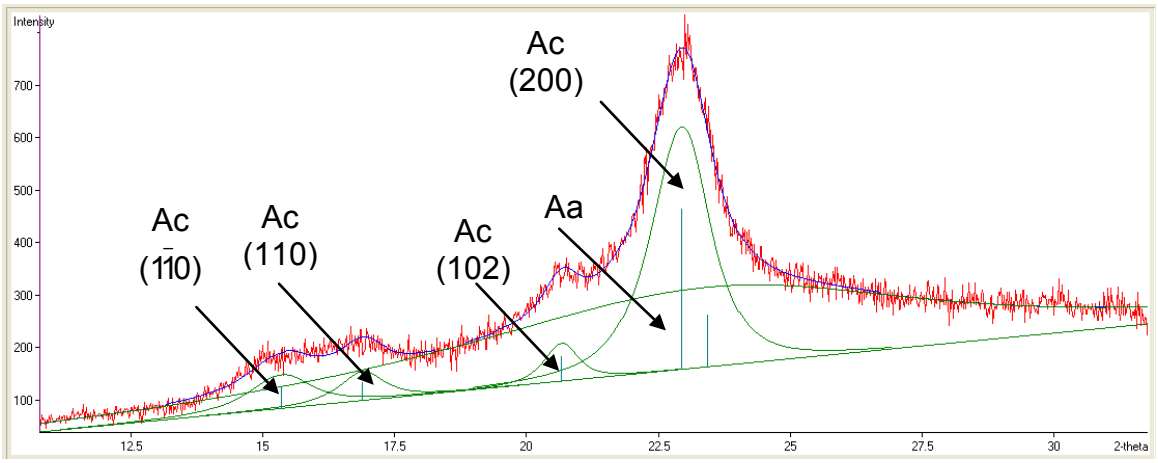

Figure B-10. XRD spectrum of cellulose processed in DMSO-Urea-supercritical CO2 at 4500 psi and 0.75 g urea (UD45075)

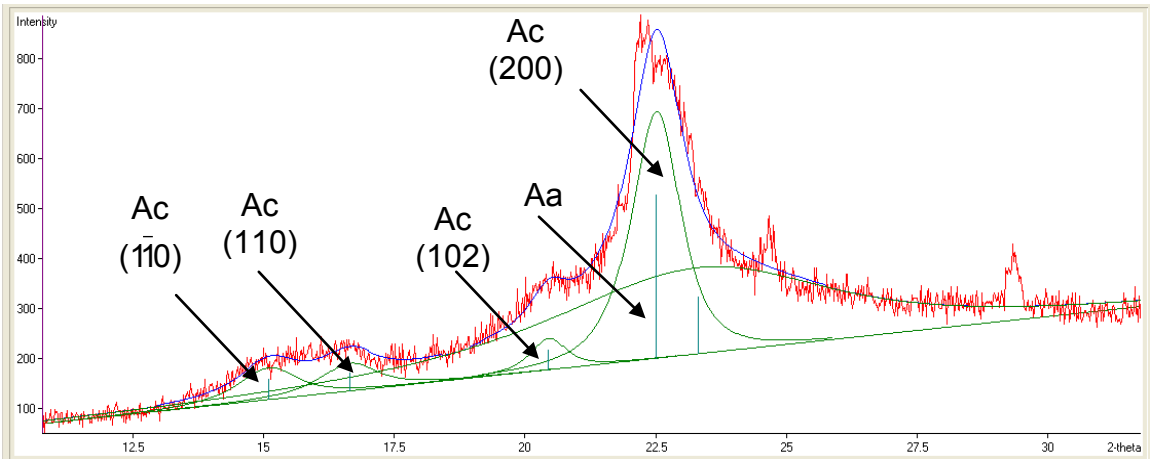

Figure B-11. XRD spectrum of cellulose processed in DMSO-Urea-supercritical CO_2 at 4500 psi and 1.00 g urea (UD45010)

APPENDIX C
DRIFT – HYDROGEN BONDING DECONVOLUTED REGIONS

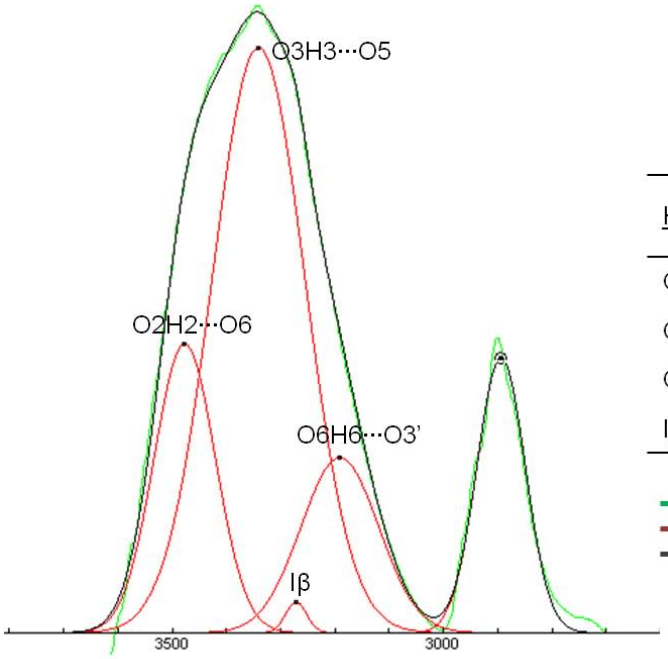

Hydrogen Bond	Type of Hydrogen Bond
O2H2···O6	Intramolecular
O3H3···O5	Intramolecular
O6H6···O3'	Intermolecular
Iβ	Hydrogen Bond

Data Points
Deconvoluted Peaks
Fitted Region

Figure C-1. DRIFT spectra of unmodified cellulose

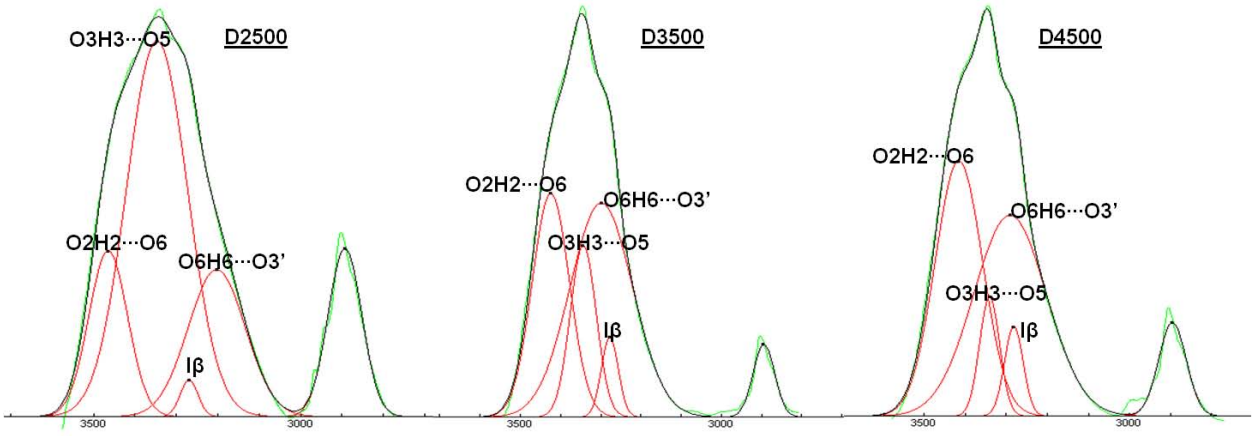

Figure C-2. DRIFT spectra of hydrogen bonding region of cellulose processed in DMSO-supercritical CO_2 at 2500 psi (D2500), 3500 psi (D3500), and 4500 psi (D4500)

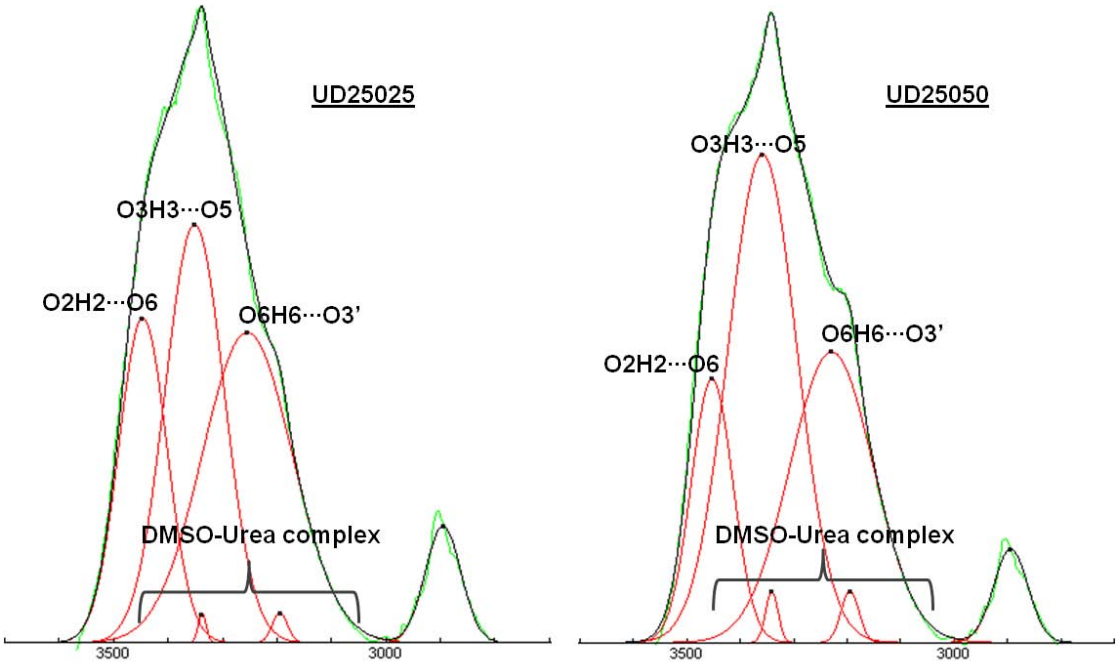

Figure C-3. DRIFT spectra of hydrogen bonding region of cellulose processed in DMSO-Urea-supercritical CO_2 at 2500 psi with urea content 0.25 g (UD25025) and 0.50 g (UD25050)

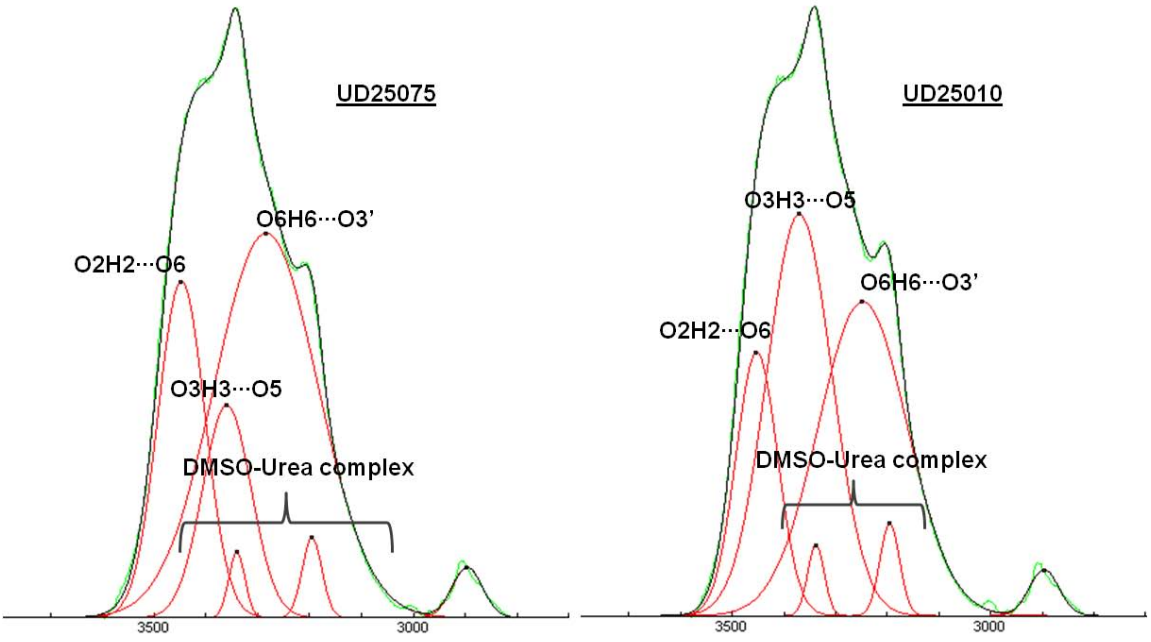

Figure C-4. DRIFT spectra of hydrogen bonding region of cellulose processed in DMSO-Urea-supercritical CO_2 at 2500 psi with urea content 0.75 g (UD25075) and 1.00 g (UD25010)

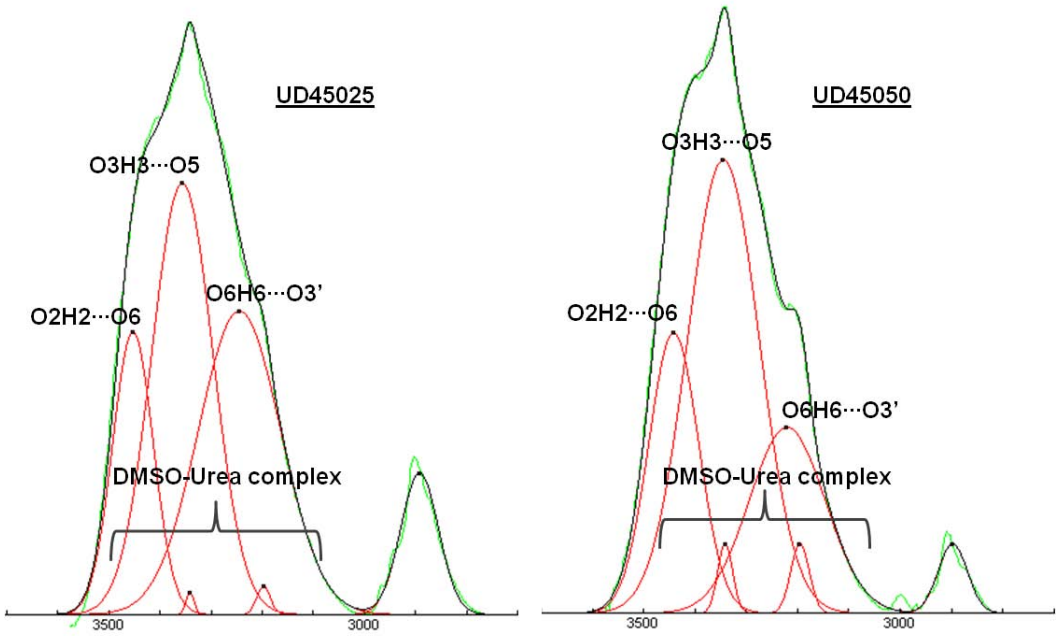

Figure C-5. DRIFT spectra of hydrogen bonding region of cellulose processed in DMSO-Urea-supercritical CO_2 at 4500 psi with urea content 0.25 g (UD45025) and 0.50 g (UD45050)

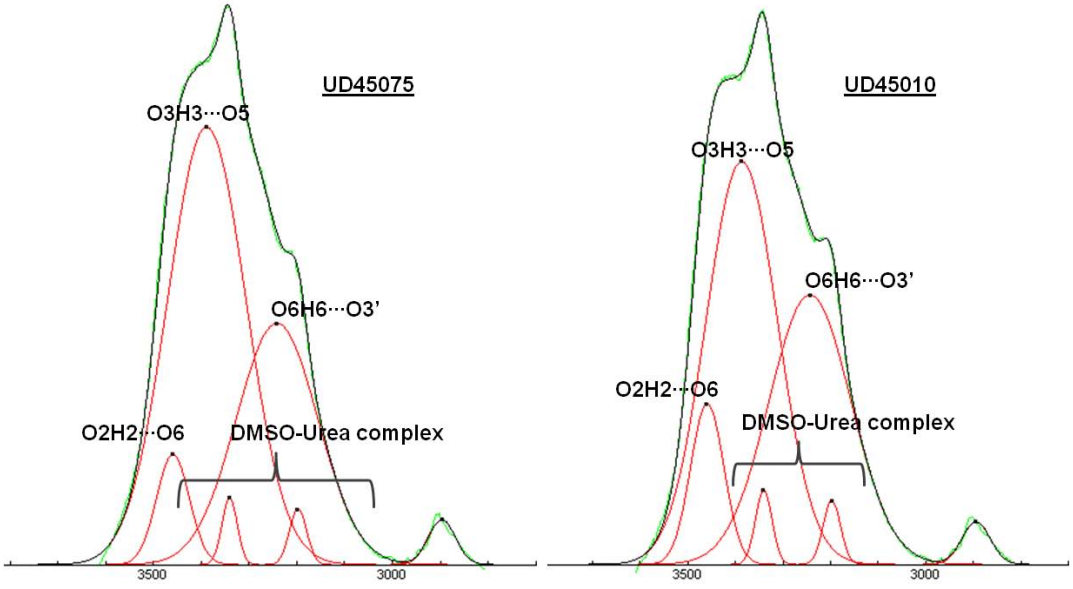

Figure C-6. DRIFT spectra of hydrogen bonding region of cellulose processed in DMSO-Urea-supercritical CO_2 at 4500 psi with urea content 0.75 g (UD45075) and 1.00 g (UD45010)

APPENDIX D
CALCULATIONS FOR AMOUNT OF DMSO EXTRACTED

Table D-1. Amount of materials and respective molar quantity

Material	Amount used	Moles
Cellulose	1.5 g	0.0093
Urea	0.25 to 1.0 g	0.0042 to 0.0167
DMSO	5 ml	0.0704

(a) For samples processed in DMSO-supercritical CO_2* –

No. of moles of DMSO extracted = Initial no. of moles of DMSO – (Integral Area of DMSO peak at 39.5 ppm x no. of moles of cellulose)

*Assuming homogeneous mixing and no cellulose loss during process

(b) For samples processed in DMSO-Urea-supercritical CO_2** –

No. of moles of DMSO extracted = Initial no. of moles of DMSO – (Integral Area of DMSO peak at 39.5 ppm x no. of moles of Urea)

**Assuming homogeneous mixing and no urea loss during process

Amount of DMSO extracted from each (a) and (b) = (No. of moles of DMSO extracted x 0.01408) ml

LIST OF REFERENCES

1. Gross, R. A.; Kalra, B., Biodegradable Polymers for the Environment. *Science* **2002,** *297* (5582), 803-807.

2. Briassoulis, D., An Overview on the Mechanical Behaviour of Biodegradable Agricultural Films. *Journal of Polymers and the Environment* **2004,** *12* (2), 65-81.

3. Klemm, D.; Heublein, B.; Fink, H.-P.; Bohn, A., Cellulose: Fascinating Biopolymer and Sustainable Raw Material. *Angewandte Chemie International Edition* **2005,** *44* (22), 3358-3393.

4. Averous, L.; Boquillon, N., Biocomposites based on plasticized starch: thermal and mechanical behaviours. *Carbohydrate Polymers* **2004,** *56* (2), 111-122.

5. Ramos, L. P., The chemistry involved in the steam treatment of lignocellulosic materials. *Química Nova* **2003,** *26*, 863-871.

6. Deguchi, S.; Tsujii, K.; Horikoshi, K., Cooking cellulose in hot and compressed water. *Chemical Communications* **2006,** (31), 3293-3295.

7. Zhang, J.; Zhang, J.; Lin, L.; Chen, T.; Zhang, J.; Liu, S.; Li, Z.; Ouyang, P., Dissolution of Microcrystalline Cellulose in Phosphoric Acid—Molecular Changes and Kinetics. *Molecules* **2009,** *14* (12), 5027-5041.

8. Nalawade, S. P.; Picchioni, F.; Janssen, L. P. B. M., Supercritical carbon dioxide as a green solvent for processing polymer melts: Processing aspects and applications. *Progress in Polymer Science* **2006,** *31* (1), 19-43.

9. Aminabhavi, T. M.; Gopalakrishna, B., Density, Viscosity, Refractive Index, and Speed of Sound in Aqueous Mixtures of N,N-Dimethylformamide, Dimethyl Sulfoxide, N,N-Dimethylacetamide, Acetonitrile, Ethylene Glycol, Diethylene Glycol, 1,4-Dioxane, Tetrahydrofuran, 2-Methoxyethanol, and 2-Ethoxyethanol at 298.15 K. *Journal of Chemical & Engineering Data* **1995,** *40* (4), 856-861.

10. Krässig, H., *Cellulose: structure, accessibility, and reactivity*. Gordon and Breach Science: 1993.

11. Kim, K. H.; Hong, J., Supercritical CO2 pretreatment of lignocellulose enhances enzymatic cellulose hydrolysis. *Bioresource Technology* **2001,** *77* (2), 139-144.

12. Taherzadeh, M.; Karimi, K., Pretreatment of Lignocellulosic Wastes to Improve Ethanol and Biogas Production: A Review. *International Journal of Molecular Sciences* **2008,** *9* (9), 1621-1651.

13. Fernandez Cid, M. V.; Gerstner, K. N.; van Spronsen, J.; van der Kraan, M.; Veugelers, W. J. T.; Woerlee, G. F.; Witkamp, G. J., Novel Process to Enhance the Dyeability of Cotton in Supercritical Carbon Dioxide. *Textile Research Journal* **2007,** *77* (1), 38-46.

14. Markarian, S. A.; Gabrielyan, L. S.; Grigoryan, K. R., FT IR ATR Study of Molecular Interactions in the Urea/Dimethyl Sulfoxide and Urea/Diethyl Sulfoxide Binary Systems. *Journal of Solution Chemistry* **2004,** *33* (8), 1005-1015.

15. Catchpole, O. J.; Tallon, S. J.; Dyer, P. J.; Lan, J. S.; Jensen, B.; Rasmussen, O. K.; Grey, J. B., Measurement and modelling of urea solubility in supercritical CO2 and CO2 + ethanol mixtures. *Fluid Phase Equilibria* **2005,** *237* (1-2), 212-218.

16. Nada, A.-A. M. A.; Kamel, S.; El-Sakhawy, M., Thermal behaviour and infrared spectroscopy of cellulose carbamates. *Polymer Degradation and Stability* **2000,** *70* (3), 347-355.

17. Rajasingam, R.; Lioe, L.; Pham, Q. T.; Lucien, F. P., Solubility of carbon dioxide in dimethylsulfoxide and N-methyl-2-pyrrolidone at elevated pressure. *The Journal of Supercritical Fluids* **2004,** *31* (3), 227-234.

18. Vega Gonzalez, A.; Tufeu, R.; Subra, P., High-Pressure Vapor−Liquid Equilibrium for the Binary Systems Carbon Dioxide + Dimethyl Sulfoxide and Carbon Dioxide + Dichloromethane. *Journal of Chemical & Engineering Data* **2002,** *47* (3), 492-495.

19. Kovalenko. V. I, K. V. I., ChemInform Abstract: Crystalline Cellulose: Structure and Hydrogen Bonds. *ChemInform* **2010,** *41* (34).

20. Klemm, D.; Schmauder, H.-P.; Heinze, T., *Cellulose*. Wiley-VCH Verlag GmbH & Co. KGaA: 2005.

21. Miller, S. A.; Landis, A. E.; Theis, T. L., Feature: Environmental Trade-offs of Biobased Production. *Environmental Science & Technology* **2007,** *41* (15), 5176-5182.

22. Muradov, N. Z.; Veziroglu, T. N., "Green" path from fossil-based to hydrogen economy: An overview of carbon-neutral technologies. *International Journal of Hydrogen Energy* **2008,** *33* (23), 6804-6839.

23. Sudesh, K.; Iwata, T., Sustainability of Biobased and Biodegradable Plastics. *CLEAN – Soil, Air, Water* **2008,** *36* (5-6), 433-442.

24. Steinbüchel, A., Non-biodegradable biopolymers from renewable resources: perspectives and impacts. *Current Opinion in Biotechnology* **2005,** *16* (6), 607-613.

25. Yosita Rudeekit, J. N., Monchai Tajan, Phasawat Chaiwutthinan, Thanawadee Leejarkpai, Determinin Biodegradability of Polylactic Acid under Different Environments. *Journal of Metals, Materials and Minerals* **2008,** *18* (2), 83-87.

26. Schacht, C.; Zetzl, C.; Brunner, G., From plant materials to ethanol by means of supercritical fluid technology. *The Journal of Supercritical Fluids* **2008,** *46* (3), 299-321.

27. Satyanarayana, D.; Chatterji, P. R., Biodegradable Polymers: Challenges and Strategies. **1993,** *33* (3), 349 - 368.

28. O'Sullivan, A., Cellulose: the structure slowly unravels. *Cellulose* **1997,** *4* (3), 173-207.

29. Zhang, Y.; Lynd, L., Toward an aggregated understanding of enzymatic hydrolysis of cellulose: Noncomplexed cellulase systems. *Biotechnol Bioeng* **2004,** *88*, 797 - 824.

30. Garvey, C. J.; Parker, I. H.; Simon, G. P., On the Interpretation of X-Ray Diffraction Powder Patterns in Terms of the Nanostructure of Cellulose I Fibres. *Macromolecular Chemistry and Physics* **2005,** *206* (15), 1568-1575.

31. Newman, R. H., Estimation of the lateral dimensions of cellulose crystallites using 13C NMR signal strengths. *Solid State Nuclear Magnetic Resonance* **1999,** *15* (1), 21-29.

32. Müller, M.; Czihak, C.; Schober, H.; Nishiyama, Y.; Vogl, G., All Disordered Regions of Native Cellulose Show Common Low-Frequency Dynamics. *Macromolecules* **2000,** *33* (5), 1834-1840.

33. Kondo, T.; Sawatari, C.; Manley, R. S. J.; Gray, D. G., Characterization of hydrogen bonding in cellulose-synthetic polymer blend systems with regioselectively substituted methylcellulose. *Macromolecules* **1994,** *27* (1), 210-215.

34. Ilharco, L. M.; Garcia, A. R.; Lopes da Silva, J.; Vieira Ferreira, L. F., Infrared Approach to the Study of Adsorption on Cellulose: Influence of Cellulose Crystallinity on the Adsorption of Benzophenone. *Langmuir* **1997,** *13* (15), 4126-4132.

35. Scott, G., *Degradable polymers: principles and applications*. Kluwer Academic Publishers: 2002.

36. Vo, L. T. T.; Siroká, B.; Manian, A. P.; Bechtold, T., Functionalisation of cellulosic substrates by a facile solventless method of introducing carbamate groups. *Carbohydrate Polymers* **2010,** *82* (4), 1191-1197.

37. Simon, J.; Müller, H. P.; Koch, R.; Müller, V., Thermoplastic and biodegradable polymers of cellulose. *Polymer Degradation and Stability* **1998,** *59* (1-3), 107-115.

38. Agarwal, U.; Reiner, R.; Ralph, S., Cellulose I crystallinity determination using FT–Raman spectroscopy: univariate and multivariate methods. *Cellulose* **2010,** *17* (4), 721-733.

39. Sun, S.; Mitchell, J. R.; MacNaughtan, W.; Foster, T. J.; Harabagiu, V.; Song, Y.; Zheng, Q., Comparison of the Mechanical Properties of Cellulose and Starch Films. *Biomacromolecules* **2009,** *11* (1), 126-132.

40. Liu, C.-F.; Ren, J.-L.; Xu, F.; Liu, J.-J.; Sun, J.-X.; Sun, R.-C., Isolation and Characterization of Cellulose Obtained from Ultrasonic Irradiated Sugarcane Bagasse. *Journal of Agricultural and Food Chemistry* **2006,** *54* (16), 5742-5748.

41. Gerhard Zuckerstätter, G. S., PetraWollboldt, Thomas Röder, Hedda K. Weber, and Herbert Sixta, The Elucidation of Cellulose Supermolecular Structure by 13C CP-MAS NMR *Lenzinger Berichte* **2009,** *87*, 38-46.

42. Wada, M.; Okano, T.; Sugiyama, J., Synchrotron-radiated X-ray and neutron diffraction study of native cellulose. *Cellulose* **1997,** *4* (3), 221-232.

43. Saka, S., Recent progress in supercritical fluid science for biofuel production from woody biomass. *Forestry Studies in China* **2006,** *8* (3), 9-15.

44. Heinze, T.; Koschella, A., Solvents applied in the field of cellulose chemistry: a mini review. *Polímeros* **2005,** *15*, 84-90.

45. Heinze, T.; Liebert, T., Unconventional methods in cellulose functionalization. *Progress in Polymer Science* **2001,** *26* (9), 1689-1762.

46. Liebert, T., Cellulose Solvents - Remarkable History, Bright Future. In *Cellulose Solvents: For Analysis, Shaping and Chemical Modification*, American Chemical Society: 2010; Vol. 1033, pp 3-54.

47. (a) Fukaya, Y.; Hayashi, K.; Wada, M.; Ohno, H., Cellulose dissolution with polar ionic liquids under mild conditions: required factors for anions. *Green Chemistry* **2008,** *10* (1), 44-46; (b) Zhu, S., Use of ionic liquids for the efficient utilization of lignocellulosic materials. *Journal of Chemical Technology & Biotechnology* **2008,** *83* (6), 777-779.

48. Ostlund A.; Lundberg, D.; Nordstierna, L.; Holmberg, K. ; Nyden, M., Dissolution and Gelation of Cellulose in TBAF/DMSO Solutions: The Roles of Fluoride Ions and Water. *Biomacromolecules* **2009,** *10* (9), 2401-2407.

49. Flieger, M.; Kantorov; aacute; , M.; Prell, A.; Rezanka, T.; Votruba, J., *Biodegradable plastics from renewable sources*. 2003; Vol. 48, p 27-44.

50. D. R. Lu, C. M. X., S. J. Xu, Starch-based completely biodegradable polymer materials. *eXPRESS Polymer Letters* **2009,** *3* (6), 366-375.

51. Peressini, D.; Bravin, B.; Lapasin, R.; Rizzotti, C.; Sensidoni, A., Starch-methylcellulose based edible films: rheological properties of film-forming dispersions. *Journal of Food Engineering* **2003,** *59* (1), 25-32.

52. Vroman, I.; Tighzert, L., Biodegradable Polymers. *Materials* **2009,** *2* (2), 307-344.

53. Ratto, J. A.; Stenhouse, P. J.; Auerbach, M.; Mitchell, J.; Farrell, R., Processing, performance and biodegradability of a thermoplastic aliphatic polyester/starch system. *Polymer* **1999,** *40* (24), 6777-6788.

54. Mani, R.; Bhattacharya, M., Properties of injection moulded blends of starch and modified biodegradable polyesters. *European Polymer Journal* **2001,** *37* (3), 515-526.

55. Schenzel, K.; Fischer, S.; Brendler, E., New method for determining the degree of cellulose I crystallinity by means of FT Raman spectroscopy. *Cellulose* **2005,** *12*, 223 - 231.

56. Bansal, P.; Hall, M.; Realff, M. J.; Lee, J. H.; Bommarius, A. S., Multivariate statistical analysis of X-ray data from cellulose: A new method to determine degree of crystallinity and predict hydrolysis rates. *Bioresource Technology* **2010,** *101* (12), 4461-4471.

57. Park, S.; Baker, J.; Himmel, M.; Parilla, P.; Johnson, D., Cellulose crystallinity index: measurement techniques and their impact on interpreting cellulase performance. *Biotechnology for Biofuels* **2010,** *3* (1), 10.

58. Segal, L.; Creely, J.; Martin, A.; Conrad, C., An empirical method for estimating the degree of crystallinity of native cellulose using the x-ray diffractometer. *Tex Res J* **1962,** *29*, 786 - 794.

59. Thygesen, A.; Oddershede, J.; Lilholt, H.; Thomsen, A.; Stahl, K., On the determination of crystallinity and cellulose content in plant fibres. *Cellulose* **2005,** *12*, 563 - 576.

60. Michell, A. J., Second-derivative F.t.-i.r. spectra of native celluloses. *Carbohydrate Research* **1990,** *197*, 53-60.

61. Lewis, D. M.; Wang, J. C., The use of fourier transform infrared (FT-IR) spectroscopy to study the state of heterobifunctional reactive dyes. *Dyes and Pigments* **1998,** *39* (2), 111-123.

62. Fengel, D., Influence of Water on the OH Valency Range in Deconvoluted FTIR Spectra of Cellulose. *Holzforschung* **1993,** *47* (2), 103-108.

63. Saalwachter, K.; Burchard, W.; Klufers, P.; Kettenbach, G.; Mayer, P.; Klemm, D.; Dugarmaa, S., Cellulose Solutions in Water Containing Metal Complexes†. *Macromolecules* **2000,** *33* (11), 4094-4107.

64. Fengel, D.; Jakob, H.; Strobel, C., Influence of the Alkali Concentration on the Formation of Cellulose II. Study by X-Ray Diffraction and FTIR Spectroscopy. *Holzforschung* **1995,** *49* (6), 505-511.

65. Oh, S. Y.; Yoo, D. I.; Shin, Y.; Kim, H. C.; Kim, H. Y.; Chung, Y. S.; Park, W. H.; Youk, J. H., Crystalline structure analysis of cellulose treated with sodium hydroxide and carbon dioxide by means of X-ray diffraction and FTIR spectroscopy. *Carbohydrate Research* **2005,** *340* (15), 2376-2391.

66. Yin, C.; Li, J.; Xu, Q.; Peng, Q.; Liu, Y.; Shen, X., Chemical modification of cotton cellulose in supercritical carbon dioxide: Synthesis and characterization of cellulose carbamate. *Carbohydrate Polymers* **2007,** *67* (2), 147-154.

67. Gardner, K. H.; Blackwell, J., The hydrogen bonding in native cellulose. *Biochimica et Biophysica Acta (BBA) - General Subjects* **1974,** *343* (1), 232-237.

68. Maréchal, Y.; Chanzy, H., The hydrogen bond network in I[beta] cellulose as observed by infrared spectrometry. *Journal of Molecular Structure* **2000,** *523* (1-3), 183-196.

69. Kokot, S.; Czarnik-Matusewicz, B.; Ozaki, Y., Two-dimensional correlation spectroscopy and principal component analysis studies of temperature-dependent IR spectra of cotton–cellulose. *Biopolymers* **2002,** *67* (6), 456-469.

70. Watanabe, A.; Morita, S.; Kokot, S.; Matsubara, M.; Fukai, K.; Ozaki, Y., Drying process of microcrystalline cellulose studied by attenuated total reflection IR spectroscopy with two-dimensional correlation spectroscopy and principal component analysis. *Journal of Molecular Structure* **2006,** *799* (1-3), 102-110.

71. Sugiyama, J.; Persson, J.; Chanzy, H., Combined infrared and electron diffraction study of the polymorphism of native celluloses. *Macromolecules* **1991,** *24* (9), 2461-2466.

72. Newman, R. H.; Ha, M.-A.; Melton, L. D., Solid-State 13C NMR Investigation of Molecular Ordering in the Cellulose of Apple Cell Walls. *Journal of Agricultural and Food Chemistry* **1994,** *42* (7), 1402-1406.

73. Earl, W. L.; VanderHart, D. L., High resolution, magic angle sampling spinning carbon-13 NMR of solid cellulose I. *Journal of the American Chemical Society* **1980,** *102* (9), 3251-3252.

74. Atalla, R.; Vanderhart, D., Native cellulose: a composite of two distinct crystalline forms. *Science* **1984,** *223*, 283 - 285.

75. Evans, R.; Newman, R.; Roick, U., Changes in cellulose crystallinity during kraft pulping. Comparison of infrared, x-ray diffraction and solid state NMR results. *Holzforschung* **1995,** *49*, 498 - 504.

76. Newman, R.; Davidson, T., Molecular conformations at the cellulose–water interface. *Cellulose* **2004,** *11* (1), 23-32.

77. Dudley, R. L.; Fyfe, C. A.; Stephenson, P. J.; Deslandes, Y.; Hamer, G. K.; Marchessault, R. H., High-resolution carbon-13 CP/MAS NMR spectra of solid cellulose oligomers and the structure of cellulose II. *Journal of the American Chemical Society* **1983,** *105* (8), 2469-2472.

78. Hult, E.; Larsson, P.; Iversen, T., A comparative CP/MAS 13C-NMR study of cellulose structure in spruce wood and kraft pulp. *Cellulose* **2000,** *7*, 35 - 55.

79. Heux, L.; Dinand, E.; Vignon, M. R., Structural aspects in ultrathin cellulose microfibrils followed by 13C CP-MAS NMR. *Carbohydrate Polymers* **1999,** *40* (2), 115-124.

80. Atalla, R.; Vanderhart, D., The role of solid state 13C NMR spectroscopy in studies of the nature of native celluloses. *Solid State Nucl Magn Reson* **1999,** *15*, 1 - 19.

81. Larsson, P.; Wickholm, K.; Iversen, T., A CP/MAS C-13 NMR investigation of molecular ordering in celluloses. *Carbohydr Res* **1997,** *302*, 19 - 25.

82. Larsson, P. T.; Hult, E.-L.; Wickholm, K.; Pettersson, E.; Iversen, T., CP/MAS 13C-NMR spectroscopy applied to structure and interaction studies on cellulose I. *Solid State Nuclear Magnetic Resonance* **1999,** *15* (1), 31-40.

83. Nocanda, X.; Larsson, P. T.; Spark, A.; Bush, T.; Olsson, A.; Madikane, M.; Bissessur, A.; Iversen, T., Cross polarisation/magic angle spinning 13C-NMR spectroscopic studies of cellulose structural changes in hardwood dissolving pulp process. *Holzforschung* **2007,** *61* (6), 675-679.

84. R. Zhang, Q. Y., H. Qi, J. Zhou, L. Zhang, Preparation and Properties of Cellulose/Poly(vinyl alcohol) Blend Films Based on Dissolution in a Non-Toxic Solvent System. *Journal of Biobased Materials and Bioenergy* **2009,** *3*, 199-204.

85. Schartel, B.; Wendling, J.; Wendorff, J. H., Cellulose/Poly(vinyl alcohol) Blends. 1. Influence of Miscibility and Water Content on Relaxations. *Macromolecules* **1996,** *29* (5), 1521-1527.

86. Mooney, B. P., The second green revolution? Production of plant-based biodegradable plastics. *Biochem J* **2009,** *418* (2), 219-232.

87. Yu, Q.; Wu, P.; Xu, P.; Li, L.; Liu, T.; Zhao, L., Synthesis of cellulose/titanium dioxide hybrids in supercritical carbon dioxide. *Green Chemistry* **2008,** *10* (10), 1061-1067.

88. Kosaka, P. M.; Kawano, Y.; Petri, H. M.; Fantini, M. C. A.; Petri, D. F. S., Structure and properties of composites of polyethylene or maleated polyethylene and cellulose or cellulose esters. *Journal of Applied Polymer Science* **2007,** *103* (1), 402-411.

89. Rogovina, S.; Vikhoreva, G., Polysaccharide-based polymer blends: Methods of their production. *Glycoconjugate Journal* **2006,** *23* (7), 611-618.

90. Thomas J. Heinze, W. G. G., *Cellulose derivatives: Modification, characterization, and nanostructures*. 1998.

91. Rogovina, S. Z.; Akopova, T. A.; Vikhoreva, G. A.; Gorbacheva, I. N., Solid state production of cellulose-chitosan blends and their modification with the diglycidyl ether of oligo(ethylene oxide). *Polymer Degradation and Stability* **2001,** *73* (3), 557-560.

92. Rogovina, S.; Aleksanyan, K.; Novikov, D.; Prut, E.; Rebrov, A., Synthesis and investigation of polyethylene blends with natural polysaccharides and their derivatives. *Polymer Science Series A* **2009,** *51* (5), 554-562.

93. Sawatari, C.; Kondo, T., Interchain Hydrogen Bonds in Blend Films of Poly(vinyl alcohol) and Its Derivatives with Poly(ethylene oxide). *Macromolecules* **1999,** *32* (6), 1949-1955.

94. (a) Masson, J. F.; Manley, R. S. J., Cellulose/poly(4-vinylpyridine) blends. *Macromolecules* **1991,** *24* (22), 5914-5921; (b) Masson, J. F.; Manley, R. S. J., Miscible blends of cellulose and poly(vinylpyrrolidone). *Macromolecules* **1991,** *24* (25), 6670-6679.

95. Nishioka, N.; Hamabe, S.; Murakami, T.; Kitagawa, T., Thermal decomposition behavior of miscible cellulose/synthetic polymer blends. *Journal of Applied Polymer Science* **1998,** *69* (11), 2133-2137.

96. Ołdak, D.; Kaczmarek, H.; Buffeteau, T.; Sourisseau, C., Photo- and Bio-Degradation Processes in Polyethylene, Cellulose and their Blends Studied by ATR-FTIR and Raman Spectroscopies. *Journal of Materials Science* **2005,** *40* (16), 4189-4198.

97. Bajer, K.; Kaczmarek, H.; Dzwonkowski, J.; Stasiek, A.; Ołdak, D., Photochemical and thermal stability of degradable PE/paper waste composites obtained by extrusion. *Journal of Applied Polymer Science* **2007,** *103* (4), 2197-2206.

98. Marsden, W. L.; Gray, P. P.; Mandels, M., Enzymatic Hydrolysis of Cellulose in Lignocellulosic Materials. *Critical Reviews in Biotechnology* **1985,** *3* (3), 235-276.

99. Keskin, S.; Kayrak-Talay, D.; Akman, U.; Hortaçsu, Ö., A review of ionic liquids towards supercritical fluid applications. *The Journal of Supercritical Fluids* **2007,** *43* (1), 150-180.

100. Wen, D.; Jiang, H.; Zhang, K., Supercritical fluids technology for clean biofuel production. *Progress in Natural Science* **2009,** *19* (3), 273-284.

101. Zheng, Y.; Lin, H. M.; Tsao, G. T., Pretreatment for Cellulose Hydrolysis by Carbon Dioxide Explosion. *Biotechnology Progress* **1998,** *14* (6), 890-896.

102. Leitner, W., Reactions in Supercritical Carbon Dioxide. In *Modern Solvents in Organic Synthesis*, Knochel, P., Ed. Springer Berlin / Heidelberg: 1999; Vol. 206, pp 107-132.

103. Wypych, G., *Handbook of solvents*. ChemTec: 2001.

104. Johnston, K. P.; Shah, P. S., Making Nanoscale Materials with Supercritical Fluids. *Science* **2004,** *303* (5657), 482-483.

105. Zheng, Y.; Tsao, G. T., Avicel hydrolysis by cellulase enzyme in supercritical CO2. *Biotechnology Letters* **1996,** *18* (4), 451-454.

106. Kjellow, A. W.; Henriksen, O., Supercritical wood impregnation. *The Journal of Supercritical Fluids* **2009,** *50* (3), 297-304.

107. Sihvonen, M.; Järvenpää, E.; Hietaniemi, V.; Huopalahti, R., Advances in supercritical carbon dioxide technologies. *Trends in Food Science & Technology* **1999,** *10* (6-7), 217-222.

108. Kanakubo, M.; Aizawa, T.; Kawakami, T.; Sato, O.; Ikushima, Y.; Hatakeda, K.; Saito, N., Studies on Solute−Solvent Interactions in Gaseous and Supercritical Carbon Dioxide by High-Pressure 1H NMR Spectroscopy. *The Journal of Physical Chemistry B* **2000,** *104* (12), 2749-2758.

109. Tsai, C.-C.; Lin, H.-m.; Lee, M.-J., Solubility of 1,5-Diaminobromo-4,8-dihydroxyanthraquinone in Supercritical Carbon Dioxide with or without Cosolvent†. *Journal of Chemical & Engineering Data* **2008,** *54* (5), 1442-1446.

110. Mukhopadhyay, M.; Dalvi, S. V., Partial molar volume fraction of solvent in binary (CO2-solvent) solution for solid solubility predictions. *The Journal of Supercritical Fluids* **2004,** *29* (3), 221-230.

111. Fleming, O. S.; Kazarian, S. G., *Polymer Processing with Supercritical Fluids*. Wiley-VCH Verlag GmbH & Co. KGaA: 2006; p 205-238.

112. Kazarian, S. G., Polymer Processing with Supercritical Fluids. *Polymer Science Series C* **2000,** *42* (1), 78-101.

113. Cooper, A. I., *Polymer synthesis and processing using supercritical carbon dioxide*. Royal Society of Chemistry: Cambridge, ROYAUME-UNI, 2000; Vol. 10.

114. Tomasko, D. L.; Li, H.; Liu, D.; Han, X.; Wingert, M. J.; Lee, L. J.; Koelling, K. W., A Review of CO2 Applications in the Processing of Polymers. *Industrial & Engineering Chemistry Research* **2003,** *42* (25), 6431-6456.

115. Kung, E.; Lesser, A. J.; McCarthy, T. J., Morphology and Mechanical Performance of Polystyrene/Polyethylene Composites Prepared in Supercritical Carbon Dioxide. *Macromolecules* **1998,** *31* (13), 4160-4169.

116. Woods, H. M.; Silva, M. M. C. G.; Nouvel, C.; Shakesheff, K. M.; Howdle, S. M., Materials processing in supercritical carbon dioxide: surfactants, polymers and biomaterials. *Journal of Materials Chemistry* **2004,** *14* (11), 1663-1678.

117. Li, H.; Lee, L. J.; Tomasko, D. L., Effect of Carbon Dioxide on the Interfacial Tension of Polymer Melts. *Industrial & Engineering Chemistry Research* **2003,** *43* (2), 509-514.

118. Elkovitch, M. D.; Tomasko, D. L.; Lee, L. J., Supercritical carbon dioxide assisted blending of polystyrene and poly(methyl methyacrylate). *Polymer Engineering & Science* **1999,** *39* (10), 2075-2084.

119. Zhang, J.; Busby, A. J.; Roberts, C. J.; Chen, X.; Davies, M. C.; Tendler, S. J. B.; Howdle, S. M., Preparation of a Poly(methyl methacrylate)/Ultrahigh Molecular Weight Polyethylene Blend Using Supercritical Carbon Dioxide and the Identification of a Three-Phase Structure: An Atomic Force Microscopy Study. *Macromolecules* **2002,** *35* (23), 8869-8877.

120. Lee, M.; Tzoganakis, C.; Park, C. B., Extrusion of PE/PS blends with supercritical carbon dioxide. *Polymer Engineering & Science* **1998,** *38* (7), 1112-1120.

121. Lan, H.-Y.; Tseng, H.-C., Study on the Rheological Behavior of PP/Supercritical CO_2 Mixture. *Journal of Polymer Research* **2002,** *9* (3), 157-162.

122. Plastics, E. S., *ANTEC'97*. SPE: 1997.

123. Muljana, H.; Picchioni, F.; Heeres, H. J.; Janssen, L. P. B. M., Supercritical carbon dioxide ($scCO_2$) induced gelatinization of potato starch. *Carbohydrate Polymers* **2009,** *78* (3), 511-519.

124. Kiran, E.; Pöhler, H., Alternative solvents for cellulose derivatives:: Miscibility and density of cellulosic polymers in carbon dioxide+acetone and carbon dioxide+ethanol binary fluid mixtures. *The Journal of Supercritical Fluids* **1998,** *13* (1-3), 135-141.

125. Haimer, E.; Wendland, M.; Potthast, A.; Henniges, U.; Rosenau, T.; Liebner, F., Controlled precipitation and purification of hemicellulose from DMSO and DMSO/water mixtures by carbon dioxide as anti-solvent. *The Journal of Supercritical Fluids* **2010,** *53* (1-3), 121-130.

126. Tsai, C.-C.; Lin, H.-m.; Lee, M.-J., Solubility of disperse yellow 54 in supercritical carbon dioxide with or without cosolvent. *Fluid Phase Equilibria* **2007,** *260* (2), 287-294.

127. O'Sullivan, A., Cellulose: the structure slowly unravel. *Cellulose* **1997,** *4*, 173 - 207.

128. Hult, E.-L.; Liitiä, T.; Maunu, S. L.; Hortling, B.; Iversen, T., A CP/MAS 13C-NMR study of cellulose structure on the surface of refined kraft pulp fibers. *Carbohydrate Polymers* **2002,** *49* (2), 231-234.

129. Ishii, R.; Cho, D. C.; Mori, T.; Mizutani, T.; Ishioka, M. In *Electrical properties of low-density polyethylene prepared by different manufacturing process*, Electrical Insulation and Dielectric Phenomena, 1999 Annual Report Conference on, 1999; 1999; pp 642-645 vol.2.

130. Gururajan, G.; Shan, H.; Lickfield, G.; Ogale, A. A., Real-time wide-angle X-ray diffraction during polyethylene blown film extrusion. *Polymer Engineering & Science* **2008,** *48* (8), 1487-1494.

131. Focher, B.; Palma, M. T.; Canetti, M.; Torri, G.; Cosentino, C.; Gastaldi, G., Structural differences between non-wood plant celluloses: evidence from solid state NMR, vibrational spectroscopy and X-ray diffractometry. *Industrial Crops and Products* **2001,** *13* (3), 193-208.

132. Zhou, D.; Zhang, L.; Guo, S., Mechanisms of lead biosorption on cellulose/chitin beads. *Water Research* **2005,** *39* (16), 3755-3762.

133. Haberhauer, G.; Gerzabek, M. H., Drift and transmission FT-IR spectroscopy of forest soils: an approach to determine decomposition processes of forest litter. *Vibrational Spectroscopy* **1999,** *19* (2), 413-417.

134. Yu, P., Plant-based food and feed protein structure changes induced by gene-transformation, heating and bio-ethanol processing: A synchrotron-based molecular structure and nutrition research program. *Molecular Nutrition & Food Research* **2010,** *54* (11), 1535-1545.

135. Kaewgun, S.; Nolph, C.; Lee, B., Enhancing Photocatalytic Activity of Polymorphic Titania Nanoparticles by NMP Solvent-based Ambient Condition Process. *Catalysis Letters* **2008,** *123* (3), 173-180.

136. Kaewgun, S.; Nolph, C. A.; Lee, B. I.; Wang, L.-Q., Influence of hydroxyl contents on photocatalytic activities of polymorphic titania nanoparticles. *Materials Chemistry and Physics* **2009,** *114* (1), 439-445.

137. Swann, G. E. A., Patwardhan, S. V., Application of Fourier Transform Infrared Spectroscopy (FTIR) for assessing biogenic silica sample purity in geochemical analyses and palaeoenvironmental research. *Clim. Past* **2011,** *7* (1), 65-74.

138. Mishra, A. K.; Chattopadhyay, D. K.; Sreedhar, B.; Raju, K. V. S. N., FT-IR and XPS studies of polyurethane-urea-imide coatings. *Progress in Organic Coatings* **2006,** *55* (3), 231-243.

139. Watanabe, A.; Morita, S.; Ozaki, Y., Study on Temperature-Dependent Changes in Hydrogen Bonds in Cellulose Iβ by Infrared Spectroscopy with Perturbation-Correlation Moving-Window Two-Dimensional Correlation Spectroscopy. *Biomacromolecules* **2006,** *7* (11), 3164-3170.

140. Fawcett, W. R.; Kloss, A. A., Attenuated total reflection fourier-transform IR spectroscopic study of dimethyl sulfoxide self-association in acetonitrile solutions. *Journal of the Chemical Society, Faraday Transactions* **1996,** *92* (18), 3333-3337.

141. Skripkin, M. Y.; Lindqvist-Reis, P.; Abbasi, A.; Mink, J.; Persson, I.; Sandstrom, M., Vibrational spectroscopic force field studies of dimethyl sulfoxide and hexakis(dimethyl sulfoxide)scandium(iii) iodide, and crystal and solution structure of the hexakis(dimethyl sulfoxide)scandium(iii) ion. *Dalton Transactions* **2004,** (23), 4038-4049.

142. Martens, W. N.; Frost, R. L.; Kristof, J.; Theo Kloprogge, J., Raman spectroscopy of dimethyl sulphoxide and deuterated dimethyl sulphoxide at 298 and 77 K. *Journal of Raman Spectroscopy* **2002,** *33* (2), 84-91.

143. Yilgör, E.; Burgaz, E.; Yurtsever, E.; Yilgör, I., Comparison of hydrogen bonding in polydimethylsiloxane and polyether based urethane and urea copolymers. *Polymer* **2000,** *41* (3), 849-857.

144. Li, Z.-f.; Li, J.-y.; Sun, J.; Sun, B.-q.; Wang, J.-j.; Shen, Q., Investigation of kinetics and morphology development for polyurethane-urea extended by DMTDA. *Frontiers of Materials Science in China* **2008,** *2* (2), 200-204.

145. Liu, J.-Y.; Yang, C.-C.; Wang, Y.-Z., Miscibility and physical properties of conducting poly(urea-urethane) thermoplastic elastomers. *Journal of Applied Polymer Science* **2007,** *103* (6), 3803-3810.

146. Cao, Y.; Tan, H., Effects of cellulase on the modification of cellulose. *Carbohydrate Research* **2002,** *337* (14), 1291-1296.

147. Yong, S.; Lu, L.; Haibo, D.; Jiazhe, L.; Beihai, H.; Runchang, S.; Pingkai, O., College of Natural Resources, North Carolina State University: 2008.

148. VanderHart, D. L.; Atalla, R. H., Studies of microstructure in native celluloses using solid-state carbon-13 NMR. *Macromolecules* **1984,** *17* (8), 1465-1472.

149. Atalla, R.; Vanderhart, D., Native Cellulose: A Composite of Two Distinct Crystalline Forms. *Science* **1984,** *223* (4633), 283-285.

150. Park, S.; Johnson, D.; Ishizawa, C.; Parilla, P.; Davis, M., Measuring the crystallinity index of cellulose by solid state 13C nuclear magnetic resonance. *Cellulose* **2009,** *16* (4), 641-647.

BIOGRAPHICAL SKETCH

Aniket Selarka was born with a twin sister in Wardha, India. He received his bachelor's degree in production engineering from Amravati University in 2002. After that, he pursued post graduate diploma in plastics engineering from Central Institute of Plastics Engineering and Technology, Chennai. He then worked for Shriram Institute for Industrial Research – a non-profit organization in New Delhi as a graduate engineer trainee for one year. In year 2005, he joined General Electric Company's Research and Development Center (John F. Welch Technology Center) in Bangalore, India. After working there for one and half years he decided to pursue PhD in materials science and engineering at University of Florida in Gainesville, USA. Aniket graduated in 2011 and is looking forward to work in the field of polymeric materials and product development.